

IOWA STATE UNIVERSITY

Digital Repository

Graduate Theses and Dissertations

Iowa State University Capstones, Theses and
Dissertations

2014

Analysis of surface wind speed distributions: A look into NARCCAP models and ASOS data throughout the Contiguous United States

Rachel Hatteberg
Iowa State University

Follow this and additional works at: <https://lib.dr.iastate.edu/etd>

 Part of the [Meteorology Commons](#)

Recommended Citation

Hatteberg, Rachel, "Analysis of surface wind speed distributions: A look into NARCCAP models and ASOS data throughout the Contiguous United States" (2014). *Graduate Theses and Dissertations*. 13882.
<https://lib.dr.iastate.edu/etd/13882>

This Thesis is brought to you for free and open access by the Iowa State University Capstones, Theses and Dissertations at Iowa State University Digital Repository. It has been accepted for inclusion in Graduate Theses and Dissertations by an authorized administrator of Iowa State University Digital Repository. For more information, please contact digirep@iastate.edu.

**Analysis of surface wind speed distributions: A look into NARCCAP models and
ASOS data throughout the Contiguous United States**

by

Rachel Hatteberg

A thesis submitted to the graduate faculty
in partial fulfillment of the requirements for the degree of
MASTER OF SCIENCE

Major: Meteorology

Program of Study Committee:
Eugene Takle, Major Professor
William Gutowski
Brian Hornbuckle

Iowa State University
Ames, Iowa
2014

Copyright © Rachel Hatteberg, 2014. All rights reserved

DEDICATION

I would like to dedicate this Master's Thesis to my parents, Nancy and Don Hatteberg, for without their support, patience, and encouragement, this project would not have been possible. Thank you both for being such wonderful and loving parents to me.

TABLE OF CONTENTS

	Page
DEDICATION	ii
NOMENCLATURE	vi
ACKNOWLEDGEMENTS	vii
ABSTRACT	viii
CHAPTER 1 INTRODUCTION: SURFACE WIND SPEEDS	1
CHAPTER 2 LITERATURE REVIEW	8
2.1 Surface wind speed measurements	8
2.2 Climatology of surface wind speeds throughout the United States	9
2.3 Surface wind speed characteristics across regions of study.....	10
2.3.1 Seasonal characteristics of surface wind speeds	11
2.3.2 Weibull distribution	14
2.3.3 Surface wind speed trends	16
2.3.3.1 Low wind speed trends	17
2.3.3.2 High wind speed trends	18
2.3.4 Interannual variability.....	19
2.3.5 Implications of wind speed trends	19
2.4 Model simulated surface wind speeds	20
2.5 Possible explanations on surface wind speed trends	23
CHAPTER 3 DATA AND METHODOLOGY	25
3.1 ASOS	25
3.1.1 Pre-ASOS compared to current ASOS	26
3.1.2 Limitations associated with wind observational data	28
3.1.3 Missing data and quality control	30
3.2 Defining “extreme” high and low wind speeds	31
3.3 Cities of Interest	33
3.4 NARCCAP.....	36
3.5 RCMs	37
3.6 GCMs	37
3.7 Inclusion of model spin-up data.....	38
3.8 Schematics of study	38
CHAPTER 4 SURFACE WINDS REPRESENTED BY ASOS OBSERVATIONS..	39

4.1 Introduction	39
4.2 Pre-ASOS vs ASOS observations.....	41
4.2.1 Seasonal distributions	41
4.3 Surface wind speed distribution.....	43
4.4 “Extreme” high winds.....	45
4.5 “Extreme” low winds.....	46
 CHAPTER 5 SURFACE WINDS REPRESENTED BY THE NARCCAP MODELS	48
5.1 Introduction	48
5.2 RCM results with NCEP boundary conditions	48
5.2.1 Surface wind speed distributions	48
5.2.2 “Extreme” high winds represented by models.....	52
5.2.3 “Extreme” low winds represented by models.....	53
5.2.4 Seasonal distributions	56
5.3 Contemporary scenario model simulations.....	60
5.3.1 Surface wind speed distributions	60
5.3.2 “Extreme” high winds represented by models.....	62
5.3.3 “Extreme” low winds represented by models.....	63
5.3.4 Seasonal distributions	64
5.4 Future scenario model simulations	68
5.4.1 Surface wind speed distributions	68
5.4.2 “Extreme” high winds represented by models.....	69
5.4.3 “Extreme” low winds represented by models	69
5.4.4 Seasonal distributions	70
5.5 Model compared to observational data.....	74
5.6.1 RCM/NCEP models compared to observational data.....	74
5.6.2 RCM/GCM contemporary model scenarios compared to observational data	76
5.6 Contemporary and future scenario comparison	77
5.5.1 Surface wind speed distributions	77
5.5.2 Seasonal distributions	82
 CHAPTER 6 SUMMARY AND CONCLUSIONS	86
REFERENCES	92
APPENDIX A: ASOS SITE INFORMATION	96
APPENDIX B : PERCENT DIFFERENCE: ASOS VS PRE-ASOS	100
APPENDIX C1-3: ANALYSIS OF LOW WINDS	104

APPENDIX D: DIFFERENCE PLOTS: CONTEMPORARY AND FUTURE SCENARIOS	116
APPENDIX E: SEASONAL DISTRIBUTIONS	120

NOMENCLATURE

ASOS	Automated Surface Observing System
CCSM	Community Climate System Model
CGCM3	Third Generation Coupled Global Climate Model
CRCM	Canadian Regional Climate Model
GCM	Global Climate Model
KFTY	Atlanta, GA, ASOS Site
KHOU	Houston, TX, ASOS Site
KHSI	Hastings, NE, ASOS Site
KJMS	Jamestown, ND, ASOS Site
KLAF	Lafayette, IN, ASOS Site
KLBL	Liberal, KS, ASOS Site
KMCW	Mason City, IA, ASOS Site
MM5I	5th Generation Mesoscale Model (PSU/NCAR Mesoscale Model)
NARCCAP	North American Regional Climate Change Assessment Program
NOAA	National Oceanic and Atmospheric Administration
NWS	National Weather Service
PBL	Planetary Boundary Layer
RCM	Regional Climate Model
WRFG	Weather and Research Forecasting Model

ACKNOWLEDGEMENTS

I would like to thank my committee chair, Gene Takle, and my committee members, Bill Gutowski, and Brian Hornbuckle, for their guidance and support throughout the course of this research.

In addition, I would also like to thank my friends, colleagues, the department faculty and staff for making my time at Iowa State University a wonderful experience. I will enthusiastically carry onward the education I received at this institution into my lifelong career in atmospheric sciences. I want to offer my appreciation to Dave Flory and Jasmeet Singh, who helped me with various coding tasks, without whom, this thesis would not have been possible. I would also like to express my gratitude to John Hobbs, for his statistical analysis guidance.

Finally, thanks to my family for their encouragement, patience, support and love.

ABSTRACT

Our ability to numerically simulate near surface winds is a challenging, yet necessary component within meteorological and climate models. There are many societal implications of winds both high and low such as wind energy, air pollution dispersion, agricultural productivity, as well as the sometimes catastrophic damage to life and property. Due to these impacts, we seek answers to the question of how well our weather forecast and climate models with low resolution simulate near surface winds. We also seek to know how these models simulate surface winds into the future with respect to climate change.

We evaluated the characteristics of three regional climate models forced by NCEP reanalysis II data across five locations in the Midwest, United States: Mason City, IA, Lafayette, IN, Hastings, NE, Liberal, KS, and Jamestown, ND; and two southern metropolitan cities: Houston, TX, and Atlanta, GA. The first part of the analysis was carried out to provide a baseline to test these climate models' ability to accurately simulate surface wind conditions using observational data as a reference point. There is a general negative bias in both the climate models with NCEP reanalysis data as well as the contemporary climate models at all of the locations except Houston, TX, and Atlanta, GA, which had a positive bias. It also appears that the CGCM3 GCM introduces significant error into the contemporary scenarios at four of the seven locations. These are factors to take into account while formulating conclusions on the accuracy of the future scenario trends as well as the overall comparison between the future and contemporary climates.

Contemporary (1968-2000) and future (2038-2070) scenarios simulated by these regional climate models were also evaluated. Both low and high ends of the "extreme" wind spectrum were analyzed, in which our low-end "extreme" threshold is defined to be at or below the 10th percentile, and the high-end extreme to be at or above the 90th percentile. Seasonal distributions were also

evaluated amongst each of the climate models. Overall, the contemporary and future scenarios appear to simulate the general timing of seasonal minimum winds (June, July, and August), whereas, they do not simulate seasonal maximum winds with accuracy (March, April, and May).

When comparing the difference between future and contemporary scenarios, it is evident that near-calm winds show to be increasing in frequency across all of the stations analyzed and high-end winds are showing inconclusive trends throughout the climate models studied. The MM5I displayed an anomalously high frequency of low-end winds at six out of the seven locations compared to the other regional climate models. This unusual feature needs to be further investigated because of air pollution dispersion and agricultural implications. There is large variance among the climate models, so it is recommended to exercise caution when using a single model for applications or references.

CHAPTER I

INTRODUCTION

Wind, the movement of air from one place to another, plays a significant role in everyday societal tasks and is constantly evolving and varying on time scales from minutes, days, years, and decades. Wind speeds have innumerable impacts on society, ranging, but not limited to agricultural, recreational, air quality and health issues, structural and personal damages, and wind energy production. In this study, we will be focusing on characteristics of surface wind speeds across specific regions of the United States by analyzing observational and model simulated wind data. A portion of this research project will investigate climate extremes, specifically wind speeds at both extremes, both high and low, as these classes are where the majority of societal impacts listed above are resultant upon. According to the Intergovernmental Panel on Climate Change (IPCC) (2013a), a climate or weather extreme is defined as the occurrence of a value of a weather or climate variable above (or below) a threshold value near the upper (or lower) ends of the range of observed values of the variable.

A deeper look into the behaviors and trends of wind speed distributions at specific locations throughout the contiguous United States is possible through the investigation of surface wind speed characteristics through model and observational data. More specifically, five locations throughout the Midwest, and two in the South, will be examined to gain a better insight into surface wind speed trends and characteristics from nearly the past four decades. Through the usage of simulated model data as far out into the future as the year 2070, wind speed distribution trends, mainly at the extremes, will be identified and analyzed. Observational data are reference points for evaluation of the models being used to estimate future surface wind speed regimes in

this study. Furthermore, researchers have actively been investigating whether climate change is affecting wind speed trends throughout the contiguous United States, and if so, what role will surface wind changes play in this planet's future socioeconomic state?

Over several meteorological scales, wind speeds have been known to reach very high-end values that may be life-threatening and can cause significant structural damage. Whether it is a deep synoptic-scale mid-latitude cyclone sweeping through the Midwest, or convectively produced downdrafts on the mesoscale level, winds can reach damaging levels over both small and large spatial scales. Model representation of winds of this magnitude is crucial in understanding long-term climatological trends: are these damaging winds increasing in frequency or magnitude? Furthermore, it is important to understand the tendencies of high-end wind speeds and to see if there is a possible link between any temporal trends and observed climate change factors. The results of this inquiry could largely affect future structural engineering so that damage to life and property could be mitigated.

Disaster mitigation is used to refer to actions that attempt to limit further negative conditions once disaster has materialized. In other words, mitigation of the damages sustained from these extreme wind events could refer to focusing on designing more sound structures in which climate which has the capability to sustain such events in the future (IPCC, 2013a). It is difficult to study such extreme events because their occurrence in nature is rare, which means there is minimal data available to make assessments regarding changes in their frequency or intensity.

As well as extreme wind speeds, other attributes of wind can cause extreme impacts. Trends in average wind speeds influences evaporation, and ultimately, water availability and droughts. Evaporation processes are highly dependent on temperature, moisture availability,

surface area, pressure, and wind. Surface winds also influence evapotranspiration (ET) rates, which is the sum of evaporation and plant transpiration. In both cases of evaporation and ET, the rate of these processes is directly proportional to the magnitude of the surface wind speed, such that the stronger the wind, the more evaporation or ET can occur per unit time (Seginer, 1971). These processes play large roles in water availability, thus, increased knowledge about surface wind speed trends will aid in understanding future tendencies of the hydrologic cycle.

On the other end of the spectrum of extremes, calm, or low surface wind speeds are also significant, such that, air stagnation events over populous cities can cause dramatic health issues to its residents. Air pollution is an acknowledged problem in select locations throughout the contiguous United States such as Los Angeles, CA, Fresno, CA, Washington, DC, Dallas, TX, and Houston, TX (American Lung Association, 2013). Air pollutants are various particles and molecules (both natural and man-made pollutants) suspended in the air that are harmful to humans, animals, and agriculture when they are inhaled or ingested. Considering air pollution in this study is crucial because wind is the primary mechanism for dispersing these harmful particles. If there are reduced wind speed trends, pollution-prone cities may face ventilation problems more frequently, in return, increasing the exposure to pollutants, and thereby, exacerbating cases of lung and heart diseases (American Lung Association, 2013). On the other hand, if wind speeds increase over time, air pollution will ideally become less of an issue for large metropolitan regions, as air pollutants would be pushed downstream more effectively. If wind speeds wane, boundary layer meteorology would be largely affected; moreover, the efficiency of heat and moisture transport between the Earth's surface and the atmosphere would decline, which would lead to amplification of any increases in surface temperatures. Studies have found that weaker winds in a warmer climate led to higher concentrations in pollution plumes

and can have implications on transport of pollen and mold in the area. Heat and moisture transfer between the Earth's surface and the atmosphere is attenuated if wind speed decreases over the period, which can lead to human discomfort, especially during summer (Munn, 1976).

Wind influences agriculture in two primary ways: physiologically and mechanically. Higher transpiration rates occur with increased wind, and wind processes increases turbulence in the atmosphere and availability of CO₂, thereby increasing photosynthesis. On the other hand, plants are also affected mechanically by wind; strong prevailing winds induce erosion processes, and if the surface winds are strong enough, crops can even be damaged or destroyed. Aeolian processes (wind processes influencing the Earth's surface) significantly influence the formation and evolution of arid and semi-arid environments, being strongly linked to soil and vegetation change. Soil erosion is harmful to agricultural land because important soil nutrients are removed or displaced from its original location. Another way erosion is harmful to plants is from "pedestaling," which is a process where the soil surface is lowered by Aeolian processes, which exposes plant roots and can result in plant mortality (Okin et al., 2001). According to the United Nations Environmental Program (UNEP), crop yield across the globe is dramatically affected by Aeolian processes such as wind erosion or erosion-induced degradation. UNEP (1990) estimates that about 20 million ha of agricultural land are destroyed each year, and becomes essentially unprofitable as a result of Aeolian processes. Wind is also necessary for pollination of plants as well as cooling from the hot sun. If surface winds are too weak, plant health is significantly degraded (Cooke, Jones and Kaye, 2006).

Trends in surface wind speeds have the potential to affect the yield and sustainability of agriculture. As will be mentioned in the following chapters, numerous studies have shown that surface wind speeds are exhibiting general decreasing trend (more frequency of near-calm

winds) (Klink, 2002; Abhishek et al., 2010; Vautard et al., 2010). There are a few concepts to keep in mind while considering possible outcomes of changing surface wind speeds: evaporative processes are directly proportional to wind speed, such that as wind speeds increase, so does the amount of evaporation. On the other hand, lighter magnitudes of wind speeds at the surface results in smaller amounts of evaporation which can take place. Evaporative processes are essential for plant's sustainability as it acts as a cooling mechanism and lowers the internal temperature of crops. If lighter winds results in less efficient evaporation, plant structures will experience general warming temps, which may or may not be favorable for overall crop health and may influence a plant's water use efficiency, defined by Hatfield, Sauer, and Prueger (2001) as the ratio of crop yield to the amount of evapotranspiration. Do the benefits of lesser efficient evaporation in plants outweigh the negatives? What are plant's adaptation capabilities to less evaporation?

Pollination is dependent on wind as the mechanical transfer of the pollen downwind. Do lighter magnitudes of surface winds result in less efficient pollination? Also impacted by wind-borne dispersion processes is the spread of diseases/fungal spores among crops. The quantity of fungal spores being released and transported throughout the air is directly proportional to wind speed, such that the greater the wind speeds, the more efficient transport of fungal spores will be. On the other hand, wind not only transports spores, but also has the capability to remove them from infected crops (Cooke, Jones and Kaye, 2006). Overall, trends in wind speeds possess both positive and negative outcomes for the yield and sustainability of vegetation.

In arid regions, dust storms are contingent on surface wind speeds along with other factors like precipitation and soil moisture as well as land use. The primary force for the production of dust storms is the surface wind associated with cold frontal systems sweeping

across arid and semi-arid regions and lifting soil particles in the atmosphere. There have been numerous dust storms throughout our nation's history, which were significantly damaging to life and property. Understanding trends in surface wind speeds may allow for better understanding or prediction of the frequency of such events.

Surface wind speeds also affect tourism and recreational activities across the globe. Various sports and activities rely on wind, such as sailing, wind surfing, or kite flying. On the other hand, wind can prohibit various activities, such as canoeing, playing tennis, having a picnic or a bonfire, and so on. To reiterate on an earlier statement, wind speeds at the surface have large implications on this planet's day-to-day activities, sustainability, and general well-being.

There are still many unknowns in regards to the relationship between surface winds and other parts of the climate system. Also, we know little about the connections between surface winds, small-scale features such as topography or land use, and large-scale atmospheric circulation patterns. Because wind speed is a function of the pressure gradient, which in turn is related to temperature, it is possible that changes in surface temperature may produce systematic changes in surface winds.

Overall, this thesis project aims to gain a better understanding regarding surface wind speed characteristics, through the analysis of observational and model data, predominantly at the extremes, both high and low. Acquiring better knowledge of the occurrence, nature, and trends of these events will allow for better preparation, and ultimately mitigation of the loss of property and life in the future.

Motivation and thesis organization

This project was inspired by my senior thesis completed in the fall of 2009, which focused on derechos. Similar datasets were used as herein, in an effort to analyze NCEP-driven

RCMs' capabilities of simulating these extreme high-end surface wind speeds. Following the completion of that project, curiosity drove me to further analyze surface wind speeds with the NARCCAP dataset, looking at both contemporary and future climate scenarios, and finally, comparing the results to observational data.

Chapter 2 contains a literature review in which historical studies dealing with surface wind speed observations and distributions will be discussed. Contemporary studies will be reviewed in which extremes and modeling projects are examined.

Next, the data used and implemented methodologies in this project will be described in Chapter 3. Following this, Chapter 4 examines surface wind speed characteristics and trends at seven cities throughout the United States (five in the Midwest and two in the South) through the collection of observational data obtained from Automated Surface Observing System (ASOS) equipment. An emphasis will be made on searching for temporal trends and analyzing winds at the extreme ends of the distributions. The analysis of observational data will serve as a foundation to which we will compare and contrast model data in the forthcoming chapter.

Similarly to Chapter 4, Chapter 5 will display results of surface wind characteristics. However, this chapter will examine various Regional Climate Models' (RCMs) simulated data which uses different Global Climate Models (GCMs) as initial boundary conditions. This chapter can be broken into two main sections: contemporary and future scenario model simulations, both of which will be heavily examined. A similar approach to analyzing the data as in Chapter 4 will be carried out in this chapter.

Lastly, Chapter 6 gives an overview of the general conclusions that can be made based on the analyzed data sets.

CHAPTER 2

LITERATURE REVIEW

Studies have reported seasonal trends, the fitting of near-surface wind data to distribution functions, and interannual variability of wind speed data (Takle, Brown, and Davis, 1978; Takle and Brown, 1978; Stewart and Essenwanger, 1978; Tuller and Brett, 1984; Klink, 1999, 2002; Pryor et al., 2010). Another focal point of wind research has been the occurrence of extreme winds near the surface. Specifically speaking, these “extreme” events can fall into two categories: the calm, or near-zero winds, and the “extreme” high-end winds, both of which are significant because their occurrences are associated with the majority of the societal impacts mentioned in Chapter 1 (IPCC, 2013a). Attribution of trends in thesis data is also analyzed.

2.1 Surface wind speed measurements

Automated instruments were not implemented into the United States until the mid to late 1990’s, prior to which, data was observed and recorded manually (ASOS, 1999). Further detail regarding measurement of the wind speed data used in this study will be discussed in Chapter 3.

There is a lack of consistency and “completeness” of wind speed measurements over long time span; therefore, it is necessary to use caution while evaluating this type of meteorological data (ASOS, 1998; DeGaetano, 1998; IPCC, 2013a). Klink (2002) uses a guideline which regulates whether a dataset is complete enough, which states that the data source should be omitted from the analysis if it possesses more than 1% missing data. Klink’s guideline provides a threshold which ensures the data used are representative and continuous. Additionally, data should be checked for conformance to the established observing practice, such that the

equipment is commissioned by a governmental agency and is subject to routine maintenance (ASOS, 1998).

2.2 Climatology of surface wind speeds throughout the United States

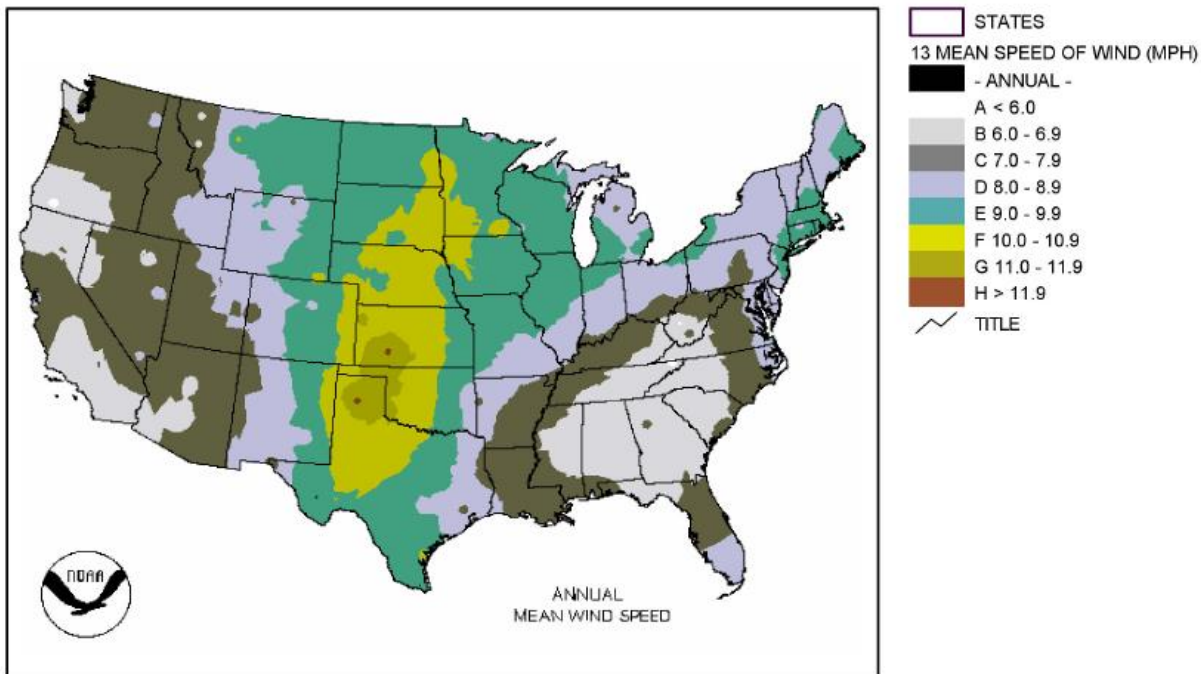


Figure 2-1. Annual daily mean surface wind speed from 1961-1990 (NOAA, 2005)

Klink (1999) has shown through observational research that mean maximum wind speeds generally are highest in the central and northeastern United States and in some locations in the west where topographic channeling may enhance surface winds.

Calm or near-calm winds at the surface occur frequently throughout the country; however, these low-end winds are typically observed less frequently in the central and northeastern United States (Klink, 1999). This lack of calm or near-calm winds in these regions can be attributed to the flat to gently rolling topography as well as the frequently passing cyclone and anticyclone systems (Klink, 1999). Nevertheless, low wind speeds are frequently observed in the southeastern portion of the United States because of the recurring high pressure synoptic regime.

Figure 2-1 is a climatological map which displays the annual daily mean surface wind speed data (in mph) from 1961-1990 (NOAA, 2005). It can be noted that there is a minimum in wind speed magnitude found in the southeast, which reinforces the aforementioned conclusions we outlined from Klink (1999). Also, there is an axis of maximum annual mean wind speeds which is oriented in the north-south direction stretching from Texas northward up to the Missouri River Valley. It should be noted that the locations encompassed within this maximum will be an area of focus within this study.

2.3 Surface wind speed characteristics across regions of study

This research project will examine surface wind speeds throughout select regions of the United States, primarily in the southeast and Midwest. These locations will be further defined in Chapter 3.3. Klink (2002) analyzed surface wind speed observations across northern Midwestern stations over climate records of 22-35 years. The records varied in length due to inconsistencies in the data, primarily due to differences in anemometer heights. Klink obtained the largest possible climate record for each of the locations based on having constant anemometer heights and locations, those of which ranged from beginning in 1959 to 1966 and ending in 1983 to 1995. This study (Klink, 2002) is of particular interest because of its geographic focus, being the Midwest, which, as stated previously, is a main region of interest in this thesis project. Results of this study exhibited that the wind speed distribution is more sharply peaked at locations such as Duluth and International Falls, MN, which point towards fewer occurrences of the mean wind speed values, but perhaps, are more condensed at the low and high ends of the distribution. On the other hand, Fargo, ND, and Rochester, MN, show more rounded peaks in their frequency distributions, which is an indication that surface winds in these locations occur in the middle-ranges more often than the low or high ends. Klink attributed the difference in the shapes of the

distributions to different anemometer heights among the stations as well as the varying periods of study. On the contrary, it was noted that the shapes differ among stations with like heights and period of records (e.g., Huron, SD; Duluth, and International Falls, MN), thus, a complete attribution of variation in distribution shape cannot be placed on measurement height differences. The theoretical explanation behind the shape or “peakedness” of the distributions will be further discussed in Section 2.3.2.

In general terms of climatology, the two regions of interest for this study fall under two prominent categories: higher mean annual surface wind speeds found in the Midwest, and generally lower mean annual wind speeds in the South and Southeast, which, again, can be observed in Figure 2-1 (NOAA, 2005).

2.3.1 Seasonal characteristics of surface wind speeds

Takle, Brown, and Davis (1976) studied the characteristics of wind and wind energy in Iowa and focused on mean monthly wind speed data. Their study showed that the average wind speed is the least in the months of July and August, and then gradually increases in strength throughout the fall and winter until it peaks in April and then begins diminishing as the summer minimum approaches. Similarly, Klink (1999) averaged monthly winds among stations across the entire contiguous United States over the period of 1961 to 1990 and found that surface wind speeds are largest in magnitude in the spring months (March, April, May) and smallest during the summer (June, July, August). Klink (1999) found an increasing trend in the monthly maximum surface wind speeds and a decreasing trend in minimum speeds throughout all months of the year, with the smallest reductions in summer and the largest in spring.

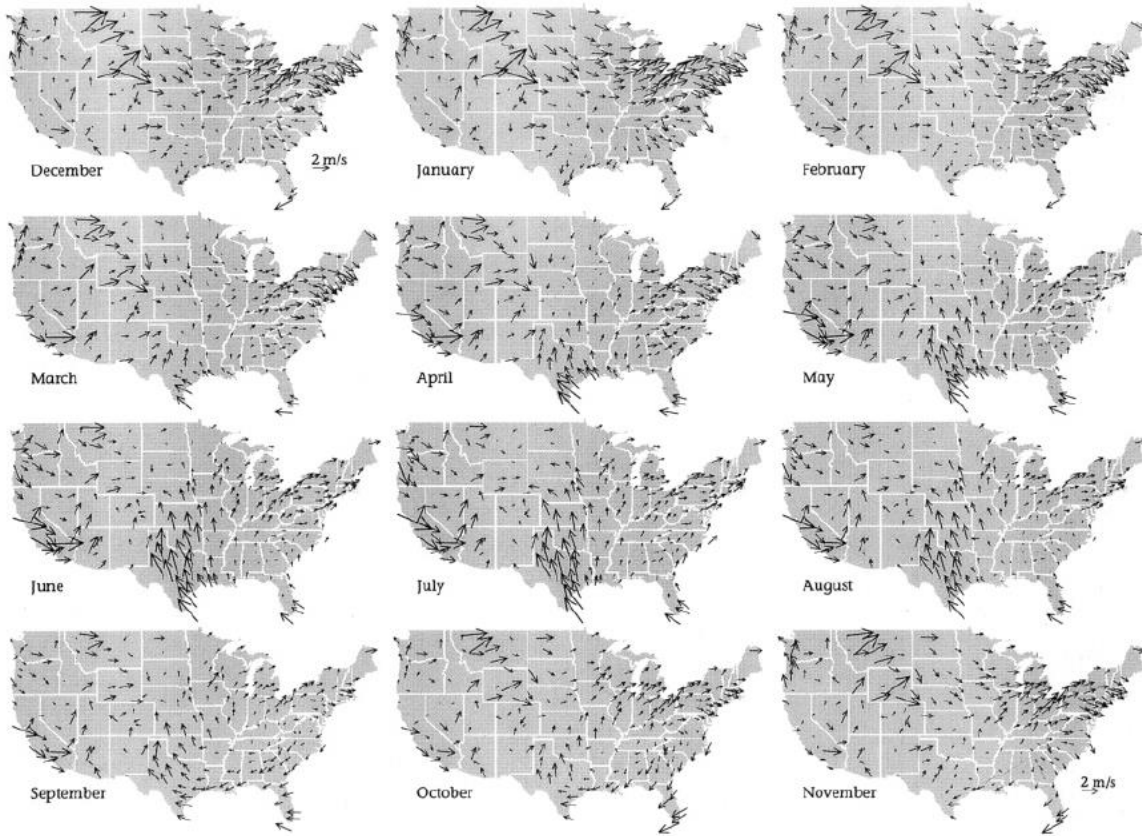


Figure 2-2. Monthly mean surface wind speed from 1961-1990 (NOAA, 2005)

Figure 2-2 displays the monthly mean surface wind speed data from 1961-1990 (NOAA, 2005). This reference is in agreement in regards to the aforementioned observations made by Stewart and Essenwanger (1978), and Takle, Brown, and Davis (1976) which asserts that speeds are largest in magnitude in the spring months (March, April, May) and smallest during the summer (June, July, August).

Table 2-1. Seasonal surface wind speed distributions (in m s^{-1}) over the years 1961-1990 (NREL, 2005).

City, State	Lat (°N)	Lon (°W)	Jan	Feb	Mar	Apr	May	Jun	Jul	Aug	Sep	Oct	Nov	Dec	Annual
Fargo, ND	46.90	96.80	5.5	5.4	5.6	5.8	5.4	4.9	4.5	4.6	4.9	5.3	5.2	5.1	5.2
Duluth, MN	46.83	92.18	5.1	4.8	5.3	5.2	4.9	4.5	4.0	4.0	4.4	4.6	4.9	4.8	4.7
Minneapolis, MN	44.88	93.22	4.7	4.6	5.1	5.4	4.8	4.6	4.2	4.1	4.3	4.6	4.7	4.6	4.6
Mason City, IA	43.15	93.33	5.9	5.5	5.9	5.9	5.4	4.9	4.0	3.8	4.3	4.9	5.4	5.6	5.1
Dodge City, KS	37.77	99.97	5.9	6.0	6.7	6.7	6.3	5.8	5.5	5.8	5.8	5.8	5.9	5.9	6.0
Indianapolis, IN	39.73	86.28	4.7	4.6	5.1	4.7	4.1	3.7	3.3	3.1	3.4	3.8	4.1	4.6	4.1
Houston, TX	29.98	95.37	4.0	4.2	4.4	4.4	3.0	3.6	3.2	3.0	3.3	3.4	3.8	3.9	3.8
Atlanta, GA	33.65	84.43	4.4	4.6	4.5	4.3	3.8	3.5	3.4	3.2	3.5	3.7	3.9	4.2	3.9

Focusing on the regions of interest for this research project, mean monthly surface wind speeds (in m s^{-1}) are outlined in Table 2-1 for the period of 1961-1990 (NREL, 2005). As seen in the table, all of the cities experienced a seasonal minimum (denoted by the yellow-highlighted cells) wind speed either for the month of July or August. On the other hand, the seasonal maximum was more variable in its occurrence among the cities: all of the cities with the exception of Atlanta and Mason City experienced a maximum mean monthly surface wind speed in either March or April; whereas, Atlanta's maximum fell in February, and Mason City observed a maximum in January, March, and April.

Other features which can be seen from Table 2-1 are that the Midwestern cities (i.e. Fargo, Duluth, Minneapolis, Mason City, Dodge City, and Indianapolis) overall had higher mean monthly wind speed values than the Southern

locations, such that, Houston and Atlanta's mean monthly wind speeds were generally slightly lower on average. These observations follow closely to those of Takle, Brown, and Davis (1976).

2.3.2 Weibull distribution

Typically, the probability density function (PDF) of surface winds is asymmetrical and are typically skewed to the right (Stewart and Essenwanger, 1978; Klink, 2002). It is because of this asymmetrical nature of wind's PDF, that this type of meteorological data fit the Weibull distribution (Takle et al., 1976; Takle and Brown, 1978; Steward and Essenwanger, 1978).

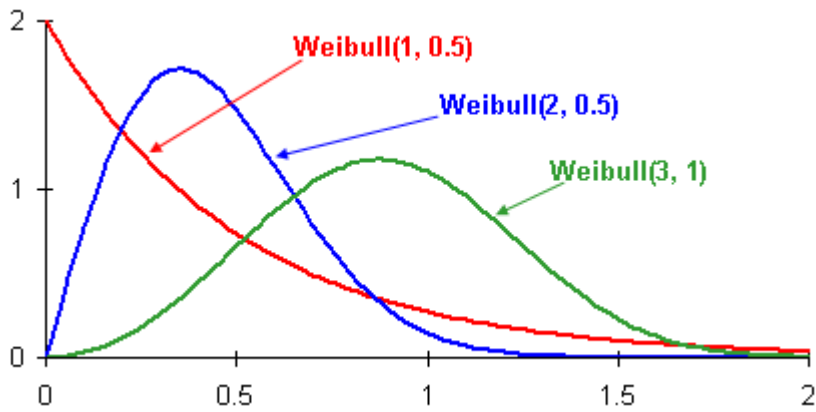


Figure 2-3. Skewed (Weibull) distribution.

Figure 2-3 illustrates the PDF for a skewed or Weibull distribution. As mentioned above, notice the skewness of each of the curves, which is a key characteristic of a Weibull distribution. Another predominant feature of this continuous distribution is that the smallest possible observable value is zero, and that the largest is unlimited, such that the density function ($p(x)$) approaches ∞ as x approaches zero. The Weibull distribution is an ideal function for winds because it accounts for the extreme nature of this phenomenon (i.e. for large values of x in Figure 2-3). Equation 2-1 is the probability density function for this distribution.

$$P_x^W(x) = \frac{k}{c} \left(\frac{x}{c}\right)^{k-1} e^{-\left(\frac{x}{c}\right)^k} \quad x \geq 0 \\ = 0, \quad \text{otherwise}$$
Eq. 2-1

The cumulative distribution function (Equation 2-2) is as follows:

$$F_x^W(x) = 1 - e^{-\left(\frac{x}{c}\right)^k}, \quad x \geq 0 \\ = 0, \quad \text{otherwise,}$$
Eq. 2-2

where $F_x^W(x)$ is the probability of the occurrence of the wind speed (x) or less, such that if $x = 0$, $F_x^W(0) = 0$, and $F_x^W(x) \rightarrow 1$ when x is large.

Parameters (c and k) in the distribution functions can be estimated via plotting on Weibull paper, or by calculating them using Equation 2-1 and 2-2. The Weibull scale parameter (c , m s^{-1}) is a measure of the distribution's central tendency (similar to the mean). The shape parameter (k , unitless) indicates the peakedness of the distribution, such that, for a given value of c , as k increases, the peak becomes more pronounced (Klink, 2002; Takle and Brown, 1978). These parameters are tools for analyzing trends within the shape of the distribution, for example, a decreasing k means that the density of the observations are spreading outwards towards the tails (which could allude to increasing occurrence of extremes, both low and high). Examples of varying shape and scale parameters (k and c , respectively) are illustrated in Figure 2-3.

There are limitations of the Weibull distribution, though, one of which being that low wind speeds are not properly accounted for. In an effort to minimize this limitation, Takle and Brown (1976, 1978) created a hybrid Weibull distribution that includes the addition of a discrete probability of the occurrence of calm wind speeds ($\sim 0 \text{ m s}^{-1}$) to the original pdf, which enhances its applicability to wind speed data sets. When this new term is not incorporated into Equation 2-1, it is assumed that $F_x^H(0) = 0$, which would mean that there is a zero probability chance that

calm wind speeds could occur in nature based on this equation. The discrete probability term (in Takle and Brown's (1978) hybrid equation) in the Weibull density function can be seen in Equation 2-3:

$$P_x^H(x) = \begin{cases} F\delta(x) + (1 - F_0)P_X^W(x), & \text{for all real } x, \\ 0, & \text{otherwise,} \end{cases} \quad (\text{Eq. 2-3})$$

where F_0 is the probability that a wind speed of zero m s⁻¹ will be observed, and $\delta(x)$ is a term called the delta function. The addition of Equation 2-2 into Equation 2-1 reduces, but does not completely eliminate the error introduced by not accurately representing low or calm wind speeds into the probability density distribution.

There is another variation of this “skewed” Weibull density function, where there are three-parameters instead of just two (c and k). The three-parameter Weibull density function includes a location parameter, Γ , along with the other two aforementioned parameters c and k. There have been mixed results in support of the three-parameter function as opposed to the two-parameter function. Some studies have shown that the two-parameter function is adequate for the task of fitting wind speed data to a continuous distribution (Takle and Brown, 1978), while others favored the three-parameter function (Stewart and Essenwanger, 1978).

There are other functions which have similar properties to those of the Weibull, and have been fit to wind speed data such as the log-normal, Rayleigh, and exponential distributions. However, research has repeatedly shown that the Weibull distribution is the best fit for this type of data, especially in the tails of the distribution (Takle and Brown, 1978; Tuller and Brett, 1984).

2.3.3 Surface wind speed trends

Through the usage of a least squares regression line as a tool to analyze a 30-year time series, Klink (1999) illustrated that mean monthly maximum surface winds are displaying a

general increasing within the United States, and on the other hand, the mean monthly minimum wind speeds are generally increasing.

As mentioned in the beginning of this section (Section 2.3), the study done by Klink (2002) used 22-35 years of observational 10-m wind speed data in the Upper Midwest. Her project focused on the 10th, 25th, 50th, 75th, and 90th percentiles of mean daily wind speeds in an effort to resolve temporal trends. It was found that these trends were found to be most pronounced at the 50th, 75th, and 90th percentiles. Klink found that each of the stations showed significant interannual variability within the mean annual wind speeds. Least squares regression analyses showed that five out of the seven locations across Minnesota and adjacent states indicated a general decreasing wind speed trend over the time period used.

Vautard et al. (2010) analyzed surface wind speeds throughout the continental mid-latitudes over the years of 1979 – 2008, and found general decreasing trends (-5 to -15 %) in surface wind observations across the mid-latitudes.

2.3.3.1 Low wind speed trends

The nature, frequency, and prediction of low wind speeds is another focal point in wind speed studies, as they are significant when considering air quality and agricultural applications. Abhishek et al. (2010) studied low winds throughout various Midwestern cities, in which they calculated the frequency of calm wind occurrence as well as the general frequency distribution trends of surface wind speeds. Their results indicated a substantial increase in the occurrence of calm winds being reported at each of the studied locations.

Abhishek et al. (2010) found that this increasing trend in the occurrence of calm winds to be more prominent during the ozone season (April through October). These findings are potentially problematic based on the fact that ozone air pollution is high when low wind speeds

are prevalent; therefore, air pollution incidences may increase in frequency and/or magnitude in those cities. Their results from a regression analysis and spatial correlation analysis support an argument that there is a large-scale atmospheric forcing which is influencing surface wind speed trends throughout the Midwest. The use of spatial correlations between various locations has been discouraged because of the inconsistencies between measuring sites (i.e. topography, anemometer height and exposure, etc.) (Klink, 2002). Wind speeds must be measured accurately and uniformly if interstation comparisons are to be made (Takle and Brown, 1976). Based on this information, skepticism arises on how to interpret the results of Abhishek et al.

2.3.3.2 High wind speed trends.

On the other end of the wind speed distribution, “extreme” high-end winds are also of great significance, as these winds have large economic, structural and agricultural impacts in our society. A changing climate can potentially lead to changes in the frequency, intensity, spatial extent, duration, and timing of extreme weather and climate events (IPCC, 2013a). One of the major concerns with regard to climate evolution is the possibility of increasing intensity or frequency of extreme events (Meehl et al. 2000), and specific to the current research, intense wind events (Della-Marta et al. 2009).

Vautard et al. (2010) found a pronounced decline (more than 5-15%) in extreme winds compared to mean winds in surface wind measurements throughout the continental mid-latitudes.

The IPCC (2013a&b) states in a recent report that there is a generally low confidence in future projections of changes in extreme high-end winds because of the relatively few studies done on projected extreme winds. This report also alluded to the fact that regional climate models (RCMs) exhibit shortcomings in their simulation of these events.

It is noteworthy to mention that individual extreme weather events alone do not indicate a changing climate, or “climate change,” but rather, it is the averaging of these events over a span of time which allows for one to draw conclusions of an evolving climate. Furthermore, extreme events cannot be directly attributed to human-induced climate change, as there is always the possibility the event might have occurred without anthropogenic forcing (IPCC, 2013a).

2.3.4 Interannual variability

Atmospheric and ocean drivers of interannual variability such as El Nino, La Nina, the North Atlantic Oscillation, Pacific Oscillation, Arctic Oscillation, etc., largely influence atmospheric circulations globally, and thus, affect wind speeds both aloft and at the surface. Pryor et al. (2010) found that there is no clear indication of a relationship which links trends in the annual mean wind speed with increasing interannual variability.

2.3.5 Implications of surface wind speed trends

As mentioned in the introductory chapter, surface winds play a large role in various agricultural processes such as evaporation (evapotranspiration), pollination, and the transport of plant diseases.

It is important to understand the difference between evaporative demand and evaporation. Pan evaporation is a measure of the evaporative demand of the atmosphere, but the actual evaporation also depends on the supply as well as the demand. Hence, a trend in observed pan evaporation does not necessarily mean an equal trend in actual evaporation. Pan evaporation is typically observed more readily than evaporation because of its more controlled nature, as it is not dependent on the supply of moisture (precipitation, groundwater, etc.).

Roderick, Farquhar, and Hobbins (2009 a & b) performed a study on global pan evaporation trends, and found that there is an overall declining trend over a 30 to 50 year period.

More specifically, they found most analyzed sites to range from -1 to -4 mm yr⁻¹, which is the equivalent to an overall reduction in annual pan evaporation of roughly 60 mm yr⁻¹ after a 30-year period. Converting this to units of energy, Roderick, Farquhar, and Hobbins (2009 a & b) showed that there has been an overall decrease of 4.8 W m⁻² over the past 30 years. These numbers are significant to understanding our evolving climate because evaporation is a large factor in the hydrologic cycle. Researchers are attributing the reduction in pan evaporation over the past several decades to be a result of decreased solar radiation (increased cloudiness) and/or decreasing trends in surface wind speeds (“stilling”) (Rong et al., 2012). On the other hand Zuo et al. (2006), resolves that there are too many meteorological factors that play a role in evaporative processes among various regions that it is too difficult to determine relationships between meteorological elements and pan evaporation.

2.4 Model simulated surface wind speeds

As previously mentioned, one of the major concerns with regard to climate evolution is focused on the possibility of increasing intensity or frequency of extreme events (Meehl et al. 2000). A changing climate can lead to unprecedented extreme weather and climate events (IPCC, 2013a). Researchers are developing and using climate models of different scales and structures in attempt to simulate future climate scenarios.

Pryor et al. (2010) analyzed 10-m wind speeds from a variety of observational data sets, reanalysis products, and regional climate model (RCM) simulations of the historical periods used (1982–2000 and 1961–1990). The data are used to quantify the magnitude and statistical significance of historical trends in wind speeds and the consistency (or inconsistency) of trends derived using different data. Also, they analyzed the data to address whether trends in the annual mean wind speed (wind climate) at specific grid cells in the various data sets show correlations

with observed changes in wind speed variance. Similarly to Klink (2002), the two observational data sets used in Pryor et al. (2010) revealed strong trends toward declining values of the 50th and 90th percentile and annual mean wind speeds, which is also the case for simulations conducted using Fifth-Generation Penn State/National Center for Atmospheric Research (NCAR) Mesoscale Model (MM5) with National Centers for Environmental Prediction – Department of Energy (NCEP-DOE) Global Reanalysis (NCEP-2) boundary conditions.

Contrary to the aforementioned results, opposing trends were found in the analysis of the North American Regional Reanalysis (NARR), other global reanalyses, and the Regional Spectral Model's (RSM) output, such that the 50th and 90th percentile and annual mean wind speeds showed a positive temporal trend. An interesting observation pointed out by Pryor et al. (2010) was that even though there is indeed an agreement among similar studies that the surface winds are in fact changing with time, and that the cause of the changes is still unknown, these studies are not in agreement in terms of the magnitude or even the sign of the temporal change.

McInnes et al. (2011) performed a study in which global surface wind speed data from Global Circulation Models (GCMs) were analyzed. Results of this study are shown in Figure 2-4.

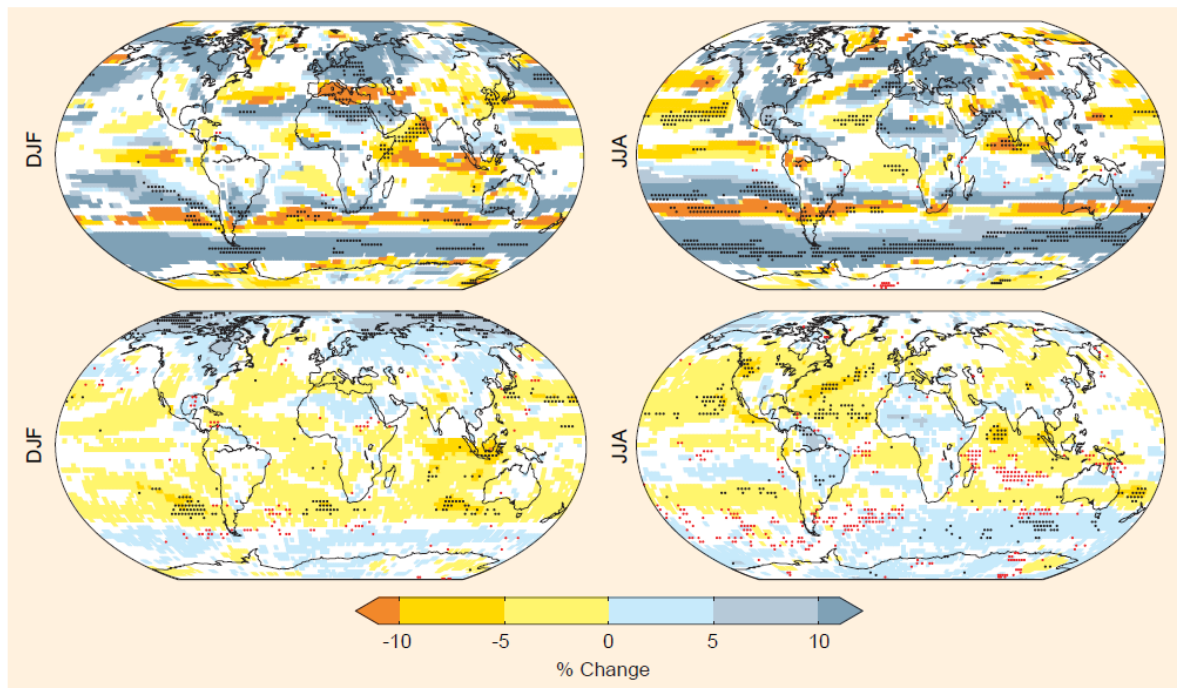


Figure 2-4. Model simulation of seasonal wind speed trends as a percent change over the periods of 2081-2100 relative to 1981-2000. Top two figures represent percent difference in daily mean values, while the bottom two figures illustrate the percent difference in the 99th percentile of wind speeds (McInnes et al., 2011).

Figure 2-4 displays model simulated percent change in global surface winds. The top two images in this figure depict percent difference of the mean of the daily averaged 10-m wind speeds during the period 2081-2100 relative to 1981-2000. The top left image displays these calculations for the months of December, January, and February (DJF), whereas, the top right image shows the months of June, July, and August (JJA). As can be seen from these images, there is a fairly inconclusive results for the Midwest during the months of DJF, such that the GCM did not project a significant percent change in the mean of the daily averaged surface wind speeds. JJA shows a strong negative signal (10+% decrease) in the Midwestern region.

The bottom two images in Figure 2-4 show the percent difference (2081-2100 relative to 1981-2000) of the 99th percentile of the daily averaged 10-m wind speed values. The (bottom) left and right images are again displayed by months DJF and JJA. DJF shows a weak negative trend (0-5% decrease) throughout much of the Midwest for the mean 99th percentile wind

speeds. JJA shows a positive signal (0-10% increase) in the northern portion of the Midwest, while there is a negative trend (0-5% decrease) in the southern part of the region.

2.5 Possible explanations on surface wind speed trends

Based on the fact that winds reflect atmospheric conditions, ranging from small-scale (~10 km) (synoptic low pressure systems, thunderstorms, orographic factors, etc.) to large-scale features (~ 10^3 km) (Rossby Waves), as well as the complex nature of wind data (i.e. variation in anemometer height, location, as well as maintenance/upkeep/calibration) it is challenging to draw precise conclusions regarding what each of these aforementioned studies' results mean. It is no possible to attribute the causes of wind speed variation to any one specific factor due to its complex nature. Possible theories of causes of the observed trends surface wind speeds include climate change, changes in interannual variability, urbanization effects, and instrumentation and observation biases. Some researchers believe that this planet's evolving climate system is affecting surface wind speeds, such that winds are being affected by changes in atmospheric circulations (i.e. mid-latitude cyclone intensity, frequency, and location variations) and temperatures at the surface (Klink, 2002; Pryor et al., 2010). Vautard et al. (2010) attributes the stilling of surface wind speeds winds over most of the continental northern mid-latitudes to changes in atmospheric circulations (10-50%), and an increase in surface roughness due to vegetation increases (25-60%).

Wind speed is directly related to the surface pressure gradient, which in turn is a function of the temperature gradient. Wind is a mechanical motion which flows from an area of high pressure to lower pressure, and since cooler air is associated with higher pressure (cool air sinks and results in higher surface pressure) and warmer air is linked to lower pressure (warm air

rises), if there are changes in air temperature throughout the hemispheres, wind speed and direction will also be affected (Klink, 1999).

As mentioned previously in Section 2.3.4, Pryor et al. (2010) concluded that there is no clear signal of a relationship linking trends in the annual mean wind speed with interannual variability.

Another feature investigated is the effect of urbanization and land use change on wind speeds near the surface. As cities grow, their maximum wind speeds are reduced because of increased friction (buildings replacing open fields) which is related to a parameter used in atmospheric models known as the roughness effect or coefficient. Moreover, the minimum speeds are accelerated as a result of the enhanced heat island effect with urbanization (Klink, 1999).

Lastly, researchers have argued that temporal trends in wind speed values might be a result of the deterioration in anemometer performance over time. DeGaetano (1998) discovered that reductions in the frequency of 3 knot (1.5 m s^{-1}) wind reports and increases in the frequency of calm reports regularly occurred simultaneously. He speculated that this pattern was due to the decline of the anemometer performance due to exposure to the elements over time. Furthermore, observational trends may also be attributed to the introduction of the ASOS stations across the nation in the mid to late 1990's. The frequencies with which extremely high and low winds were reported significantly altered with the implementation of ASOS instrumentation in the late 1990's (ADEM, 2007). Ultimately, it is crucial to understand that given the natural temporal and spatial variability found in wind speed observations, it seems unlikely that errors (calibration, human error, etc.) can be identified and filtered out with a reasonable degree of certainty (Degaetano, 1998).

CHAPTER 3

DATA AND METHODOLOGY

3.1 ASOS

This project analyzes observational Automated Surface Observing System (ASOS) data as well as North American Regional Climate Change Program (NARCCAP) model simulated output. The focus of this research will be weighted heavily on model representation of surface winds, and the observational data will act as a necessary foundation for comparing the simulated results against.

ASOS is a collaborative program among the National Weather Service (NWS), the Federal Aviation Administration (FAA), and the Department of Defense (DOD) in which are networks of instruments that measure and record numerous meteorological features automatically and returns them to the users on a real-time basis. The ASOS systems are commonly viewed as the nation's primary surface weather observing network. These observing systems are considered "primary" mainly because of their dense network throughout the United States as well as the uniformity and consistency of the systems themselves. The measurements are designed to support weather forecast activities (including ingesting the observational data into meteorological models that are used for forecasting purposes), aviation operations, as well as aiding in making data available for the meteorological, hydrological, and climatological research communities' needs. These systems collect basic, yet significant meteorological data such as sky condition, visibility, basic present weather information (type and intensity for rain, snow, and freezing rain), obstructions to vision such as fog or haze, pressure (sea-level pressure and altimeter setting), ambient temperature, dew point temperature, wind (direction, speed and character), precipitation accumulation, as well as select significant remarks.

Of all of these weather parameters, wind speed will be the primary focus within this study. The modern ASOS wind sensor contains a “light chopper,” electro-optical method to determine wind speed. From this, it uses electro-magnetic signals generated by the rotating cup and wind vane which are directly converted into reportable values by ASOS. The sensor’s starting threshold for response to wind direction and speed is 2 knots. More specifically, if the computed 2-minute average wind speed is 2 knots or less, the 2-minute average wind direction and speed is reported as “calm” (00000KT). ASOS continuously and objectively measures wind direction and speed far more frequently, consistently, and accurately than a human observer could. This standard anemometer ranges from 0 to 125 knots, has an accuracy of \pm 2 knots, and a resolution of 1 knot (ASOS, 1998). ASOS processes data identically, which provides site-to-site consistency unknown in past records. Five-second wind direction and wind speed averages are computed from the 1-second measurements. These 5-second averages are rounded to the nearest degree and nearest knot and are retained for 2 minutes. These five-second averages are the fundamental units used to compute reportable wind values and are, in effect, the ASOS equivalent to the manual “instantaneous” wind observation.

These data, however, were not always computerized, as prior to the mid 1990’s, meteorological data was collected through hourly human observations.

3.1.1 Pre-ASOS compared to current ASOS

The first ASOS was installed in August 1991 in Topeka, Kansas, and marked a new beginning of automation and human-less weather observations. Furthermore, in 1996, NWS adopted the international METAR code for surface observations (significant changes in reporting variable winds and clouds). ASOS were implemented across the United States in an attempt to

minimize labor and human errors which were eliminated once these measurements were automated. On the contrary, though, the introduction of ASOS also ushered in disadvantages, which will be explained in section 3.1.2.

The frequencies at which “extremely” high and low winds were reported significantly changed with the introduction of ASOS instrumentation because of the introduced ability to record frequent observations. Comparative research studies have shown signs that ASOS-related changes in anemometer instruments and heights may be a possible explanation for increased numbers of “calms” reported (ADEM, 2007). Interestingly enough, contradictory information tells us that the use of average hourly winds may dramatically reduce the number of “calms” reports and eliminate the number of hours when winds are reported less than 6 kts with a variable direction (ADEM, 2007) DeGaetano (1998) discovered that reductions in the frequency of 3-kt (1.5 m s^{-1}) wind reports and increases in the frequency of calm reports regularly occurred simultaneously; consequently, he speculated that this pattern was due to the deterioration in anemometer performance over time. McKee et al. (2000) analyzed the differences in observed wind speed values Pre-ASOS and ASOS implementation at 12 locations in the United States. The sites displayed an average difference of -0.2 m s^{-1} (ASOS – Pre-ASOS) in the mean daily wind speeds; however, these sites displayed a range in values from -0.65 m s^{-1} to -0.15 m s^{-1} , all of which showed a decreasing trend.

In the past, observers monitored an analog or digital wind dial over a short period to determine the average wind direction and speed for the observation. Most sites also had a wind recorder device to provide a continuous documented record of measured wind direction and speed. The observer often used this device to determine the maximum instantaneous wind speed over the 10-minute period before completing the observation. The observer used visual/mental

averaging and ultimate human judgment to create an observation of wind. This method was not always consistent from site to site or from one observer to another (ASOS, 1998). The human mode of observation appears subjective and inconsistent, especially when comparing to the modern method of automated measurements through ASOS.

Aside from the form of measurement, another parameter that has evolved through time has been the height placement of the anemometer. Prior to ASOS, airport wind sensors were generally exposed 20 feet above ground level. Now, current federal standards for siting meteorological equipment specify a height of 10 m (32.8 feet) (ASOS, 1998). With that, it is trivial to conclude that it is tricky to accurately analyze wind speed measurements both before and after the switch from human to automated observations in one grouping based on the inconsistencies in the anemometer height and means of taking observations. A better approach might be to separate the data into two time periods of similar properties: pre-ASOS and ASOS.

3.1.2 Limitations associated with ASOS wind measurements

Though there were numerous advantages to upgrading to automated measuring systems, primarily as it eliminated subjectivity due to human perception and judgment, it is necessary to consider the downfalls that are present while dealing with wind data and proceed with caution when analyzing this information. A few limitations associated with ASOS wind measurements include errors resulting from the exposure of the anemometer, calibration and functioning of the anemometer, as well as proper data collection (Arrakis, 2004; Klink, 1999).

Small scale factors that may influence ASOS data may include the acceleration or deceleration of the local flow if the anemometer is exposed to small hills or elevation changes in the vicinity, turbulence of the air from small buildings, trees, or hills, and finally, the slowing of

the wind near the ground due to surface roughness (frictional) features. The effects surface roughness has on wind speed and direction is significant on the microscale level ($r \sim 1$ km) of meteorology. Surface roughness can be denoted by a roughness length, or Z_0 . A high roughness tends to decrease wind speed. Typical values of Z_0 are expressed in Table 3-1 (Arrakis, 2004).

Table 3-2. Typical Z_0 values (given in m) (Arrakis, 2004).

Surface	Example Surfaces	Z_0 Values
Flat	Beach, ice, snow, ocean	$Z_0 = 0.005$
Open	Low grass, airports, empty crop	$Z_0 = 0.03$
	High grass, low crops	$Z_0 = 0.10$
Rough	Tall row crops, low woods	$Z_0 = 0.25$
Very Rough	Forests, orchards	$Z_0 = 0.50$
Closed	Villages, suburbs	$Z_0 = 1.0$
Towns	Town centers, open spaces in forests	$Z_0 > 2$

Wind shear, or the variation of wind speed with height, can be estimated using Equation 3-1.

Where, $V(z)$ and $V(z_r)$ are the target and reference height wind speeds, respectively; z and z_r are the target and reference heights, and z_0 is the roughness length (according to Table 3-1). Wind

$$\frac{V(z)}{V(z_r)} = \frac{\ln(z/z_0)}{\ln(z_r/z_0)} \quad Eqn. 3-1$$

shear is a function of both height and Z_0 , such that wind shear is directly proportional to height and inversely proportional to values of Z_0 (Equation 3-1). Meteorological models commonly use these variables while calculating boundary layer parameters, such as wind.

Another factor to pay attention to while analyzing the potential features that have the ability to influence wind measurements is the air turbulence that is generated from trees and small buildings. Wind flowing around buildings or over rough surfaces such as trees causes rapid changes in speed and sometimes direction called turbulence. Around trees, turbulence is

exhibited in the leeward direction as much as 10-15 times the height of the trees and upwind nearly 5 times the height of the obstructing object (Arrakis, 2004).

Anemometer functionality and calibration are also important to consider while analyzing potential limitations of ASOS wind data. Unlike sonic anemometers, which can measure wind speeds with pristine accuracy to as low as less than ± 0.5 kts and with a resolution of roughly 0.2 kts, standard ASOS equipment measures accurately to ± 2 kts and has a resolution of 1 kt. Thus, when wind speeds are significantly low, perhaps near or below the 2 kts threshold, the instrument cannot accurately discern the wind speed, instead, it just lumps the observation into the category of “calm.” On the other end, looking at high wind speeds are shown to be subject to error called u-error or “overspeeding” (Kaganov, 1976). This phenomenon is produced by the non-linearity of rotary cup anemometers, such that the instrument responds more quickly to an increase in speed than to a decrease (Mage, 1979).

ASOS equipment, like any other instrument, requires routine maintenance and calibration to sustain excellent working condition. Often times, while routine maintenance takes place, the hourly Meteorological Aerodrome Report (METAR) will send out a missing report, as there is no data to be sent. Furthermore, duration and frequency of data gaps at ASOS stations are more recurrent than at observer-based stations (ADEM, 2007).

3.1.3 Missing data and quality control

Several studies have noted the sharp increase in quantity of missing data when the NWS changed over from human observations to ASOS (EPA, 1997; ADEM, 2007). For the purposes of this study, if an ASOS location possessed 5% or more missing data, the station was omitted from this study. Furthermore, locations were screened based on the length of wind speed records

available. For instance, Ames, IA (KAMW) has less than 5% missing data, but its period of record began in September, 1996, whereas, nearby stations (KMCW, KHSI, KJMS, etc.) provide data prior to the 1970's; thus, KAMW was omitted from this study. Table 3-2 in Section 3.3 displays the quantities of missing data within the ASOS dataset at each of the seven cities.

3.2 Defining “extreme” high and low wind speeds

While defining what qualifies as an extreme value or event, it is important to understand that quantitatively, the extremity of a weather or climate event of a given magnitude naturally varies substantially based on the geographic location which is being considered (IPCC, 2013a). Keeping in mind the impacts extreme wind events have on our modern society (listed throughout Chapter 1), it is also necessary to note that while an event may not be considered extreme in a statistical sense, it may still lead to extreme conditions or impacts, either by crossing a critical threshold in a social, ecological, or physical system, or by occurring simultaneously with other events. It is because of this, and the fact that the “threshold” as to when an event is considered “extreme” or not, is highly variable based on geography, that we define this threshold with caution. The issue with geography and the variation in what is “extreme” for individual regions of the United States (and the globe) can be neglected once we define our “extremes” through using percentiles, not actual magnitudes of wind speeds. Various studies define these extreme thresholds based on the use “extreme indices,” which can either be based on the likelihood of occurrence of given quantities or surpassing a given threshold quantity such as being less than the 5th or 10th percentile or greater than the 90th, 95th, or 99th percentiles (IPCC, 2013a).

There is no generally accepted definition of what constitutes a low wind speed. Based solely on ASOS algorithms, “calm” winds are defined as winds less than or equal to 2 kts (1.03

m s^{-1}). Smith (1993) defines low wind speeds as being when the mean wind speed is comparable or less than the root-mean-square turbulent horizontal velocity. Smith stated that low wind speeds could be defined as being when the influence of the geostrophic wind becomes small/negligible (i.e. small pressure gradient) when compared to topographic influences. Smith also defined low wind speeds in a relative context, such that wind speeds will be significantly lower when the atmosphere is dominated by stable conditions, whereas, winds will be higher under convective conditions. Agreeing with Smith (1993), Deaves and Lines (1998) suggested that it is not appropriate to define “low wind speeds” by a single threshold wind speed value because of varying atmospheric stability conditions and geographic characteristics. Interestingly enough, Deaves and Lines (1998) ultimately used a single threshold value of less than 5 kts (2.57 m s^{-1}) as a “low wind speed” because this threshold corresponds to the magnitude wind speed where standard meteorological data may be “misleading” and the applicability of dispersion models may need to be considered more carefully. If a magnitude and not a percentile is used to assign a threshold, one can argue from the previous statement that the “low wind speed” definition should be decreased from less than 5 kts to less than 2 kts (1.03 m s^{-1}), as that is the minimum wind speed a standard ASOS anemometer can reasonably resolve without introducing large error (ASOS, 1998). For this research project, “extreme low wind speeds” will be statistically defined to be equal or less than the 10th percentile value.

Similarly to low winds, a threshold for defining an “extreme” high-end wind speed is best defined as a percentile value rather than an absolute magnitude. A percentile threshold will effectively eliminate the variations in wind speed distributions which can be found across different geographical regions. For this project, we will define an “extreme” high wind to be at or

above the 90th percentile, such that, its occurrence is statistically rare in nature, and typically has high impacts as a result.

For this study, we will set our threshold for a wind to be considered “extremely” low at the 10th percentile and “extremely” high at the 90th percentile.

3.3 Cities of Interest

This study takes an in-depth look at six specific cities across the United States. Four of the cities are dependent on wind for agricultural health as well as for wind energy production. The other two cities are largely populated and industrial; therefore, they depend on wind to disperse air pollution away from the urban areas. The Midwestern, agricultural cities used are: Ames IA, Lafayette IN, Hastings NE, Liberal KS, Jamestown ND, and the more urbanized locations are Houston TX, and Atlanta GA. Detailed information regarding these ASOS locations are presented in Table 3-2. The Midwestern cities were selected in such a manner so that the Central United States is represented equally spatially in the north-south and east-west directions.

Table 3-2. Detailed information for each of the cities used in this study.

City, State	ASOS ID	Lat (°N)	Lon (°W)	Elevation (ft)
Mason City, IA	KMCW	43.16	93.33	1194
Lafayette IN	KLAF	40.43	86.93	623
Hastings NE	KHSI	40.61	98.43	1955
Liberal KS	KLBL	37.05	100.97	2956
Jamestown ND	KJMS	46.93	98.68	1492
Houston TX	KHOU	29.65	95.28	85
Atlanta GA	KFTY	33.78	84.52	863

A note regarding these ASOS locations is that each of these locations is positioned at airports, which is valuable information because topography in vicinities of airports is generally flat and surrounded by little vegetation. Terrain that is primarily open creates only minimal

orographic and surface influence on wind characteristics near the ground (Arrakis, 2004).

Satellite images of each of the seven cities are given in Appendix A. As can be observed in the aerial images in Appendix A, there are minimal buildings or clusters of trees within the vicinity ($\frac{1}{2}$ - 1 km) of the airport runways and ASOS instrumentation; thus, the generalization about airports not usually having large obscuring structures or clusters of trees in the surrounding area is verified in these instances. Looking closer at KFTY and KHOU (Figure 3-2a and 3-2b), however, there are trees and/or small buildings in the close vicinity ($\frac{1}{2}$ km) of the ASOS equipment, which may ultimately influence the wind measurements slightly from resulting

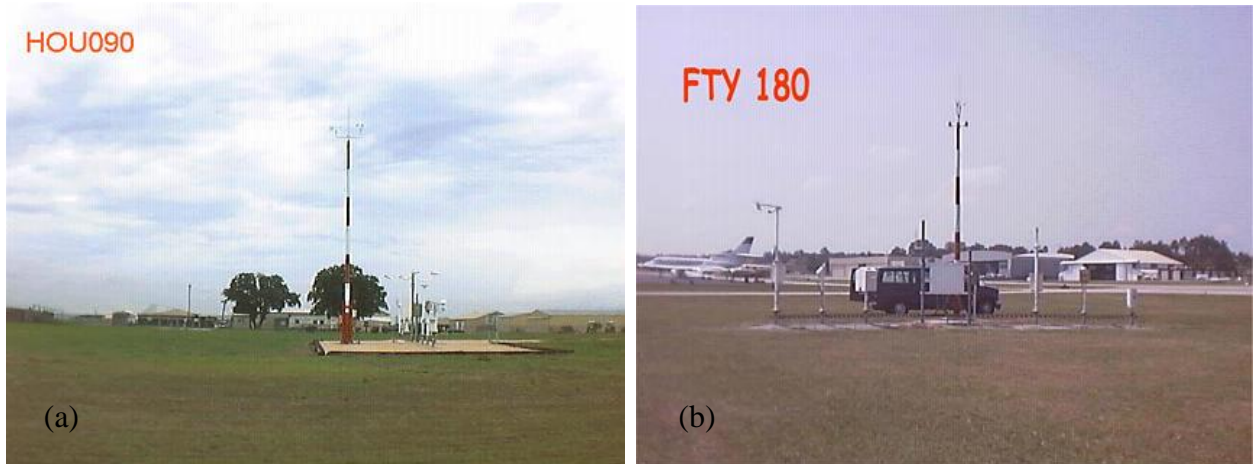


Figure 3-1 a & b. Illustration of flat terrain typically observed in the vicinities of ASOS instrumentation. (a) KHO090 ASOS from a northerly perspective, (b) KFTY 180 ASOS from a southerly perspective.

small-scale wind shear or turbulence, depending on the direction of the prevailing wind.

As mentioned in Section 3.1, ASOS data is occasionally be discontinuous due to exposure or maintenance circumstances, and therefore, have periods of time with missing data. Table 3-3 displays this quantity of missing data found at each of the seven cities. Table 3-3 is broken into two separate tables, where the Pre-ASOS and ASOS wind speed records are isolated.

All of the cities, with the exception of KLBL display an increase in percent missing data from Pre-ASOS to ASOS.

Table 3-3. Missing data for each of the selected cities in this study, in which the top table displays the quantity of missing data found in the Pre-ASOS dataset, while the bottom table shows the missing data Post-ASOS installation.

Site ID	Period of Interest: Pre-ASOS Implementation	Number of Observations	Missing Observations	% Missing
KMCW	Jan 01, 1973 - Aug 17, 2000	239,615	226	0.0943
KLAF	Jan 01, 1973 - Jan 15, 1998	210,263	695	0.331
KHSI	Jan 01, 1973 - May 30, 1995	87,164	636	0.730
KLBL	Jan 01, 1973 - Jan 01, 1998	132,664	3,393	2.558
KJMS	Jan 01, 1973 - Oct 05, 2000	218,667	675	0.309
KHOU	Jan 01, 1973 - Aug 12, 1998	217,786	548	0.252
KFTY	Jan 01, 1973 - Oct 28, 1998	187,960	763	0.410

Site ID	Period of Interest: Post-ASOS Implementation	Number of Observations	Missing Observations	% Missing
KMCW	Aug 17, 2000 - Jan 01, 2013	116,120	737	0.635
KLAF	Jan 15, 1998 - Jan 01, 2013	148,436	5,361	3.612
KHSI	May 30, 1995 - Jan 01, 2013	135,945	2,214	1.629
KLBL	Jan 01, 1998 - Jan 01, 2013	367,570	4,747	1.291
KJMS	Oct 05, 2000 - Jan 01, 2013	151,942	2,158	1.420
KHOU	Aug 12, 1998 - Jan 01, 2013	127,117	851	0.669
KFTY	Oct 28, 1998 - Jan 01, 2013	142,626	2,565	1.798

It is important to note is that KLBL did not have an official implementation date of when it became automated because unlike the other sites, this location was commissioned by the FAA. As a result of this missing information, a general date of automation was selected for this location (Jan 01, 1998), and thus, because of this estimation, some error in the analysis might be introduced, so conclusions for KLBL will be made with caution. The dates of ASOS implementation are crucial because this information allows for an analysis of strictly Pre-ASOS compared to ASOS observations. Details of this comparison will be described further in Chapter 4.

3.4 NARCCAP

The NARCCAP dataset contains high-resolution climate change scenario simulation output from various Regional Climate Models (RCMs) which are coupled within different Atmosphere-Ocean General Circulation Models (AOGCMs) for 30-year current and future periods. The AOGCMs are also known in this study as Global Circulation Models (GCMs) for shorthand, and act as drivers of the initial boundary conditions used in the RCMs.

The RCMs are run at 50-km (0.5° latitude/longitude) spatial resolution across a domain spanning the contiguous United States and most of Canada; results are recorded at 3-hourly instantaneous intervals. These simulation results are ideal for the analysis of model performance and uncertainty in regional-scale projections of future climate regimes throughout North America (Mearns et al., 2012).

Specifically, the wind data within the NARCCAP output are recorded at a 3-hourly instantaneous interval based on the UTC time scale, placing the data at 00, 03, 06, 09, 12, 15, 18, and 21 UTC.

The 10-m zonal (u) and meridional (v) winds were obtained from the NARCCAP archived data set, from that, we calculated the total wind speed using the following equation:

$$U = \sqrt{u^2 + v^2} \quad Eqn. 3-2$$

U (Equation 3-2) is then assumed to be the surface wind speed throughout the entire study. Since 10-m is the standard observing level, the NARCCAP wind data in the archive have been interpolated to this level from the lowest model grid point.

3.5 RCMs

Table 3-4. Models used in study.

	NCEP	GFDL	CGCM3	HADCM3	CCSM
CRCM	X		X		X
ECPC					
HRM3					
MM5I	X				X
RCM3					
WRFG	X		X		X
Timeslice					

The NARCCAP data set is comprised of six Regional Climate Models (RCMs), three of which will be used in this study (Table 3-4): 5th Generation Mesoscale Model (MM5I), Weather Research and Forecasting Model (WRFG), and the Canadian Regional Climate Model (CRCM). These RCMs are nested within the GCMs for the contemporary (1968-2000) and future (2038-2070) scenarios to provide finer-resolution (50 x 50 km). As a baseline for evaluating the performance of these models, the RCMs are driven with NCEP/DOE AMIP-II Reanalysis data spanning 1979-2004 (Mearns et al., 2009). Further details regarding these models can be found on the NARCCAP website: <http://www.narccap.ucar.edu/>

3.6 GCMs

Two of the four AOGCMs were selected from the NARCCAP data set to be used as the driver for the RCMs (Table 3-4): Community Climate System Model (CCSM) and the Third Generation Coupled Global Climate Model (CGCM3). The GCMs provide the RCMs with initial conditions such as soil moisture, sea surface temperatures, and sea ice (updated every six hours) as well as lateral meteorological conditions such as temperature, pressure, and humidity. Last, the global models provide responses to forcing at large scales ($\sim 10^2$ km).

GCMs have been forced with the SRES A2 emissions scenario for the 21st century. The A2 scenario was selected for the NARCCAP because it is at the higher, more extreme end of the SRES emissions scenarios which allows for a dramatic illustration of possible impacts of climate change (Mearns, et al., 2009). Further details regarding these models are available on the NARCCAP website: <http://www.narccap.ucar.edu/>

3.7 Inclusion of model spin-up data

For this study, we elected to include the archived dataset in its entirety, including during the model “spin-up” period (initial three years). Through statistical significance testing, the null hypothesis was supported; such that, through using an independent, two-tailed T-Test with a significance level of 0.01, it was definitively shown that data within the typical model “spin-up” period is not different from the rest of the data.

3.8 Schematics of study

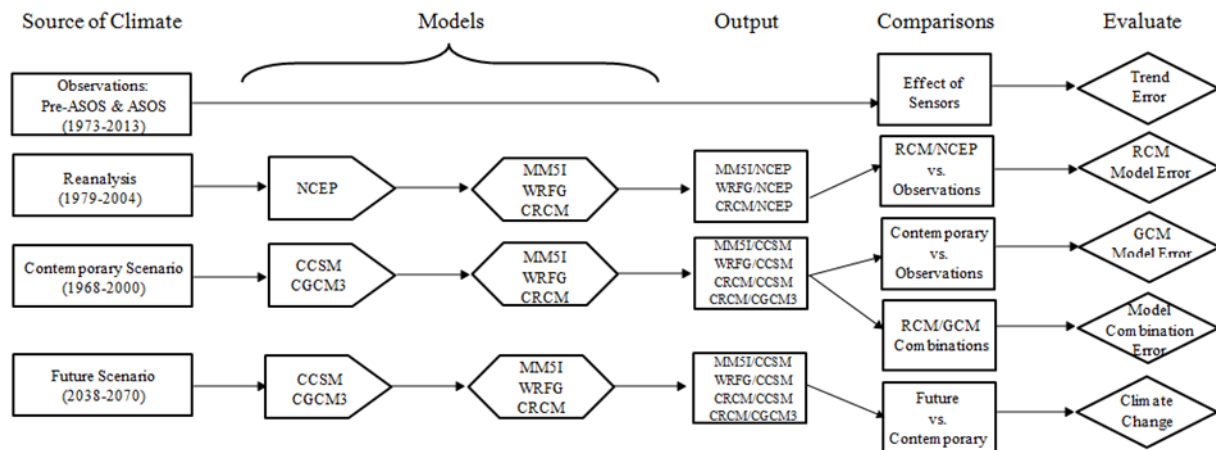


Figure 3-2 is a schematic diagram of the various sources of climate, output, comparisons, and the evaluations made from the data used in this study.

CHAPTER 4

SURFACE WINDS REPRESENTED BY ASOS OBSERVATIONS

4.1 Introduction

As previously mentioned, automated observations were not fully in place throughout the United States until the mid-1990's, and that prior to that time, wind speeds measurements were taken by human observers at each of the designated stations. The issue is the resulting inconsistencies between Pre-ASOS and ASOS data, such that Pre-ASOS records may be arguably subjective. Another inconsistency between the two data sets is the observed increase in missing data with ASOS data due to maintenance issues. This chapter does not add to analysis of specific quantitative differences, but rather, acknowledges that there is indeed, a change in reported wind speeds once measurements became automated.

Evidence of human subjectivity is revealed when the Pre-ASOS data are collected and plotted. For example, there is a large number of reports of wind speeds of 5, 8, 10, 12, 16, 18 and 20 kts and relatively low number of occurrences of 6, 9, 11, 13, 16 and 19 kts, suggesting a tendency to report wind speeds as even integers or multiples of 5 (Takle and Brown, 1976). This trend can be seen in Figure 4-1. This observation is an example of human error believed to be due to rounding prior to the automation of wind speed measurements. Data in Figure 4-1 is formatted in kts instead of m s^{-1} , unlike other figures in this study. This is done because wind speed observations are typically measured in kts, thus, this human subjectivity feature is easily deduced using the original units. All other plots will be converted into m s^{-1} so that the observational data conforms to the model data (m s^{-1}). The last bin, labeled "Other" encompasses all data > 30 kts. Of course certain bins (such as 1 kt) are empty when wind speeds are converted

from integer values of m s^{-1} to kts due to rounding errors. The shape of the two datasets are largely different; the ASOS distribution is smooth and continuous with the exception of observations < 3 kts

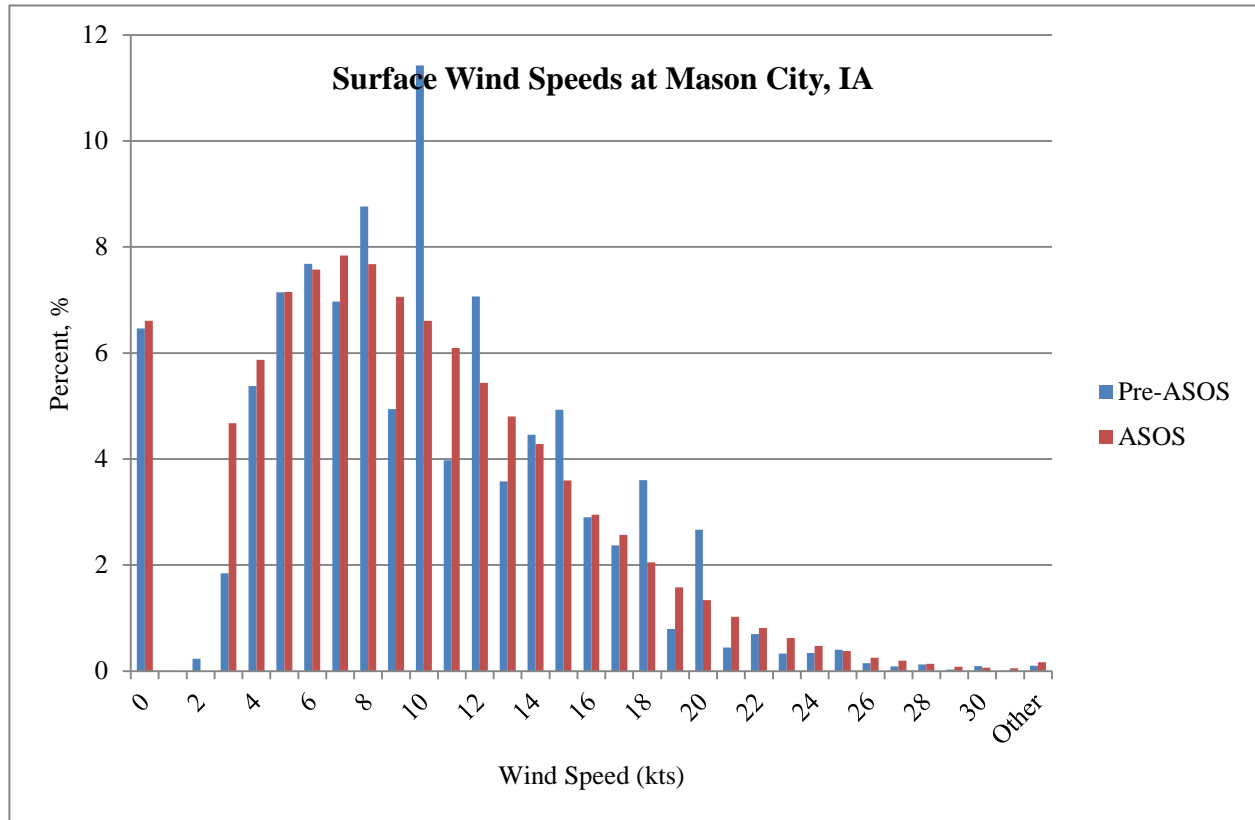


Figure 4-1. Pre-ASOS (Jan. 01, 1971 – Aug. 17, 2000) compared to ASOS (Aug. 17, 2000 - Dec. 31, 2012) surface wind speeds at Mason City, IA.

(1.54 m s^{-1}), which is the known threshold for the cup anemometers used at ASOS locations. Wind speeds $<$ than 3 kts are not accurately read by the instrument, thus, are recorded as 0 kts, which is a potentially misleading feature of automated measurements (ASOS, 1998). Unlike ASOS data, Pre-ASOS possesses a more erratic-looking curve, such that there is a higher percent of observations at even integers (2, 4, 6, etc.) than odd (1, 3, etc.). It can also be noticed that there are relatively more observations at intervals of 5 (5, 10, 15, etc.), all of which agrees with

the findings of Takle and Brown (1976). Such trends can be seen at all seven locations used in this study.

Calculated percentile (10^{th} , 90^{th} , 95^{th} , 99^{th} , and 99.9^{th}) (in m s^{-1}) and corresponding linear regression values (in $\text{m s}^{-1} \text{ yr}^{-1}$) are provided in Table 4-1. The data in this table are representative of the entire period of study (1973-2013) encompassing observations both prior to and after the automation of measurements. General trends from this table are that KFTY consistently has the lowest magnitude of observed wind speeds across all percentile values. On the other hand, KHSI and KLBL generally possess the highest wind speeds across the majority of the percentile thresholds.

Observational Data (Pre-ASOS and ASOS)
Percentiles (1973-2013)

	10^{th}	90^{th}	95^{th}	99^{th}	99.9^{th}	Mean
KMCW	1.94 / -0.01	8.84 / -0.01	10.09 / 0.01	12.51 / 0.04	15.65 / 0.06	5.04 / -0.01
KLAF	0.85 / -0.04	7.00 / -0.01	7.79 / 0.01	9.91 / 0.02	12.94 / 0.03	3.93 / 0.41
KHSI	1.72 / 0.03	8.83 / -0.08	10.37 / -0.08	13.43 / -0.11	17.19 / -0.15	5.14 / 0.64
KLBL	1.33 / 0.09	9.66 / 0.01	11.02 / 0.03	14.05 / 0.03	17.85 / 0.01	5.18 / -0.15
KJMS	2.19 / -0.02	9.03 / 0.01	8.59 / -0.20	12.80 / 0.05	15.94 / 0.03	5.23 / 0.01
KHOU	0.57 / -0.03	6.79 / -0.03	7.59 / -0.03	9.47 / -0.02	12.27 / -0.00	3.68 / 0.12
KFTY	0.00 / 0.00	5.11 / -0.02	6.02 / -0.01	7.73 / 0.00	10.91 / 0.04	2.36 / -0.07

Table 4-1. ASOS percentile (m s^{-1}) and trends ($\text{m s}^{-1} \text{ yr}^{-1}$) over the entire period of study (1973-2013).

4.2 Pre-ASOS vs ASOS Observations

4.2.1 Seasonal distributions

As described in Section 2.3.1, Takle, Brown, and Davis (1976) and Klink (2002) found that surface winds are climatologically at their minimum in the summer months, typically in July or August.

Table 4-2. Mean monthly wind speeds (m s^{-1}) at each location. This set of tables isolates Pre-ASOS and ASOS data. The bottom table displays the percent difference between the two datasets.

Pre-ASOS	Jan	Feb	Mar	Apr	May	Jun	Jul	Aug	Sep	Oct	Nov	Dec	Annual
KMCW	5.73	5.46	5.85	5.93	5.23	4.83	4.02	3.72	4.20	4.93	5.43	5.45	5.07
KLAF	4.80	4.55	4.95	4.76	4.09	3.66	3.30	3.08	3.38	3.90	4.45	4.55	4.12
KHSI	5.37	5.54	6.21	6.55	5.78	5.26	4.67	4.57	5.11	5.33	5.62	5.52	5.46
KLBL	4.63	4.97	5.84	6.19	5.60	5.29	5.17	4.59	5.09	5.16	4.98	4.81	5.19
KJMS	5.56	5.53	5.73	5.75	5.69	5.10	4.35	4.54	4.99	5.42	5.38	5.44	5.29
KHOU	4.42	4.52	4.60	4.37	3.87	3.42	2.90	2.68	3.13	3.55	4.11	4.21	3.81
KFTY	2.86	3.10	3.16	2.93	2.40	2.16	2.21	2.01	2.16	2.18	2.45	2.73	2.53

ASOS	Jan	Feb	Mar	Apr	May	Jun	Jul	Aug	Sep	Oct	Nov	Dec	Annual
KMCW	5.73	5.57	5.48	5.89	5.57	4.50	3.50	3.34	4.02	4.78	5.30	5.53	4.93
KLAF	4.09	4.15	4.18	4.46	3.47	2.88	2.53	2.36	2.57	3.19	3.72	3.88	3.46
KHSI	4.78	5.07	5.17	5.84	5.19	4.58	3.78	3.59	3.94	4.65	4.57	4.75	4.66
KLBL	5.00	5.45	5.94	6.57	6.16	6.27	5.36	5.05	5.36	5.49	5.43	5.11	5.60
KJMS	5.42	5.41	5.60	5.67	5.80	4.76	4.01	4.08	4.42	5.07	5.38	5.42	5.09
KHOU	4.00	4.06	3.95	4.03	3.70	3.02	2.56	2.48	2.95	3.15	3.40	3.84	3.43
KFTY	2.56	2.64	2.74	2.57	2.26	2.02	1.90	1.74	1.94	1.88	2.01	2.34	2.22

% Diff	Jan	Feb	Mar	Apr	May	Jun	Jul	Aug	Sep	Oct	Nov	Dec	Annual
KMCW	0.00	2.06	-6.34	-0.65	6.47	-6.90	-13.00	-10.21	-4.28	-3.04	-2.51	1.45	-2.60
KLAF	-14.72	-8.81	-15.73	-6.30	-15.17	-21.40	-23.30	-23.27	-24.07	-18.15	-16.31	-14.81	-16.16
KHSI	-11.01	-8.51	-16.67	-10.93	-10.22	-13.00	-19.18	-21.48	-22.98	-12.86	-18.61	-13.94	-14.71
KLBL	8.15	9.66	1.75	6.26	9.98	18.44	3.60	9.83	5.35	6.43	8.92	6.06	7.80
KJMS	-2.52	-2.30	-2.20	-1.45	1.80	-6.67	-7.84	-10.15	-11.41	-6.45	0.04	-0.24	-3.85
KHOU	-9.42	-10.26	-14.15	-7.85	-4.49	-11.59	-11.77	-7.29	-5.84	-11.18	-17.36	-8.89	-10.15
KFTY	-10.66	-14.88	-13.14	-12.30	-5.94	-6.44	-13.69	-13.68	-9.90	-13.77	-18.17	-14.30	-12.36

Table 4-2 displays three calculations: (top) monthly mean wind speed data prior to automation (Jan 01, 1973 – ASOS implementation); (middle) monthly mean wind speed data post-automation (implementation date – Jan 01, 2013); (bottom) and finally, the percent difference between the two studied periods (% difference = [(ASOS/Pre-ASOS) -1]). Table 4-2 illustrates that all seven analyzed ASOS stations in this study show that the lowest mean monthly wind speeds occur during the months of July and August. Furthermore, winds display a tendency to gradually increase in strength throughout the fall and winter months until they peak in April and then begin diminishing as the summer minimum approaches once again. Houston shows an exception to the pattern, such that once the measurements were automated (ASOS), there was a larger spread of times during the year in which the maximum winds occurred (February through April).

The bottom table within Table 4-2 displays the percent difference between Pre-ASOS and ASOS seasonal trends. Five out of the seven cities display an overall decreasing trend throughout every month. The exceptions to this negative trend are Mason City, IA (KMCW) which shows both increasing and decreasing trends throughout the seasons, and Liberal, KS (KLBL) which had an overall increase in wind speed magnitude during every month.

4.3 Surface wind speed distribution

Similarly to the findings of historical wind research, surface wind speed distributions by ASOS data show a continuous and right-skewed distribution. Figure 4-2 illustrates the typical distribution found for surface wind speed data. Notice the semi-smooth nature of the curve, which is comprised of the addition of Pre-ASOS and ASOS data used in Figure 4-1.

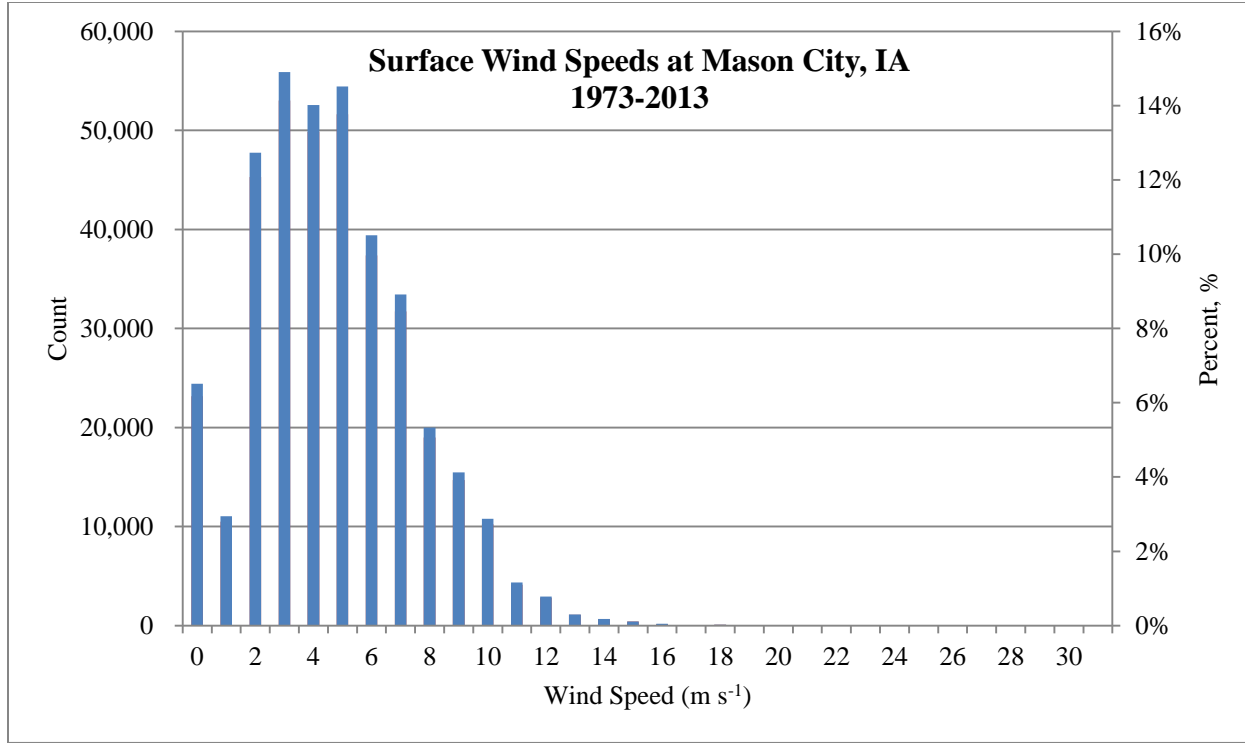


Figure 4-2. Surface wind speed distribution at Mason City, IA (KMCW) over the years of 1973-2013

Figure 4-3 shows the calculated percent difference between the two datasets: ASOS – Pre-ASOS at Mason City, IA (KMCW). Again, note the last bin, labeled “Other” which encompasses all observational data which exceeds 30 m s^{-1} . Trends that can be deduced from this plot are that there is a slight increase in observations in bins $\geq 22 \text{ kts}$ and a general increase in values between 3 and 4 kts. Also, there is a decrease in even integers (8, 10, 12, 14, 18, and 20 kts) and an increase in odd integers (7, 9, 11, 13 and 19 kts) which is partially attributed to the introduction of automated measurements, and thus, the removal of human subjectivity to “nicely-rounded” values. These general trends can be seen throughout all seven locations used in this study. For specifics regarding percent changes among all other stations, see Appendix B.

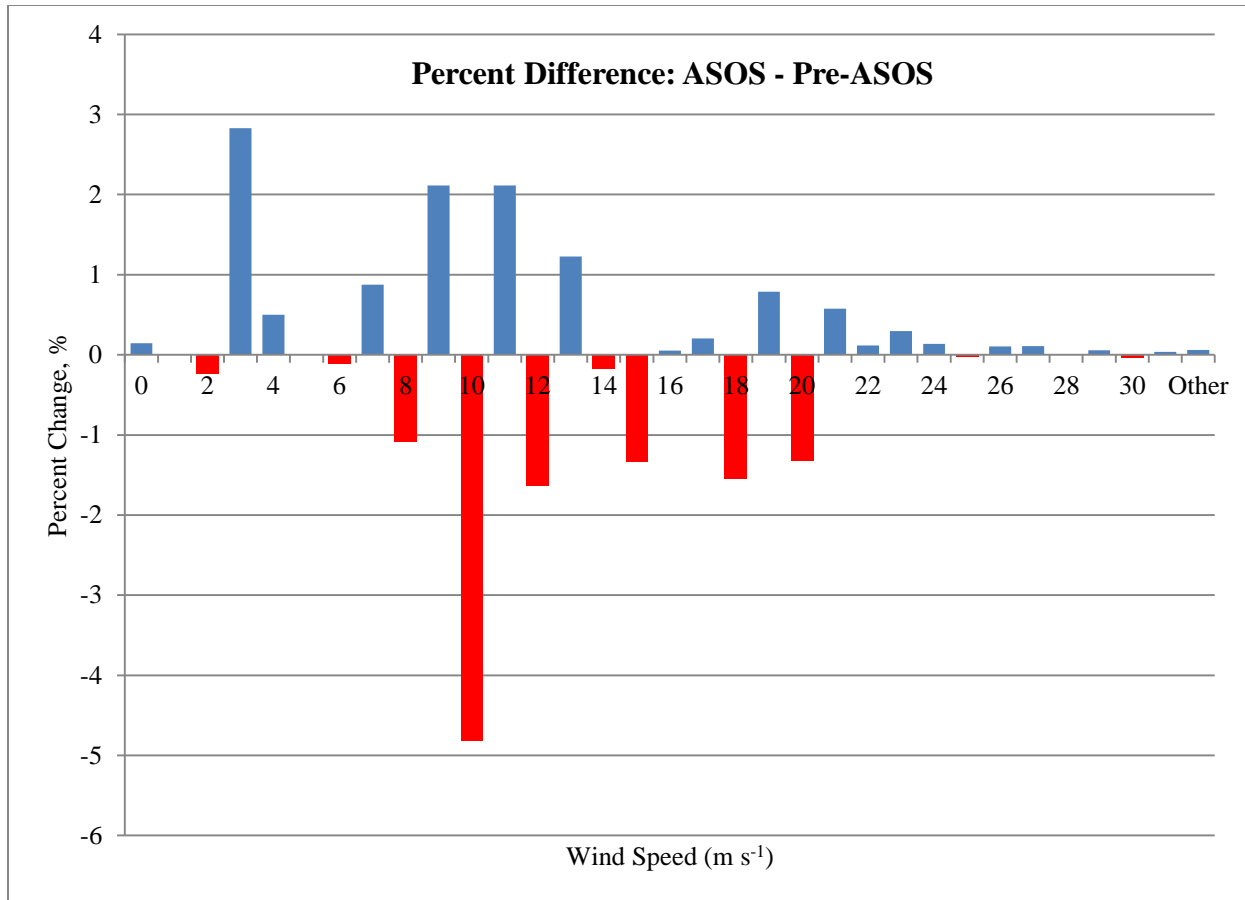


Figure 4-3. Difference in wind speeds (in kts) from Pre-ASOS to ASOS at Mason City, IA (KMCW)

4.4 “Extreme” high winds

In Section 3.2, we defined “extreme” high-end winds to be those at or exceeding the 90th percentile. Typical values of these “extreme” winds among the various locations are outlined in Table 4-1. In reference to the linear regression calculations, there are slight temporal trends at the 90th percentile: five out of the seven cities display a negative trend, while, KLBL and KJMS slightly increases in magnitude during the years 1973 to 2013. KLBL has the highest “extreme” value, being 9.659 m s^{-1} ; whereas, KFTY has the lowest, at 5.114 m s^{-1} .

4.5 “Extreme” low winds

On the other end of the spectrum of extremes, low-end winds (≤ 3 kts/ 1.54 m s^{-1}) make up, on average, anywhere from 7 to nearly 40 percent of the wind speed observations during the period of study for this research project (Jan. 01, 1973 – Jan. 01, 2013). Table 4-3 shows this feature of calm and near-calm winds. This table displays that calm and near-calm winds occur most frequently (39.242%) at Atlanta, GA, whereas, they occur most infrequently at Liberal, KS, and Jamestown, ND (7.481 and 7.481%, respectively).

Table 4-3. Count and percent calculation of wind speeds to be at $\leq 3 \text{ m s}^{-1}$.

	Frequency	%
KMCW	33578	9.439
KLAF	62070	17.304
KHIS	20447	8.772
KLBL	36581	7.481
KJMS	29049	7.838
KHOU	65435	18.972
KFTY	129725	39.242

According to a report by the Environmental Protection Agency (EPA, 1997), ASOS data contains a higher frequency of occurrence of calm surface conditions than observer data (Pre-ASOS) for all stations across the entire United States. Figure 4-4 illustrates this observation, such that throughout each of the stations (with the exception of Liberal, KS), there is an increase in which winds ≤ 3 kts (1.54 m s^{-1}) between Pre-ASOS and ASOS time periods.

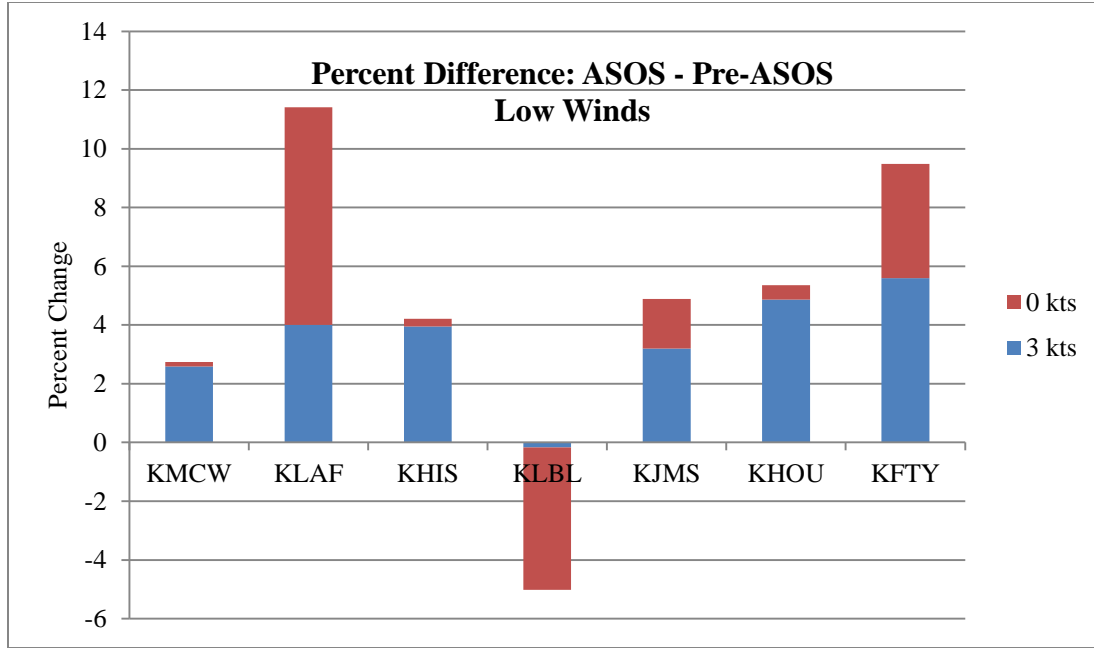


Figure 4-4. Percent difference in calm or near-calm winds: ASOS - Pre-ASOS. Red bars represent wind speeds at 0 m s^{-1} and blue are winds $\leq 3 \text{ kts}$.

For the purpose of this study, we previously defined “extreme” low winds to be any surface wind speed at or below the 10th percentile. Recall Table 4-1; features of wind speeds at the 10th percentile are that three of the seven locations (KMCW, KLAF, KJMS) have an overall negative linear regression trend, while three others (KHIS, KLBL, KHOU) display an increasing trend, and finally, one location (KFTY) has a linear regression value of 0.00 m s^{-1} , such that there is no overall change in the 10th percentile wind values during the years 1973-2013. Similarly to the data analyzed in Section 4.4, KFTY displays the lowest 10th percentile value at 0.00 m s^{-1} , while KJMS has the highest at 2.186 m s^{-1} . Furthermore, KFTY displays the lowest values among all of the analyzed cities at each of the calculated: 10th, 90th, 95th, 99th, and 99.9th percentiles.

CHAPTER 5

SURFACE WINDS REPRESENTED BY THE NARCCAP MODELS

5.1 Introduction

Simulations of various model combinations of near-surface wind speeds are analyzed to reveal general conclusions on the nature, distribution, and temporal trends. The seven cities which were outlined in the previous chapter will be used as a general guide for which of the model's grid points will be used in this analysis. Each city will be represented by a single 50 x 50 km grid box, as this is the finest grid resolution of the NARCCAP models.

5.2 RCM results with NCEP boundary conditions

5.2.1 Surface wind speed distributions

For the first part of the model analysis, output from three RCMs will be examined. These RCMs are MM5I, CRCM, and WRFG, all of which are initiated with boundary conditions from NCEP reanalysis data. Figure 5-1 shows examples of annual distributions of surface wind speeds found across the seven cities which are used in this study. Similarly to observations made by previous studies, these distributions are continuous, asymmetrical, and skewed to the right (Takle et al., 1976; Takle and Brown, 1978; Stewart and Essenwanger, 1978; Klink, 2002). These cities vary widely in the frequencies at which each wind speed value occurs, but all of the distributions have the same resemblance, with the exception of Houston, TX (KHOU), where the shape cumulative frequency distribution resembles more of a Normal, or Gaussian distribution. (Figure 5-1).

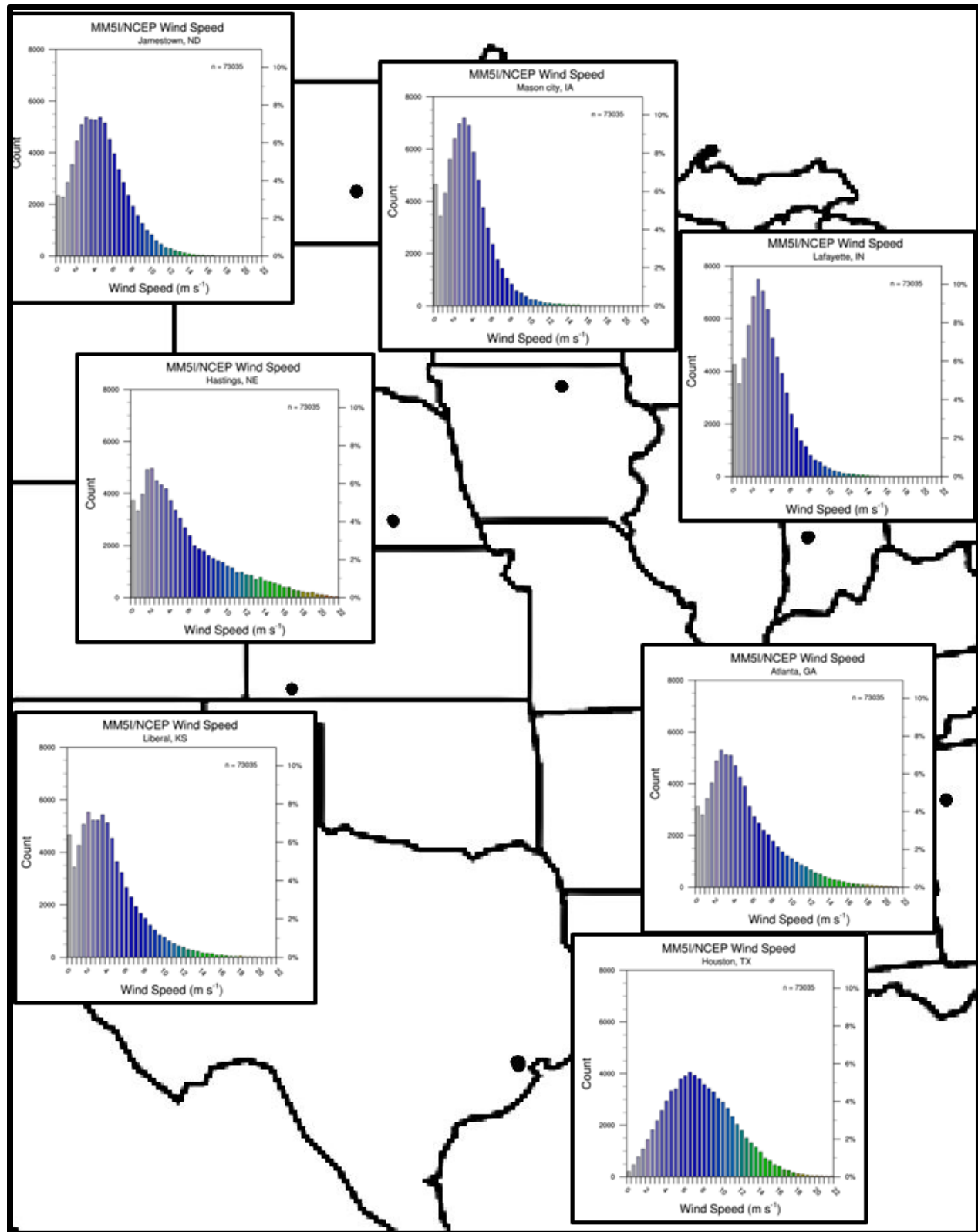


Figure 5-1. Annual distributions of surface wind speeds across the seven locations used in this study. Model simulation of MM5I with NCEP reanalysis data over the years of 1979-2004.

Table 5-1. Model calculated percentiles with NCEP-driven reanalysis data. Mean winds reported in m s^{-1} and trends are reported in $\text{m s}^{-1} \text{yr}^{-1}$.

NCEP Model Reanalysis Output Percentiles (1979-2004)							
Site ID	Model	10 th	90 th	95 th	99 th	99.9 th	Mean
KMCW	MM5I	0.904 / -0.0062	6.636 / -0.028	7.909 / -0.037	10.593 / -0.070	13.507 / -0.106	3.647 / -0.014
	WRFG	1.699 / 0.0062	9.597 / 0.050	11.437 / 0.062	14.900 / 0.334	17.864 / 0.004	5.055 / 0.017
	CRCM	0.535 / -0.0023	4.100 / -0.013	4.727 / -0.005	5.864 / -0.026	6.868 / -0.021	2.308 / -0.002
KLAF	MM5I	0.880 / 0.0187	6.600 / 0.020	7.845 / 0.019	10.447 / 0.007	13.551 / 0.021	3.563 / 0.019
	WRFG	1.703 / 0.0015	10.025 / 0.053	12.031 / 0.065	15.422 / 0.085	18.629 / 0.128	5.344 / 0.021
	CRCM	0.552 / 0.000	3.781 / 0.004	4.379 / 0.000	5.548 / -0.001	6.765 / -0.024	2.095 / 0.003
KHSI	MM5I	1.038 / 0.002	12.340 / 0.013	14.793 / 0.015	18.776 / -0.021	21.843 / -0.077	5.625 / 0.005
	WRFG	1.543 / 0.008	7.434 / 0.011	8.549 / 0.003	10.931 / -0.037	13.604 / -0.075	4.330 / 0.009
	CRCM	0.641 / -0.002	5.424 / 0.002	6.167 / 0.000	7.843 / 0.021	9.346 / 0.025	3.116 / 0.003
KLBL	MM5I	0.898 / -0.007	8.627 / -0.031	10.509 / -0.035	14.201 / -0.059	17.727 / -0.088	4.370 / -0.014
	WRFG	1.302 / 0.005	6.300 / 0.008	7.325 / 0.011	9.272 / 0.012	11.130 / 0.008	3.553 / 0.005
	CRCM	0.858 / 0.002	4.872 / 0.004	5.607 / 0.006	7.202 / 0.011	9.006 / 0.046	2.852 / 0.003
KJMS	MM5I	1.473 / -0.003	8.428 / -0.015	9.742 / -0.020	12.309 / -0.015	15.262 / -0.007	4.784 / -0.008
	WRFG	1.871 / -0.005	7.752 / -0.012	8.804 / 0.000	10.806 / 0.001	12.756 / 0.012	4.625 / -0.010
	CRCM	1.559 / 0.006	9.465 / 0.011	11.121 / 0.002	14.138 / -0.001	16.399 / 0.059	5.272 / 0.008
KHOU	MM5I	3.380 / 0.001	12.799 / -0.002	14.317 / 0.004	17.276 / -0.002	20.322 / -0.006	7.903 / 0.001
	WRFG	3.690 / -0.014	13.669 / 0.002	15.257 / -0.002	18.057 / 0.027	20.671 / 0.004	8.545 / -0.013
	CRCM	2.654 / 0.006	10.545 / 0.013	11.712 / 0.031	13.929 / 0.018	15.880 / 0.004	6.343 / 0.008
KFTY	MM5I	1.227 / 0.007	10.268 / -0.014	14.734 / -0.007	16.434 / -0.002	20.703 / 0.041	5.130 / 0.001
	WRFG	3.153 / -0.011	13.545 / -0.016	15.204 / -0.007	18.439 / -0.002	21.309 / 0.036	8.091 / -0.015
	CRCM	2.377 / 0.125	11.298 / 0.021	12.856 / 0.028	15.942 / 0.022	18.450 / 0.048	6.432 / 0.008

Table 5-1 is an overview of percentile calculations from the studied RCMs (MM5I, WRFG, and CRCM) with NCEP boundary conditions. The calculated percentiles capture quantitative values that are representative of the “extreme” low-end winds (10th percentile) and the “extreme” high-end winds (90th, 95th, 99th, and 99.9th percentiles). These percentiles (in m s^{-1}) are the resulting mean value of the entire time period for the models, which for this dataset, runs from 1979-2004. The other calculation within Table 5-1

is a trend statistically determined by a linear regression equation for each RCM/NCEP model combination (measured in $\text{m s}^{-1} \text{yr}^{-1}$). It is noteworthy that the WRFG RCM consistently simulates the highest value at the 10th percentile and the CRCM showed the lowest value at this threshold in five out of the seven cities. Throughout the remaining percentiles, there was no clear trend at which model runs consistently higher or lower in comparison to the other models.

MM5I at Mason City, IA (KMCW), Liberal, KS (KLBL), and Jamestown, ND (KJMS) displays an overall decreasing trend in winds throughout each of the percentiles; whereas, they have shown to increase at Lafayette, IN (KLAF). Hastings, NE (KHSI), Houston, TX (KHOU), and Atlanta, GA (KFTY), had mixed results, such that various percentiles had positive (increasing) trends, and others did not.

WRFG shows an increasing trend in wind speeds throughout the majority of the percentiles at each of the seven cities. Exceptions of this observation are at Atlanta, GA, where a decreasing trend is apparent throughout each of the percentiles except at 99.9th threshold. The other exceptions are at Jamestown, ND, with the 10th and 90th percentiles and Houston, TX, with the 10th and 95th percentiles.

Last, CRCM simulated a positive trend in wind speeds at Liberal, KS, Houston, TX, and Atlanta, GA. Jamestown, ND, primarily showed an increasing trend with the exception at the 99th percentile, which had a slight decrease. The overall mean trend though, was positive. Two out of the seven cities had an overall positive trend in the mean wind speed across all models: Lafayette, IN, and Liberal, KS.

In several instances, the CRCM and WRFG display peculiarly large trends, which might insinuate model error. Specifically, the CRCM shows a positive trend of $0.125 \text{ m s}^{-1} \text{ yr}^{-1}$ at the 10th percentile at Atlanta, GA, the WRFG displays a trend of $0.334 \text{ m s}^{-1} \text{ yr}^{-1}$ for the 99th percentile at Mason City, IA, a value of $0.128 \text{ m s}^{-1} \text{ yr}^{-1}$ at the 99.9th percentile at Lafayette, IN, and finally, the MM5I shows a decreasing trend of $0.106 \text{ m s}^{-1} \text{ yr}^{-1}$ at the 99.9th percentile at Mason City, IA, all of which are at least one order of

magnitude larger than the other models at each of the cities. These values, curiously large, might be a sign of model error.

Comparison of model and observational data will be discussed in Section 5-6.

5.2.2 “Extreme” high winds represented by models

As defined by the IPCC (2013a), extreme events are defined as the occurrence of a value of a weather or climate variable above (or below) a threshold value near the upper (or lower) ends ('tails') of the range of observed values of the variable. Recall, we previously defined a threshold for extreme winds as the 90th percentile (Section 3.2).

As previously indicated, there is large variance among the three models in the 90th percentile and above (Table 5-1). More specifically, the CRCM simulates the lowest values at five out of the seven cities, with the exception of Jamestown, ND (KJMS), and Atlanta, GA (KFTY). Furthermore, at the 95th, 99th, and 99.9th percentiles, the CRCM also tends to simulate the lowest wind speeds among six out of the seven cities (except Jamestown, ND). Values range from as low as 3.8 m s⁻¹ simulated by the CRCM at Lafayette, IN to as high as 13.7 m s⁻¹ by the WRFG at Houston, TX at the 90th percentile.

5.2.3 “Extreme” low winds represented by models

Referring back to Table 5-1, the WRFG consistently simulates the highest value at the 10th percentile and the CRCM showed the lowest value at this threshold in five out of the seven cities. Values simulated by the CRCM are such like 0.4 m s⁻¹ at Mason City, IA to 2.7 m s⁻¹ at Houston, TX.

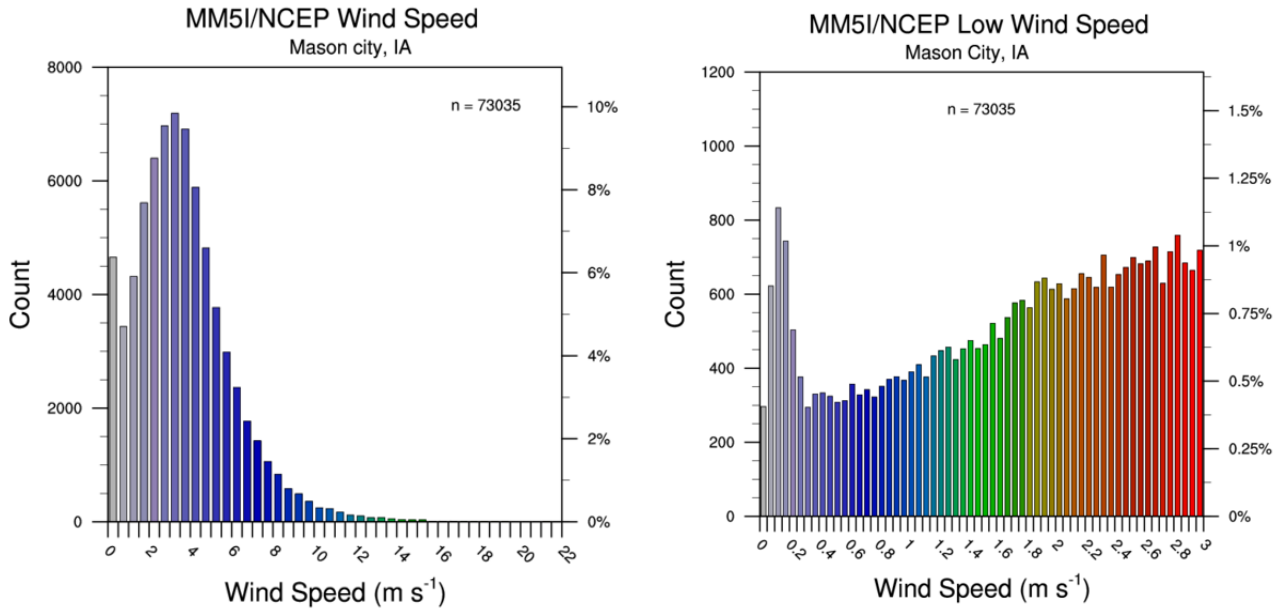


Figure 5-2. Annual distributions of surface wind speeds simulated by MM5I with NCEP reanalysis data at Mason City, IA. (Left) Total distribution. (Right) Partial distribution, to show emphasis on low winds (≤ 3 m s⁻¹).

A distinct feature shown by MM5I is its prominent spike in the calm or nearly calm wind speeds when initialized with the NCEP boundary conditions as well as both the contemporary and future CCSM scenarios. This unusual feature can be seen in Figure 5-2 (left), and even better in Figure 5-2 (right) which exclusively captures winds $\leq 3 \text{ m s}^{-1}$. This peculiar characteristic is also visible in the MM5I/CCSM

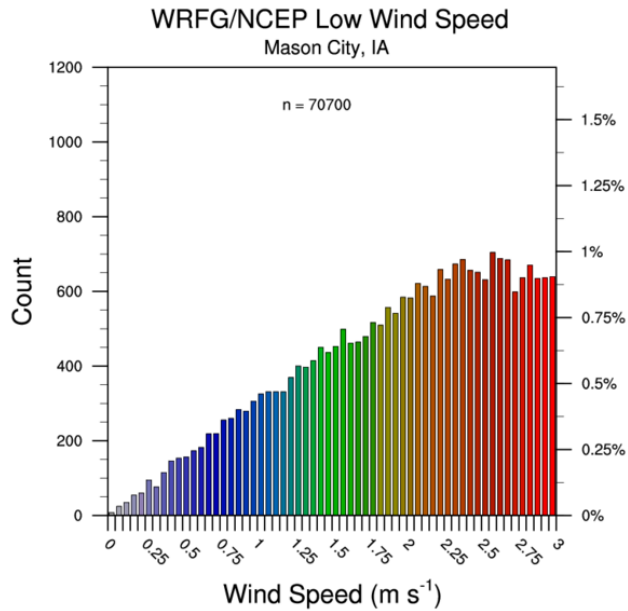


Figure 5-3. Low-end winds ($\leq 3 \text{ m s}^{-1}$) simulated by the WRFG/NCEP at Mason City, IA.

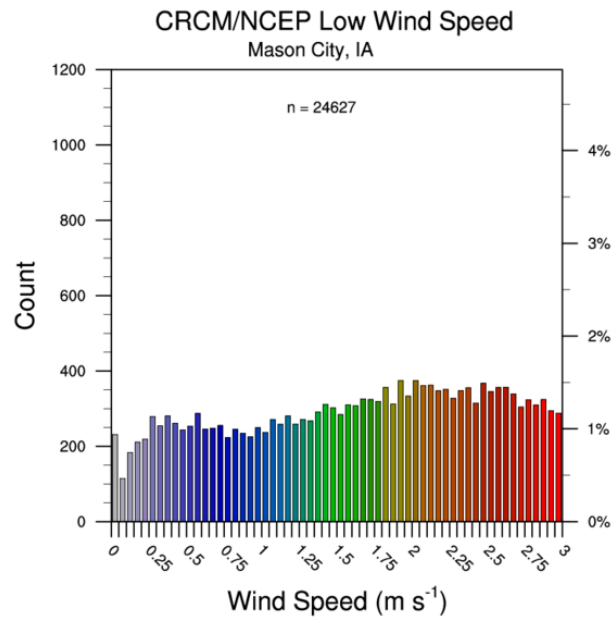


Figure 5-4. Low-end winds ($\leq 3 \text{ m s}^{-1}$) simulated by the CRCM/NCEP at Mason City, IA.

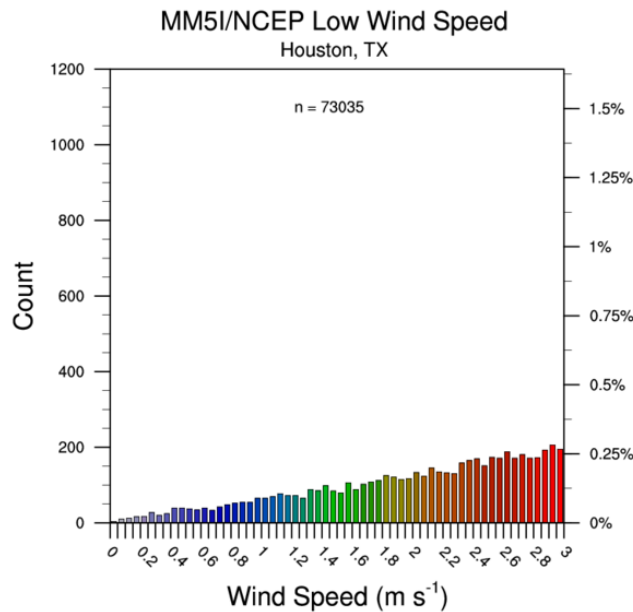


Figure 5-5. Low-end winds ($\leq 3 \text{ m s}^{-1}$) simulated by the MM5I/NCEP at Houston, TX.

contemporary and future scenarios (Section 5.3.3 and 5.4.3), but is not shown in any other model combinations such as the WRFG/NCEP (Figure 5-3) and CRCM/NCEP (Figure 5-4). This trend is observed across all of the studied locations with the exception of Houston, TX, (Figure 5-5), in which there is no apparent spike in wind speeds near 0.00 m s^{-1} .

Refer to Appendix C1-3 for a complete illustration of annual distributions of low-end wind speeds simulated by each of the model combinations at Mason City, IA, Houston, TX, and Atlanta, GA, respectively. Only select cities were chosen to show in Appendix C because of their unique features in reference to the other stations. As previously mentioned, Houston, TX, was the only city in this study which did not exhibit the spike in near-calm winds in the MM5I model simulations. Lastly, Atlanta, GA, is included in the appendix because of its climatologically-low wind speeds.

To look into this peculiar observation, we compared the planetary boundary layer (PBL) schemes used in each of the models. The MM5I, which is the RCM that shows the spike in near-calm winds, uses the Medium-Range Forecast (MRF) PBL with countergradient and non-local K components. The non-local K components takes into account the countergradient fluxes in a model that establishes the PBL depth and then constrains the vertical diffusion coefficient K which assumes a constant vertical profile over the entire depth of the PBL (Hong, Song-You, et al., 2006). The WRFG uses the Yonsei University (YSU) PBL scheme with explicit entrainment. Finally, the CRCM's PBL scheme includes a gradient Richardson number formulation as well as a Local K component. From these varying components of the PBL schemes used in these models, it is reasonable that there are widely ranging results in wind speed values.

We have brought attention to these unusual characteristics because of the significance of near-calm winds on air pollution dispersion, agricultural impacts, etc. This feature needs to be further investigated.

5.2.4 Seasonal distributions

While general trends (discussed in Section 5.2.1-5.2.3) are insightful into a better understanding of the wind environments in these seven cities, it is also beneficial to analyze the data on a seasonal timescale.

Tables 5-2, 3, and 4 display mean monthly wind speeds simulated by the RCMs with NCEP reanalysis data. These tables are color-coded to show at which month the maximum (coral) and minimum (yellow) winds have a tendency to occur during. Multiple cells were highlighted if there was another value $\leq 0.10 \text{ m s}^{-1}$ away from the defined mean monthly maximum or minimum value.

Table 5-2 illustrates mean monthly wind speeds simulated by the MM5I with NCEP boundary conditions. Recall, previous research has indicated that wind speeds are typically at their minimum during the months of June, July, and August, and at a seasonal maximum during March, April, and May (Takle, Brown, and Davis, 1976; Klink, 1999). This table shows that these model-simulated winds tend to peak in March and April, with the exception of at Liberal, KS and Houston, TX, where the mean monthly winds are the strongest during December. On the other hand, seasonally minimum winds tend to occur during June, July, and August, which agrees with findings from Chapter 4. Jamestown, ND, is the only city that defies this trend, where the minimum wind speeds tend to occur in April.

Table 5-2. Mean monthly distributions simulated by MM5I with NCEP boundary conditions. Coral-shaded cells represent the month at which the seasonal maximum wind speed occurred at, and yellow-shaded is for the seasonal minimum. Values are shown in m s^{-1} .

MM5I/NCEP	Jan	Feb	Mar	Apr	May	Jun	Jul	Aug	Sep	Oct	Nov	Dec	Total
KMCW	3.641	5.325	3.975	2.472	2.973	2.321	2.933	2.396	3.600	3.600	4.380	4.539	3.513
KLAF	3.700	4.679	6.442	4.049	3.128	2.854	2.618	2.413	3.341	2.875	4.011	4.171	3.690
KHSI	9.388	6.782	9.702	5.821	3.712	2.485	2.395	2.473	3.071	4.875	6.536	8.774	5.501
KLBL	4.582	3.559	5.826	3.246	3.496	2.520	2.015	2.105	2.984	4.807	5.272	7.997	4.034
KJMS	4.841	5.769	5.163	3.813	4.957	4.215	4.349	3.928	5.270	4.401	4.711	4.727	4.679
KHOU	8.841	6.060	8.958	7.545	7.520	6.028	5.558	6.295	7.318	9.694	9.897	10.537	7.854
KFTY	6.468	6.928	7.122	5.240	3.376	2.966	2.945	2.656	3.822	3.589	4.936	6.966	4.751

Next, Table 5-3 displays mean seasonal distributions for the WRFG/NCEP model simulated wind speeds. Seasonal maximum winds appear to occur widely from October to March, which is similar to the findings with the MM5I with NCEP boundary conditions (Table 5-2), but with more spread. The seasonal minimum winds generally occur during July and August, which is similar to results of prior research (Chapter 4) as well as results from the MM5I simulations. There are exceptions to this observation though; where minimum winds at Hastings, NE, occur during January, and Houston, TX, during December.

Table 5-3. Mean monthly distributions simulated by WRFG with NCEP boundary conditions. Coral-shaded cells represent the month at which the seasonal maximum wind speed occurred at, and yellow-shaded is for the seasonal minimum. Values are shown in m s^{-1} .

WRFG/NCEP	Jan	Feb	Mar	Apr	May	Jun	Jul	Aug	Sep	Oct	Nov	Dec	Total
KMCW	6.957	4.735	6.475	3.557	3.538	3.002	2.817	2.770	3.256	4.342	4.390	7.710	4.462
KLAF	7.241	6.539	6.899	3.518	4.186	3.328	3.384	2.910	3.962	3.807	3.979	5.184	4.578
KHSI	3.614	4.053	5.186	4.174	4.548	4.514	4.031	3.914	4.364	5.068	4.041	4.084	4.299
KLBL	4.416	3.629	4.383	3.075	2.601	3.156	2.904	3.031	3.210	3.758	3.543	4.383	3.507
KJMS	5.276	4.159	5.260	4.521	5.174	4.149	4.361	3.785	4.541	4.840	4.500	4.328	4.574
KHOU	9.656	6.482	9.565	8.717	4.548	4.514	4.031	6.200	6.215	9.948	9.693	4.084	6.971
KFTY	9.561	6.140	8.232	7.098	6.528	6.365	4.880	6.653	7.898	8.764	8.459	10.350	7.577

Finally, Table 5-4 outlines mean seasonal distributions simulated by the CRCM/NCEP. Unlike results in observational data in Chapter 4, this RCM produces seasonal maximum winds to occur primarily during December and January. On the other hand, seasonal minimum winds are simulated to occur strictly during July and August, which matches our previous research.

Table 5-4. Mean monthly distributions simulated by CRCM with NCEP boundary conditions. Coral-shaded cells represent the month at which the seasonal maximum wind speed occurred at, and yellow-shaded is for the seasonal minimum. Values are shown in m s^{-1} .

CRCM/NCEP	Jan	Feb	Mar	Apr	May	Jun	Jul	Aug	Sep	Oct	Nov	Dec	Total
KMCW	2.659	2.694	3.371	2.596	2.596	2.321	2.188	1.738	2.823	3.617	3.096	2.698	2.700
KLAF	3.368	1.751	3.342	2.477	2.477	2.005	1.689	1.592	2.955	3.602	3.335	3.907	2.708
KHSI	5.141	4.100	5.279	3.711	3.711	3.427	3.043	2.693	3.278	4.168	5.109	5.471	4.094
KLBL	4.883	3.872	5.642	3.882	3.882	3.164	2.460	2.350	2.498	3.619	4.676	5.591	3.877
KJMS	9.614	6.697	7.725	6.056	6.056	5.124	4.839	4.608	7.023	7.745	9.284	8.581	6.946
KHOU	10.335	6.357	9.646	8.604	8.604	6.855	6.562	5.927	5.838	8.802	8.774	10.168	8.039
KFTY	10.776	6.711	10.445	7.702	7.702	6.104	5.416	5.645	8.334	10.605	10.321	9.705	8.289

Figure 5-6(a-c) gives an overarching visual reference as to how each of the cities compares to one another with each of the climate models. The MM5I with NCEP reanalysis data (Figure 5-6 a) shows that Houston, TX generally exhibits higher wind speeds throughout each of the months, with the exception of during January, February, and March, where Hastings, NE, is slightly higher in magnitude. On the lower end, Mason City, IA, and Lafayette, IN, consistently display the lowest wind speeds throughout the entire

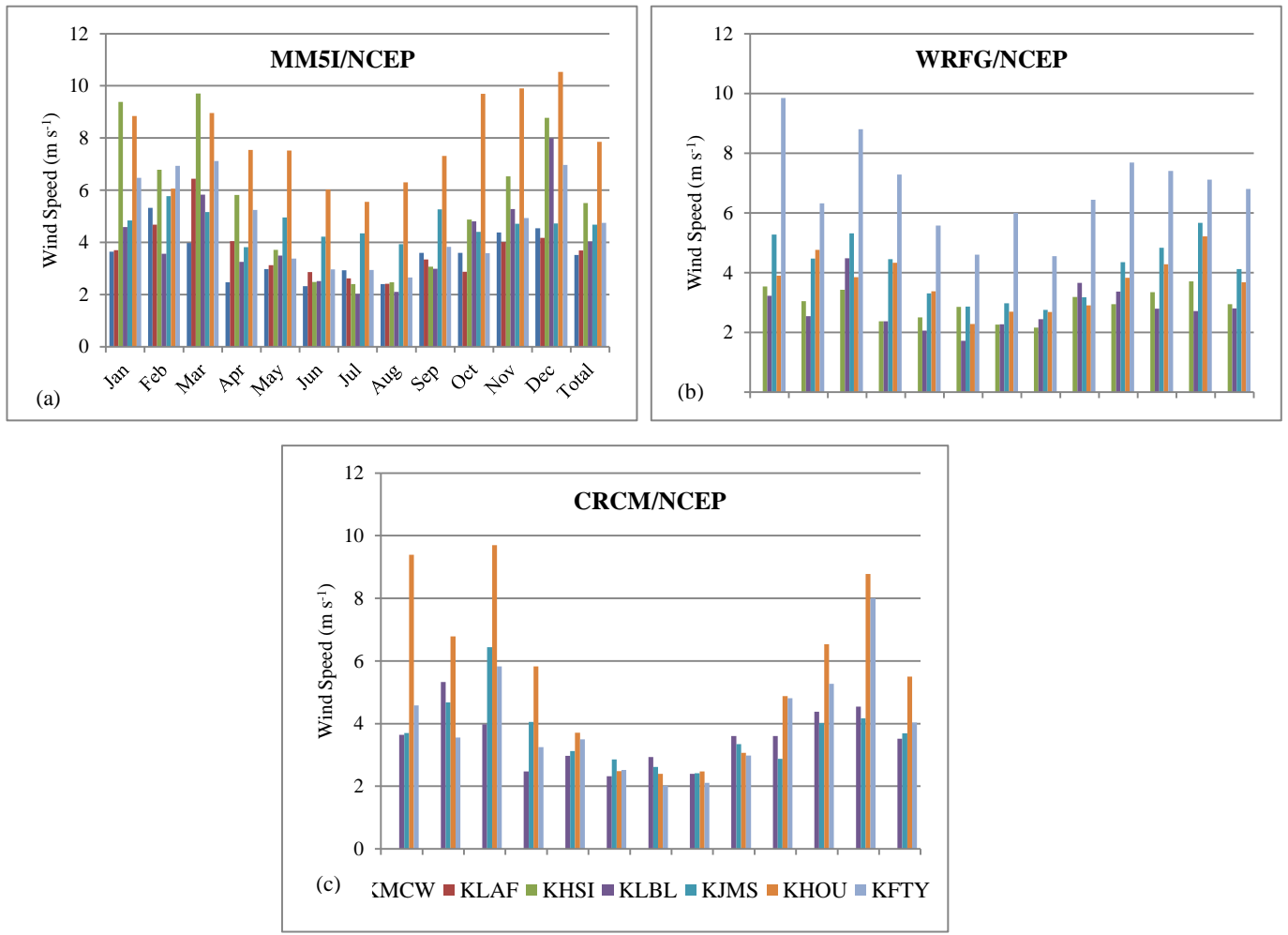


Figure 5-6. Seasonal trends simulated by MM5I (a), WRFG (b), and CRCM (c) with NCEP reanalysis data over the years of 1979-2004 with NCEP boundary conditions.

year. These features match geographical characteristics of surface wind speeds found by Klink (1999) and NOAA (2005). Historical research has demonstrated that there is an axis of relatively higher winds spanning from northern Texas through the Missouri River Valley. This spatial observation matches our

results fairly well since it is apparent that Houston, TX, generally has higher magnitude wind speeds, while Mason City, IA, and Lafayette, IN, have lower winds throughout the seasons. Interestingly enough, the magnitudes of seasonal winds at Atlanta, GA, closely follow Houston, TX, and Hastings, NE, but according to previous research, winds in the southeast are relatively low compared to the Midwest (NOAA, 2005).

Mean seasonal distributions simulated by the WRFG are similar to those of the MM5I; however, the CRCM displays winds at Atlanta, GA, to be nearly as strong (and sometimes even stronger) than at Houston, TX, which goes against climatological research by Klink (1999) and NOAA (2005). Following Atlanta, GA, and Houston, TX, the CRCM produces the next highest winds at Jamestown, ND, which is a feature unique to this model only.

5.3 Contemporary scenario model simulations

5.3.1 Surface wind speed distributions

Contemporary model scenarios are simulations covering years 1968-2000. As mentioned in Section 3.7, the entire data period, as well as during the typical model spin-up period is included in this study. Based on results from statistical significance testing with a significance level of 0.01, the data during the spin-up period (first three years) was proven to be no different than the rest of the period of study.

Table 5-5 displays percentile calculations for the following model combinations at each of the locations: MM5I/CCSM, WRFG/CCSM, CRCM/CCSM, and CRCM/CGCM3. Similar to Table 5-1 in Section 5.2.1, Table 5-5 includes the linear regression ($\text{in m s}^{-1} \text{ yr}^{-1}$) corresponding to each of the percentile values. Knowing that the initial conditions which are driving the climate models during the contemporary scenario are comprised of climatological data, we can assume that there should not be any actual model “trends” seen in the data. As a result of this assumption, we can use the linear regression values in Table 5-

5 as a “null” case to compare with the trends in the climate models with NCEP reanalysis data (Table 5-1). Any significant differences might infer model error in the climate models with NCEP boundary conditions.

Table 5-5. RCM/GCM contemporary model scenario calculated percentiles: 10th, 90th, 95th, 99th, 99.9th, and overall mean. Mean winds reported in m s⁻¹, and linear regression in m s⁻¹ yr⁻¹.

Contemporary Scenario Model Output Percentiles (1968-1999)							
		10 th	90 th	95 th	99 th	99.9 th	Mean
KMCW	MM5I/CCSM	1.050 / 0.000	7.029 / 0.007	8.221 / 0.012	10.765 / 0.022	13.733 / 0.025	3.937 / 0.003
	WRFG/CCSM	1.723 / 0.003	10.663 / 0.026	12.708 / 0.031	16.349 / 0.018	19.769 / 0.009	5.366 / 0.005
	CRCM/CCSM	0.711 / -0.002	5.328 / 0.002	6.175 / 0.005	7.805 / 0.003	9.570 / 0.016	2.952 / 0.000
	CRCM/CGCM3	0.547 / 0.001	4.177 / 0.006	4.819 / 0.008	6.002 / -0.003	7.055 / 0.001	2.341 / 0.002
KLAF	MM5I/CCSM	1.093 / 0.00	7.468 / 0.012	8.912 / 0.017	11.863 / 0.046	15.147 / 0.061	4.111 / 0.005
	WRFG/CCSM	2.021 / 0.003	11.217 / -0.008	13.497 / -0.008	17.342 / 0.001	21.065 / -0.009	5.863 / 0.002
	CRCM/CCSM	0.679 / 0.00	5.376 / -0.003	6.236 / 0.001	7.844 / 0.002	9.444 / 0.014	2.881 / -0.002
	CRCM/CGCM3	0.583 / -0.002	3.829 / -0.001	4.449 / -0.004	5.660 / -0.012	6.792 / -0.011	2.133 / -0.003
KHSI	MM5I/CCSM	1.242 / 0.000	14.149 / 0.020	16.670 / 0.020	20.557 / 0.019	24.169 / -0.006	6.506 / 0.007
	WRFG/CCSM	1.936 / -0.002	9.395 / 0.010	10.972 / 0.018	14.217 / 0.025	18.415 / 0.039	5.448 / 0.004
	CRCM/CCSM	0.804 / -0.001	7.995 / 0.005	9.386 / 0.006	12.062 / 0.023	14.715 / 0.023	4.205 / 0.000
	CRCM/CGCM3	0.704 / 0.003	5.756 / -0.001	6.737 / 0.001	8.768 / -0.004	11.113 / 0.004	3.338 / 0.000
KLBL	MM5I/CCSM	1.094 / 0.001	9.851 / 0.024	11.864 / 0.032	15.733 / 0.028	19.488 / 0.069	4.921 / 0.008
	WRFG/CCSM	1.332 / 0.004	6.741 / 0.010	8.037 / 0.010	10.273 / 0.010	12.111 / -0.003	3.704 / 0.008
	CRCM/CCSM	1.119 / -0.006	7.441 / -0.012	8.798 / -0.010	11.176 / 0.008	13.240 / 0.017	3.951 / -0.007
	CRCM/CGCM3	1.015 / -0.001	5.132 / 0.007	5.880 / 0.003	7.272 / 0.013	8.747 / 0.029	3.027 / 0.001
KJMS	MM5I/CCSM	1.630 / -0.002	8.873 / -0.001	10.183 / -0.004	12.800 / 0.008	15.687 / 0.022	5.092 / 0.000
	WRFG/CCSM	2.165 / 0.004	9.810 / 0.007	11.296 / 0.015	14.220 / 0.018	17.289 / 0.039	5.718 / 0.006
	CRCM/CCSM	2.062 / -0.007	12.998 / -0.001	14.622 / 0.002	17.423 / 0.014	20.507 / 0.036	7.238 / -0.009
	CRCM/CGCM3	1.569 / -0.004	10.291 / 0.008	11.966 / 0.013	15.370 / 0.007	18.205 / 0.014	5.615 / -0.001
KHOU	MM5I/CCSM	3.831 / 0.009	13.804 / 0.024	15.406 / 0.023	18.457 / 0.013	21.577 / 0.007	8.548 / 0.015
	WRFG/CCSM	4.028 / 0.001	14.540 / 0.009	16.254 / 0.003	19.519 / -0.001	23.141 / 0.041	8.903 / 0.005
	CRCM/CCSM	3.177 / -0.005	14.046 / 0.001	15.804 / -0.005	19.024 / 0.003	22.292 / 0.043	8.299 / 0.001
	CRCM/CGCM3	2.795 / 0.003	10.659 / 0.016	11.917 / 0.021	14.407 / -0.013	16.948 / -0.014	6.488 / 0.008
KFTY	MM5I/CCSM	1.884 / 0.008	12.627 / 0.007	15.089 / 0.003	19.842 / 0.019	24.529 / -0.053	6.557 / 0.008
	WRFG/CCSM	3.372 / 0.009	14.017 / 0.009	15.820 / 0.009	18.950 / 0.000	21.910 / -0.017	8.378 / 0.014
	CRCM/CCSM	3.098 / -0.003	15.046 / 0.009	16.906 / 0.009	20.599 / -0.012	23.995 / -0.035	8.821 / 0.002
	CRCM/CGCM3	2.421 / 0.001	11.780 / -0.009	13.348 / -0.015	16.794 / 0.005	19.972 / -0.039	6.655 / 0.000

When considering the contemporary scenario data as our “null” case, we can test the statistical significance of the trends simulated by the climate models with NCEP boundary conditions through an unpaired (heteroscedastic), two-tailed T-Test. Assuming a significance level of $p < 0.05$, nearly half of the model combinations (and cities) are statistically insignificant; thus, there is no statistical connection between the trends simulated by the models with NCEP initial conditions and the linear regressions in the contemporary scenario. On the other hand, if we test with a significance level of $p < 0.01$, only the MM5I is statistically insignificant at Liberal, KS.

5.3.2 “Extreme” high winds represented by models

According to Table 5-5, the climate models with contemporary scenario boundary conditions display large variation. Looking at the 90th percentile, the WRFG simulates the highest wind speed at three out of the seven cities (KMCW, KLAJ, and KHOU). On the other hand, the CRCM produces the lowest wind speed at six out of the seven cities (every city except KJMS). At the most “extreme” percentile (99.9th), the same trends are apparent, such that the WRFG generally simulates the highest wind speeds and the CRCM shows the lowest.

5.3.3 “Extreme” low winds represented by models

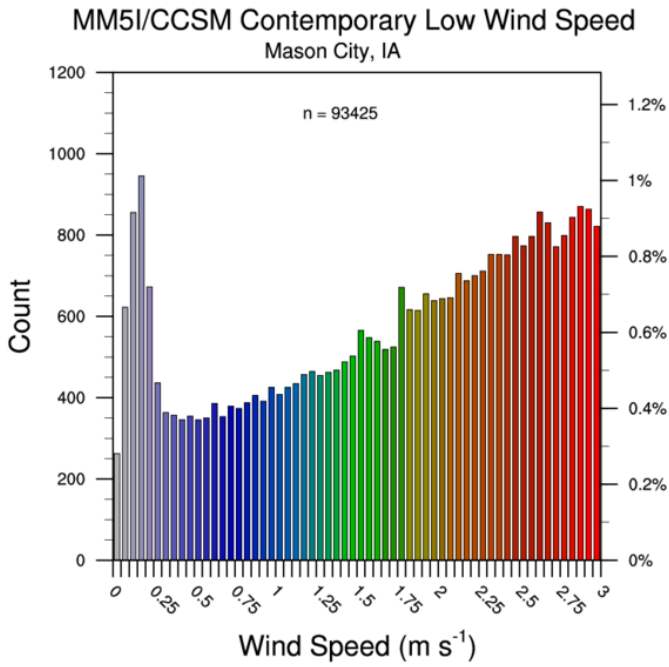


Figure 5-7. Low-end winds ($\leq 3 \text{ m s}^{-1}$) simulated by the MM5I/CCSM at Mason City, IA

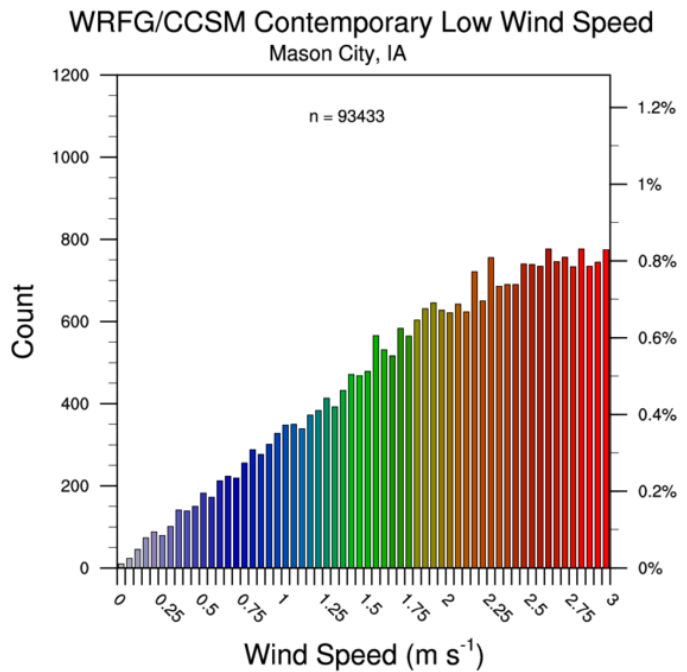


Figure 5-8. Low-end winds ($\leq 3 \text{ m s}^{-1}$) simulated by the WRFG/CCSM at Mason City, IA.

Figure 5-7 displays low-end winds ($\leq 3 \text{ m s}^{-1}$) simulated by the MM5I with CCSM contemporary boundary conditions at Mason City, IA. As mentioned in Section 5.2.3, the MM5I RCM produces a spike in near-calm winds, whereas, the other RCM/GCMs do not yield this phenomenon. Based on Figure 5-7 and the discussion in Section 5.2.3, we can deduce that the RCM, MM5I, is the primary, if not sole contributor to this spike in near-calm winds. Figure 5-8 reinforces this statement, such that the WRFG with CCSM contemporary boundary conditions does not display a spike in near-calm winds, but rather, shows a minimum occurrence of calm winds and then increases in frequency with speed.

Similar to the previous section, refer to Table 5-5 for wind speed data regarding “extreme” winds, but in this section, we will be analyzing the “extreme” low-end winds. As previously defined, for this study, “extreme” low winds are defined as anything that falls at or below the 10th percentile threshold. The WRFG simulates the highest winds at this percentile unanimously amongst all of the locations. On the

other hand, the CRCM produces the lowest winds at six out of the seven cities, with the exception of the MM5I showing the lowest winds at Atlanta, GA.

5.3.4 Seasonal distributions

Table 5-6. Mean monthly distributions simulated by the MM5I with CCSM boundary conditions. Yellow-highlighted cells represent seasonal minimum winds; coral-highlighted cells represent the seasonal maximum in m s^{-1} .

MM5I/CCSM Contemporary	Jan	Feb	Mar	Apr	May	Jun	Jul	Aug	Sep	Oct	Nov	Dec	Total
KMCW	5.187	8.045	3.658	4.181	4.220	2.598	2.258	3.358	4.070	4.731	4.252	5.953	4.376
KLAF	3.721	5.085	4.225	4.052	4.156	2.477	3.399	3.290	4.214	4.033	4.327	5.122	4.008
KHSI	8.902	11.998	7.265	10.431	6.837	3.519	2.411	2.720	5.040	7.592	7.282	8.520	6.876
KLBL	8.595	8.144	7.403	5.669	3.743	3.426	2.617	2.464	4.015	6.012	6.775	6.593	5.455
KJMS	6.974	8.996	4.795	5.825	5.186	3.800	3.233	3.636	5.909	6.797	5.001	5.958	5.509
KHOU	9.206	9.431	9.849	9.632	7.281	6.201	7.249	6.563	8.654	11.299	10.373	10.161	8.825
KFTY	5.662	11.162	6.323	9.370	7.613	3.577	4.236	3.713	5.245	7.585	8.483	7.379	6.696

Table 5-6 illustrates mean monthly distributions simulated by the MM5I with CCSM contemporary boundary conditions. Note that the yellow-highlighted cells denote the months in which the seasonal minimum winds occurred during, and the coral-colored cells represent the seasonal maximum. The seasonal minimum winds tend to occur during June, July, and August, which matches with climatological research as previously mentioned (Klink, 1999; NOAA, 2005). The MM5I/CCSM shows variation in the timing of seasonal maximum winds; peak winds occur during January and February at five out of the seven cities. The remaining cities peak during October and December in Houston, TX (KHOU), and Lafayette, IN (KLAF), in turn.

Table 5-7. Mean monthly distributions simulated by the WRFG with CCSM boundary conditions Yellow-highlighted cells represent the seasonal minimum winds; coral-highlighted cells represent the seasonal maximum in m s^{-1} .

WRFG/CCSM Contemporary	Jan	Feb	Mar	Apr	May	Jun	Jul	Aug	Sep	Oct	Nov	Dec	Total
KMCW	6.326	7.562	6.557	6.200	5.212	3.018	2.547	3.110	3.410	6.053	5.220	6.856	5.173
KLAF	7.315	10.064	6.744	6.097	5.342	3.690	3.735	3.645	4.709	6.105	4.575	6.972	5.749
KHSI	7.071	8.061	6.744	6.497	6.795	4.973	4.994	4.500	4.457	5.458	5.977	5.698	5.935
KLBL	5.733	5.595	5.642	5.165	5.167	2.726	2.668	2.572	3.408	4.025	4.826	3.748	4.273
KJMS	5.726	8.707	5.604	6.283	5.337	5.304	4.467	5.243	5.277	6.327	5.012	4.877	5.680
KHOU	9.493	9.663	10.244	9.625	7.930	6.741	6.183	6.623	6.793	11.578	11.815	10.171	8.905
KFTY	8.844	8.525	7.857	6.856	6.394	5.260	5.767	6.385	7.886	9.589	10.151	10.119	7.803

Table 5-7 illustrates mean monthly distributions simulated by the WRFG with CCSM contemporary boundary conditions.

Similar to Table 5-6, this model combination simulates seasonal minimum winds during the months of June, July, and August at six out of the seven cities. The one exception to this is at Hastings, NE, where the seasonal minimum winds occur during August and September. More than one month is highlighted, and thus, also categorized to be a seasonal minimum because September's mean was $\leq 0.10 \text{ m s}^{-1}$ different from the month of August. Seasonal peak winds occurred during November through March, which only partially matches results found in the ASOS observational data (Section 2.3.4 and Chapter 4) where seasonal maximum winds were found to occur during March, April, and May. The same can be said for the findings of Takle, Brown, and Davis (1976) and Klink (1999) at Mason City, IA, as well as Jamestown, ND. Comparisons of seasonal trends with results of Takle, Brown, and Davis (1976) as well as Klink (1999) can only be made for locations in the upper Midwest (Minnesota, North Dakota, and Iowa), because that is where the studies were performed.

Table 5-8. Mean monthly distributions simulated by the CRCM with CCSM boundary conditions. Yellow-highlighted cells represent seasonal minimum winds; coral-highlighted cells represent the seasonal maximum in m s^{-1} .

CRCM/CCSM Contemporary	Jan	Feb	Mar	Apr	May	Jun	Jul	Aug	Sep	Oct	Nov	Dec	Total
KMCW	3.538	3.049	3.431	2.374	2.508	2.851	2.267	2.161	3.184	2.945	3.345	3.710	2.947
KLAF	3.227	2.540	4.479	2.374	2.061	1.719	2.277	2.439	3.660	3.365	2.795	2.719	2.805
KHSI	5.279	4.473	5.314	4.453	3.303	2.861	2.978	2.755	3.173	4.356	4.837	5.667	4.121
KLBL	3.895	4.765	3.849	4.329	3.379	2.280	2.691	2.685	2.906	3.826	4.287	5.218	3.676
KJMS	9.851	6.321	8.807	7.282	5.577	4.608	6.003	4.549	6.438	7.683	7.402	7.117	6.803
KHOU	8.761	8.979	11.819	8.823	6.073	5.382	6.247	5.496	6.691	6.353	9.047	11.305	7.915
KFTY	9.950	8.727	12.025	7.381	6.554	7.153	5.933	8.005	9.686	9.460	8.510	9.921	8.609

Table 5-8 illustrates mean monthly distributions simulated by the CRCM with CCSM contemporary boundary conditions.

Seasonal minimum winds occur during June, July, and August, which follows previous findings in Chapter 4. Seasonal winds peak during December, January, and March, which shows that the seasonal winds are at their maximum several months too early compared to results of observational data in Chapter 4.

A noteworthy feature about this model simulation is the small variation in monthly mean wind speeds at Mason City, IA, and Lafayette, IN. The variance among the months at Mason City, IA, for the CRCM/CCSM is 0.273, whereas, it is 2.37 and 2.96 with the MM5I/CCSM and WRFG/CCSM respectively. At Lafayette, IN, the seasonal variance simulated by the MM5I/CCSM (0.539) is less than the variance simulated by the CRCM/CCSM (0.585); however, the WRFG/CCSM's seasonal variance is 3.56, which is significantly larger. At the remaining five locations, the variance among the months is more consistent between model scenarios.

Table 5-9. Mean monthly distributions simulated by the CRCM with CGCM3 boundary conditions. Yellow-highlighted cells represent seasonal minimum winds; coral-highlighted cells represent the seasonal maximum in m s^{-1} .

CRCM/CGCM3		Jan	Feb	Mar	Apr	May	Jun	Jul	Aug	Sep	Oct	Nov	Dec	Total
Contemporary														
KMCW	2.489	2.693	2.780	2.458	2.422	2.241	1.817	2.020	2.297	2.964	3.802	3.291	2.606	
KLAF	3.690	2.920	3.867	2.354	2.096	2.407	1.421	1.805	3.634	4.307	4.487	4.245	3.103	
KHSI	5.621	4.758	4.209	3.902	3.973	3.127	2.787	2.601	2.988	4.383	6.458	5.778	4.215	
KLBL	5.430	4.282	4.571	3.540	3.602	3.071	2.257	2.437	2.611	4.312	6.184	5.116	3.951	
KJMS	7.899	6.419	7.672	5.710	5.070	5.308	4.035	5.039	4.839	6.861	9.782	11.683	6.693	
KHOU	11.883	10.477	11.369	8.594	7.401	6.509	5.173	6.222	6.318	9.353	12.118	11.978	8.950	
KFTY	11.202	10.617	10.847	8.892	6.972	7.186	4.029	5.950	10.247	11.444	11.122	12.701	9.267	

Table 5-9 illustrates mean monthly distributions simulated by the CRCM with CGCM3 contemporary boundary conditions.

There appears to be an agreement in the timing of seasonal maximum and minimum winds among the seven cities, which is a feature that has not been observed by the other model combinations. The CRCM/CGCM3 simulates winds to be at their seasonal minimum during July and August, and maximum during November and December. This only partially fits with previous research and findings from this study, because the timing of winds to peak seasonally is during November and December, when climatologically, they have been shown to occur during March, April, and May. Evidently the seasonal distributions produced by this RCM/GCM combination do not resemble the other model scenarios (MM5I/CCSM, WRFG/CCSM, and CRCM/CCSM), which could infer that the GCM plays a large role in these monthly mean values.

Overall, these model scenarios appear to simulate the general timing of seasonal minimum winds (June, July, and August), whereas, they do not simulate the seasonal maximum winds with as much accuracy (March, April, and May).

5.4 Future scenario model simulations

5.4.1 Surface wind speed distributions

Similarly to the methodology in Section 5.3, the full period (2038-2070) for the future scenario will be analyzed because there is no statistically significant difference in the spin-up data compared to the full period.

Table 5-10. RCM/GCM Future model scenario calculated percentiles: 10th, 90th, 95th, 99th, 99.9th, and overall mean. Mean winds reported in m s⁻¹ and linear regression in m s⁻¹ yr⁻¹.

Future Scenario Model Output
Percentiles (2038-2070)

		10 th	90 th	95 th	99 th	99.9 th	Mean
KMCW	MM5I/CCSM	0.002 / 0.438	5.330 / 0.009	6.226 / -0.003	7.576 / 0.014	9.061 / .028	2.813 / 0.010
	WRFG/CCSM	1.623 / 0.002	9.894 / -0.028	11.937 / -0.016	15.548 / 0.006	18.743 / 0.073	5.079 / -0.008
	CRCM/CCSM	0.895 / -0.008	5.180 / 0.001	6.048 / 0.001	7.746 / 0.001	9.454 / 0.028	2.823 / 0.002
KLAF	CRCM/CGCM3	0.509 / -0.002	4.065 / -0.005	4.682 / -0.005	5.884 / -0.004	6.931 / 0.008	2.263 / -0.003
	MM5I/CCSM	0.742 / 0.015	5.401 / 0.017	6.121 / 0.015	7.419 / 0.003	8.616 / -0.021	3.036 / 0.016
	WRFG/CCSM	1.932 / 0.004	10.124 / -0.007	12.242 / -0.004	16.107 / -0.012	19.091 / 0.020	5.482 / 0.002
KHSI	CRCM/CCSM	0.638 / 0.000	5.312 / -0.006	6.221 / -0.007	7.884 / 0.000	9.450 / 0.009	2.818 / -0.002
	CRCM/CGCM3	0.557 / -0.001	3.741 / -0.001	4.355 / -0.002	5.560 / -0.005	6.715 / -0.008	2.079 / -0.002
	MM5I/CCSM	0.442 / 0.003	5.832 / 0.000	7.133 / -0.002	10.108 / -0.014	12.520 / -0.033	2.944 / 0.003
KLBL	WRFG/CCSM	1.791 / -0.001	8.825 / -0.003	10.140 / -0.003	13.096 / -0.014	16.852 / -0.036	5.139 / -0.002
	CRCM/CCSM	0.750 / -0.001	8.120 / -0.003	9.552 / 0.001	12.273 / -0.005	15.048 / -0.034	4.237 / 0.000
	CRCM/CGCM3	0.599 / 0.001	5.626 / 0.002	6.508 / 0.004	8.357 / 0.006	10.546 / 0.003	3.233 / 0.001
KJMS	MM5I/CCSM	0.388 / 0.004	4.988 / 0.011	5.798 / 0.010	7.274 / 0.013	8.709 / 0.006	2.711 / 0.007
	WRFG/CCSM	1.324 / 0.001	6.458 / 0.004	7.682 / 0.004	10.034 / 0.012	12.363 / 0.023	3.596 / 0.001
	CRCM/CCSM	1.077 / 0.001	7.282 / 0.008	8.689 / 0.011	11.111 / 0.016	13.430 / -0.005	3.852 / 0.002
KJMS	CRCM/CGCM3	0.943 / -0.436	5.010 / -0.050	5.777 / -0.011	7.337 / -0.008	8.891 / 0.003	2.929 / -0.004
	MM5I/CCSM	0.912 / 0.005	7.406 / 0.003	8.583 / 0.001	10.658 / -0.007	12.599 / -0.007	3.927 / 0.002
KJMS	WRFG/CCSM	2.136 / -0.001	9.243 / -0.011	10.621 / -0.013	12.924 / -0.014	15.922 / -0.028	5.471 / -0.003

Table 5-10 continued

	CRCM/CCSM	2.030 / 0.002	13.085 / -0.012	14.733 / -0.014	17.738 / -0.025	20.936 / 0.003	7.182 / -0.006
	CRCM/CGCM3	1.576 / 0.007	10.005 / 0.009	11.650 / 0.005	14.381 / -0.002	16.798 / -0.014	5.472 / 0.005
KHOU	MM5I/CCSM	3.351 / -0.002	9.648 / 0.012	10.759 / 0.012	13.020 / -0.023	14.878 / -0.035	6.465 / 0.002
	WRFG/CCSM	3.890 / -0.008	14.271 / -0.021	16.017 / -0.024	19.062 / -0.028	22.440 / -0.032	8.696 / -0.012
	CRCM/CCSM	3.150 / -0.003	13.558 / -0.008	15.345 / -0.010	18.623 / -0.001	21.959 / -0.012	8.062 / -0.007
	CRCM/CGCM3	2.781 / 0.693	10.552 / 0.010	11.738 / 0.006	13.932 / 0.010	16.463 / 0.028	6.364 / -0.003
KFTY	MM5I/CCSM	1.141 / 0.022	7.087 / 0.022	8.248 / 0.020	10.859 / -0.023	13.281 / -0.046	4.048 / 0.022
	WRFG/CCSM	3.319 / 0.006	14.017 / -0.013	15.898 / -0.010	19.141 / -0.006	22.343 / 0.008	8.273 / -0.003
	CRCM/CCSM	3.068 / -0.002	14.898 / -0.017	16.813 / -0.006	20.494 / 0.017	23.920 / 0.033	8.697 / -0.010
	CRCM/CGCM3	0.638 / 0.000	5.312 / -0.006	6.221 / -0.007	7.884 / 0.000	9.450 / 0.009	2.818 / -0.002

The format of Table 5-10 is similar to that of Table 5-5 in Section 5.3.1, such that the 10th, 90th, 95th, 99th, and 99.9th percentiles are calculated (m s^{-1}) as well as the overall mean values (m s^{-1}). This table also provides linear regression values for each model at each city. Notice the following unusually large linear regression values in the 10th percentile: 0.438 by the MM5I/CCSM at Mason City, and -0.436 at Liberal, KS, and 0.693 at Houston, TX, by the CRCM/CGCM3. These peculiarly large linear regression values could indicate model error and should be looked into further.

5.4.2 “Extreme” high winds represented by models

Referring to Table 5-10, the WRFG/CCSM simulates the highest winds at the 90th percentile at four of the seven locations. At the 99.9th percentile, this climate model also simulates the highest wind speeds at four of the seven locations compared to the other model combinations. The CRCM/CCSM projects the lowest wind speed values at the 90th percentile at four of the seven cities.

5.4.3 “Extreme” low winds represented by models

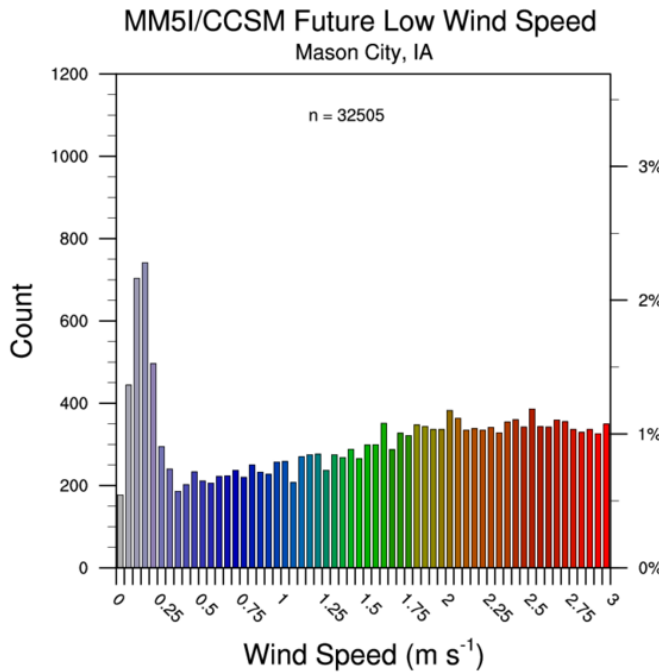


Figure 5-9. Low-end winds ($\leq 3 \text{ m s}^{-1}$) simulated by the MM5I/CCSM at Mason City, IA

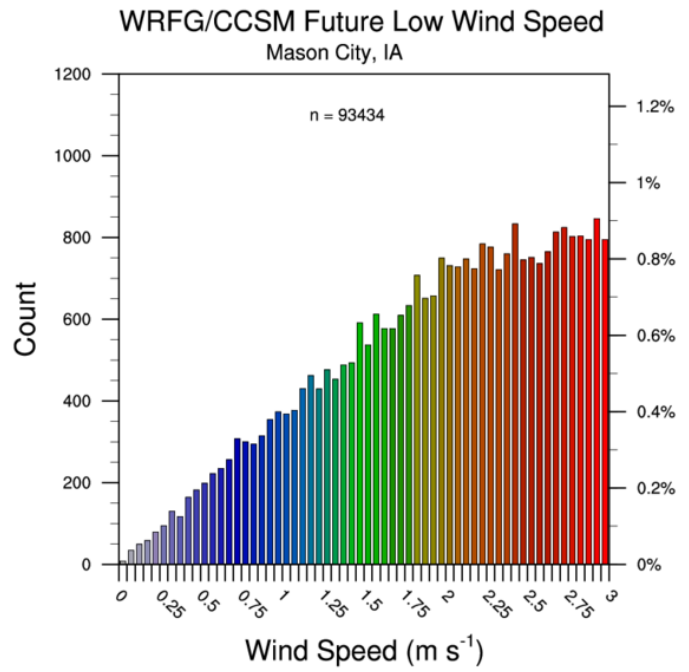


Figure 5-10. Low-end winds ($\leq 3 \text{ m s}^{-1}$) simulated by the WRFG/CCSM at Mason City, IA

As mentioned in Section 5.3.3, a unique characteristic is observed within the MM5I/CCSM (both contemporary and future scenarios), which is not found in any of the other model combinations. Figure 5-9 shows this peculiar feature within the future scenario of the MM5I/CCSM at Mason City, IA. To reinforce the peculiarity of this characteristic, Figure 5-10 illustrates yet again, that the other models do not simulate the spike in low-end wind speeds. Refer to Appendix C1-3 for complete sets of low-end wind speed distributions simulated by each of the model combinations at Mason City, IA, Houston, TX, and Atlanta, GA.

5.4.4 Seasonal distributions

The seasonal distributions found in Table 5-11 only partially resemble those found in the contemporary scenario (Table 5-6) such that the seasonal minimum winds occur during June, July, and August in the contemporary scenario, and May, July, and August in the future scenario. This shows that the variation in timing of seasonally minimum winds has shifted with time. On the other hand, the winds

peaked during October, December, January, and February during the contemporary scenario, while they occurred during October, November, and January in the future scenario. This difference may suggest that the variation in timing of seasonal peak winds has diminished with time.

Table 5-11. Mean monthly distributions simulated by the MM5I with CCSM boundary conditions. Yellow-highlighted cells represent seasonal minimum winds; coral-highlighted cells represent the seasonal maximum in m s^{-1} .

MM5I/CCSM		Jan	Feb	Mar	Apr	May	Jun	Jul	Aug	Sep	Oct	Nov	Dec	Total
Future														
KMCW		3.967	3.798	3.304	3.102	2.386	3.008	3.095	3.466	3.754	4.495	3.798	3.283	3.455
KLAF		4.190	4.049	3.524	3.650	3.039	3.531	3.111	2.795	3.786	4.155	3.868	3.601	3.608
KHSI		6.144	5.232	5.013	3.531	2.492	3.364	2.158	2.867	4.024	7.014	10.398	6.604	4.903
KLBL		5.326	4.401	4.043	3.537	3.207	3.442	2.592	2.983	2.949	5.215	5.043	4.720	3.955
KJMS		4.765	4.756	4.331	4.355	3.585	4.525	4.195	5.214	5.144	5.937	6.331	4.714	4.821
KHOU		11.752	8.976	6.726	7.459	7.900	7.733	5.378	8.332	7.522	11.284	11.162	10.062	8.690
KFTY		7.627	5.767	6.549	3.486	4.501	4.533	3.785	2.938	4.109	5.510	7.040	4.918	5.064

Output of the WRFG/CCSM future scenario is not similar to those of the contemporary scenario. Table 5-12 displays that seasonal minimum winds occur during February, March, July, August, and September, whereas the seasonal minimum winds during the contemporary scenario did not occur during February or March. Peak winds occur during November and January, unlike the contemporary scenario where they occurred during January and February. This feature suggests that the timing of the peak winds has shifted to earlier months in the year.

Table 5-12. Mean monthly distributions simulated by the WRFG with CCSM boundary conditions. Yellow-highlighted cells represent seasonal minimum winds; coral-highlighted cells represent the seasonal maximum in m s^{-1} .

WRFG/CCSM	Future	Jan	Feb	Mar	Apr	May	Jun	Jul	Aug	Sep	Oct	Nov	Dec	Total
KMCW		6.956	6.136	6.289	4.404	2.824	3.106	2.553	2.814	3.353	5.597	8.958	6.894	4.990
KLAF		8.692	7.854	7.470	4.098	3.349	4.343	3.554	3.265	4.427	5.723	6.108	6.459	5.445
KHSI		5.083	4.778	5.378	6.537	4.671	4.688	4.976	4.949	3.900	5.599	5.856	4.938	5.113
KLBL		5.947	4.482	3.863	4.112	2.900	3.082	3.071	3.203	2.818	3.219	3.884	5.135	3.810
KJMS		5.523	4.362	4.935	5.001	4.628	5.054	4.552	4.947	4.650	6.705	7.228	5.777	5.280
KHOU		12.906	10.547	7.223	8.509	8.553	7.303	5.156	7.199	7.151	10.090	11.566	10.980	8.932
KFTY		12.470	10.291	9.616	7.838	6.953	7.561	5.674	5.663	7.116	10.300	11.951	10.410	8.820

Table 5-13 displays mean monthly distributions simulated by the CRCM with CCSM future boundary conditions. This simulation shows that winds were at a seasonal minimum primarily during July, August, and September, as well as February and March, which shows that the timing of these winds occur slightly later in the year than observational results (Section 4.2.1). This also shows the occurrence of low winds during months that winds typically peak (February and March). Furthermore, Table 5-13 shows that winds peak during November and January, which is earlier in the year than previous research has shown.

22

Comparing these results to those from the contemporary scenario (Table 5-8), it appears that the variance in timing of seasonal maximum winds has shifted from December, January, and February to occurring during just November and January. The seasonal minimum winds occur later in the year during the future scenario compared to the contemporary scenario, with the exception of the minimum winds during February at Jamestown, ND, and March at Houston, TX.

Table 5-13. Mean monthly distributions simulated by the CRCM with CCSM boundary conditions. Yellow-highlighted cells represent seasonal minimum winds; coral-highlighted cells represent the seasonal maximum in m s^{-1} .

CRCM/CCSM		Jan	Feb	Mar	Apr	May	Jun	Jul	Aug	Sep	Oct	Nov	Dec	Total
Future														
KMCW		2.582	2.915	3.263	3.361	2.528	1.957	1.773	2.258	3.304	2.858	2.646	3.382	2.736
KLAF		2.538	3.142	2.627	3.516	2.607	1.831	1.664	1.895	3.501	3.924	3.860	3.584	2.891
KHSI		3.160	4.641	5.009	4.990	3.501	2.733	2.984	2.812	4.458	4.613	5.128	5.042	4.089
KLBL		4.943	4.252	4.452	4.678	3.041	2.897	2.899	2.498	3.215	4.110	3.785	3.676	3.704
KJMS		6.175	7.842	7.858	9.153	5.644	4.922	4.198	5.030	8.456	9.355	8.443	12.428	7.459
KHOU		8.717	10.737	6.804	8.779	5.852	6.598	7.191	8.064	8.282	8.502	8.338	8.531	8.033
KFTY		10.387	10.340	8.591	8.022	6.534	4.540	5.905	6.640	9.802	10.358	9.751	11.687	8.546

Table 5-14. Mean monthly distributions simulated by the CRCM with CGCM3 boundary conditions. Yellow-highlighted cells represent seasonal minimum winds; coral-highlighted cells represent the seasonal maximum in m s^{-1} .

CRCM/CGCM3		Jan	Feb	Mar	Apr	May	Jun	Jul	Aug	Sep	Oct	Nov	Dec	Total
Future														
KMCW		3.882	3.246	3.010	2.870	2.551	2.753	1.989	2.450	3.053	2.926	3.644	3.722	3.008
KLAF		4.267	3.556	3.179	2.522	3.283	2.294	1.857	2.128	3.814	4.087	4.805	2.600	3.199
KHSI		5.957	5.443	4.434	3.886	4.016	3.267	3.097	3.207	4.136	4.625	7.710	5.438	4.601
KLBL		4.736	6.219	4.796	3.223	3.343	3.256	2.552	3.045	4.097	3.708	6.079	4.754	4.151
KJMS		11.587	7.849	6.395	6.839	6.443	6.556	5.281	5.066	6.331	8.014	11.360	8.847	7.547
KHOU		10.220	12.902	9.937	6.417	8.786	7.638	5.715	8.216	8.987	9.431	11.653	10.706	9.217
KFTY		11.840	11.334	9.943	7.255	9.080	7.388	5.934	6.559	9.256	10.789	13.248	10.926	9.463

Finally, the CRCM/CGCM3 future scenario showed seasonal minimum winds consistently during July, and seasonal maximum winds occurring primarily during January and February (Table 5-14). The exception to this observation is that the mean monthly winds at Atlanta, GA, peaked during November. The output of the CRCM/CGCM3 future scenarios strongly

resemble those of Table 5-9, where there is little variation in timing of the seasonal maximum and minimum winds throughout each of the locations.

5.5 Model compared to observational data

5.5.1 RCM/NCEP models compared to observational data

Table 5-16. Comparison of RCM/NCEP model data with observational data over 1979-2004. Actual error in m s^{-1} and percent error = $[(\text{Model/Obs}) - 1] \times 100\%$ are displayed for each location.

RCM/NCEP and Observational Comparison							
		10 th	90 th	95 th	99 th	99.9 th	Mean
KMCW	MM5I	-1.09 / -53.89	-2.27 / -25.39	-2.09 / -20.89	-1.98 / -15.70	-2.33 / -13.88	-1.43 / -28.11
	WRFG	-0.48 / -23.00	0.18 / 2.23	1.05 / 10.63	1.99 / 15.83	2.03 / 13.92	-0.45 / -8.74
	CRCM	-1.46 / -72.69	-4.95 / -55.51	-5.32 / -52.99	-6.87 / -54.46	-9.00 / -56.33	-2.77 / -54.42
KLAF	MM5I	-0.17 / -49.85	-0.58 / -7.84	-0.12 / -1.41	0.33 / 3.21	0.35 / 3.07	-0.49 / -11.44
	WRFG	0.65 / 4.16	2.84 / 40.10	4.07 / 51.25	5.30 / 52.82	5.43 / 41.84	1.36 / 34.36
	CRCM	-0.50 / -65.97	-3.40 / -47.14	-3.59 / -44.86	-4.57 / -45.01	-6.43 / -48.43	-1.94 / -47.77
KHSI	MM5I	-1.04 / -51.55	3.78 / 44.87	4.73 / 47.63	5.89 / 46.26	4.94 / 30.98	0.43 / 9.17
	WRFG	-0.54 / -26.58	-1.13 / -12.75	-1.51 / -14.73	-1.95 / -14.94	-3.30 / -18.05	-0.87 / -15.87
	CRCM	-1.44 / -70.30	-3.14 / -36.22	-3.90 / -38.43	-5.04 / -38.97	-7.56 / -43.96	-2.08 / -39.53
KLBL	MM5I	-0.38 / -61.86	-0.88 / -8.40	-0.30 / -2.16	0.37 / 3.76	0.04 / 0.82	-0.67 / -12.00
	WRFG	0.03 / -40.55	-3.21 / -33.12	-3.48 / -31.91	-4.56 / -32.49	-6.56 / -36.81	-1.48 / -28.45
	CRCM	-0.42 / -60.93	-4.64 / -48.41	-5.20 / -48.01	-6.64 / -47.65	-8.68 / -48.87	-2.20 / -43.04
KJMS	MM5I	-0.79 / -33.49	-0.54 / -6.02	-0.28 / -14.29	-0.36 / -2.70	-0.75 / -3.85	-0.53 / -9.46
	WRFG	-0.39 / -15.77	-1.22 / -13.51	-1.26 / -22.91	-1.86 / -14.58	-3.16 / -19.69	-0.69 / -12.49
	CRCM	-0.71 / -29.10	0.49 / 5.64	1.08 / -2.30	1.47 / 12.06	0.49 / 3.43	-0.05 / -0.50
KHOU	MM5I	2.72 / 130.86	5.95 / 87.59	6.70 / 88.83	7.77 / 82.75	8.00 / 66.89	4.23 / 117.39
	WRFG	3.03 / 160.22	6.82 / 100.41	7.64 / 101.30	8.55 / 91.02	8.35 / 69.31	4.88 / 134.58
	CRCM	2.00 / 79.72	3.69 / 54.53	4.10 / 54.43	4.42 / 47.44	3.56 / 30.45	2.67 / 74.59
KFTY	MM5I	1.23 / N/A	5.02 / 97.21	6.23 / 102.62	8.63 / 111.99	9.53 / 91.64	2.69 / 115.07
	WRFG	3.15 / N/A	8.30 / 160.01	9.07 / 148.92	10.64 / 137.27	10.14 / 97.58	5.65 / 238.50
	CRCM	2.38 / N/A	6.05 / 116.99	6.72 / 110.47	8.14 / 105.44	7.28 / 70.88	3.99 / 169.74

Table 5-16 compares RCM model data with NCEP boundary conditions to observation data over the years of 1979-2000. The comparisons are completed through calculating the actual difference in m s^{-1} between the model and observational data as well as finding the percent error (bias) (% error = $[(\text{Model/Obs}) - 1] \times 100\%$). Although our record of observational data begins in 1973, we will only analyze data from 1979 onward because the RCM/NCEP dataset does not initialize until 1979. While comparing the model output to observational data, it is clear that there is large variance among the models and locations. Note that the percent error calculation at the 10th percentile at Atlanta, GA, are marked “N/A”, which is because the percentile value was 0.00 m s^{-1} and, thus, leaves the calculation invalid.

At the 10th percentile, the majority of locations display a negative magnitude difference with the exception of at Houston, TX, and Atlanta, GA, with each of the models as well as at Liberal, KS (0.03 m s^{-1}) and Lafayette, IN (0.65 m s^{-1}) by the WRFG. This means that the climate models with NCEP boundary conditions have an overall positive bias compared to the observational data we analyzed in Chapter 4.

Looking at the high-end winds (90th, 95th, 99th, and 99.9th percentiles), the majority of trends in actual and percent error are ambiguous throughout the locations aside from Mason City, IA, Houston, TX, and Atlanta, GA. At Mason City, IA, the MM5I displays a negative bias, with percent error values ranging from -13.9% at the 99.9th percentile to -25.4% at the 90th percentile. The CRCM also shows a considerable negative bias, with percent error ranging from -53.0% at the 95th percentile to -56.3% at the 99.9th percentile. The only model to display a positive bias at this location is the WRFG, with percent error values ranging from 2.23% at the 90th percentile to as large as 15.8% at the 99th percentile. Evaluating the model error at Houston, TX, and Atlanta, GA, it is evident that all of the models have a positive bias. These are the only two locations that unanimously show a high bias, such that all of the models over-estimate the wind speeds throughout all of the percentiles.

5.5.2 RCM/GCM contemporary model scenarios compared to observational data

Table 5-17. Comparison of RCM/GCM contemporary model scenario output to observational data over 1973-2000. Actual error in m s⁻¹ and percent error = [(Model/Obs) - 1] x 100% are displayed for each location.

Contemporary Climate Model Scenarios and Observational Comparison

		10 th	90 th	95 th	99 th	99.9 th	Mean
KMCW	MM5I/CCSM	-0.89 / -45.92	-1.81 / -20.45	-1.86 / -18.47	-1.75 / -13.98	-1.92 / -12.26	-0.96 / -19.59
	WRFG/CCSM	-0.22 / -11.26	1.83 / 20.68	2.63 / 26.04	3.84 / 30.65	4.12 / 26.31	0.47 / 9.61
	CRCM/CCSM	-0.22 / -11.26	1.83 / 20.68	2.63 / 26.04	3.84 / 30.65	4.12 / 26.31	0.52 / 10.55
	CRCM/CGCM3	-1.40 / -71.90	-4.66 / -52.73	-5.26 / -52.20	-6.47 / -51.71	-8.60 / -54.93	-2.55 / -52.18
KLAF	MM5I/CCSM	0.24 / 28.78	0.47 / 6.75	1.12 / 14.34	1.96 / 19.74	2.21 / 17.08	0.30 / 7.92
	WRFG/CCSM	1.17 / 138.10	4.22 / 60.32	5.70 / 73.16	7.44 / 75.05	8.13 / 62.84	2.05 / 53.92
	CRCM/CCSM	-0.17 / -20.02	-1.64 / -23.39	-1.56 / -20.00	-2.06 / -20.83	-3.49 / -26.99	-0.93 / -24.35
	CRCM/CGCM3	-0.27 / -31.32	-3.17 / -45.28	-3.34 / -42.91	-4.25 / -42.87	-6.14 / -47.49	-1.68 / -44.00
KHSI	MM5I/CCSM	-0.48 / -27.96	5.78 / 69.00	6.85 / 69.74	7.84 / 61.61	7.93 / 48.86	1.53 / 30.65
	WRFG/CCSM	0.21 / 12.32	1.02 / 12.22	1.15 / 11.72	1.50 / 11.76	2.18 / 13.42	0.47 / 9.40
	CRCM/CCSM	-0.92 / -53.34	-0.38 / -4.51	-0.43 / -4.43	-0.66 / -5.18	-1.52 / -9.37	-0.77 / -15.56
	CRCM/CGCM3	-1.02 / -59.05	-2.62 / -31.25	-3.08 / -31.40	-3.95 / -31.07	-5.12 / -31.55	-1.64 / -32.96
KLBL	MM5I/CCSM	-0.23 / -17.43	0.19 / 1.99	0.84 / 7.63	1.68 / 11.99	1.63 / 9.15	-0.06 / -1.26
	WRFG/CCSM	0.00 / 0.35	-2.92 / -30.21	-2.99 / -27.09	-3.78 / -26.88	-5.74 / -32.16	-1.28 / -25.69
	CRCM/CCSM	-0.21 / -15.54	-2.22 / -22.96	-2.23 / -20.19	-2.87 / -20.45	-4.61 / -25.84	-1.03 / -20.73
	CRCM/CGCM3	-0.62 / -46.71	-3.90 / -40.40	-4.29 / -38.89	-5.28 / -37.59	-6.74 / -37.75	-1.65 / -33.02
KJMS	MM5I/CCSM	-0.55 / -25.09	-0.16 / -1.72	1.39 / 15.85	0.00 / -0.02	-0.26 / -1.61	0.02 / 0.41
	WRFG/CCSM	-0.02 / -0.97	0.78 / 8.65	2.51 / 28.51	1.42 / 11.07	1.34 / 8.43	0.65 / 12.76
	CRCM/CCSM	-0.12 / -5.70	3.97 / 43.96	5.83 / 66.35	4.62 / 36.08	4.56 / 28.62	2.17 / 42.72
	CRCM/CGCM3	-0.62 / -28.18	1.26 / 13.98	3.18 / 36.14	2.57 / 20.05	2.26 / 14.18	0.54 / 10.73
KHOU	MM5I/CCSM	3.26 / 576.44	7.01 / 103.29	7.82 / 102.99	8.99 / 94.99	9.31 / 75.84	5.05 / 144.40
	WRFG/CCSM	3.44 / 607.59	7.75 / 114.12	8.66 / 114.17	10.05 / 106.2	10.87 / 88.58	5.41 / 154.54
	CRCM/CCSM	2.61 / 460.89	7.26 / 106.85	8.21 / 108.24	9.56 / 100.98	10.02 / 81.67	4.80 / 137.29
	CRCM/CGCM3	2.23 / 393.48	3.87 / 56.97	4.33 / 57.02	4.94 / 52.19	4.68 / 38.12	2.99 / 85.49
KFTY	MM5I/CCSM	1.89 / N/A	7.44 / 143.44	9.04 / 149.52	12.10 / 156.3	13.87 / 130.0	4.24 / 183.44
	WRFG/CCSM	3.37 / N/A	8.83 / 170.25	9.77 / 161.61	11.21 / 144.7	11.25 / 105.5	6.06 / 262.16
	CRCM/CCSM	3.10 / N/A	9.86 / 190.07	10.86 / 179.57	12.86 / 166.0	13.33 / 125.0	6.51 / 281.30
	CRCM/CGCM3	2.42 / N/A	6.59 / 127.12	7.30 / 120.74	9.05 / 116.88	9.31 / 87.30	4.34 / 187.69

Table 5-17 compares contemporary model data to observation data over the years of 1973-2000.

The comparisons are completed through calculating the actual error in m s^{-1} between the model and observational data as well as finding the percent error (bias) ($\% \text{ error} = [(\text{Model}/\text{Obs}) - 1] \times 100\%$).

Although the contemporary model data initializes at the year 1968, we are only comparing data from 1973 onward because that is when our observational record begins. Similar to Table 5-16, the percent error calculations at the 10th percentile at Atlanta, GA, are marked “N/A” which is because of a 0.00 m s^{-1} percentile value and leaves the calculation invalid.

Fairly similar trends in error are found in Table 5-17 as in 5-16, such that at the percentiles, there is a general negative bias amongst the majority of locations except Houston, TX, and Atlanta, GA, which have positive errors. Interestingly enough, the CGCM3 appears to be introducing additional error into the contemporary scenario. This feature is visible while comparing the mean wind speeds of the CRCM with NCEP boundary conditions in Table 5-16 to the CRCM/CCSM and CRCM/CGCM3 in Table 5-17, specifically at Mason City, IA. The percent error associated with the CRCM with NCEP reanalysis data is -54.4% and -52.2% for the CRCM/CGCM3; however, when you compare these values to those of the CRCM/CCSM (10.6%), it is clear that the CGCM3 is responsible for introducing significant error into the contemporary scenario. The same observation is seen throughout Lafayette, IN, Hastings, NE, and Liberal, KS, in the mean winds.

5.6 Contemporary and future scenario comparison

5.6.1 Surface wind speed distributions

Finally, we will evaluate the compare and contrast the contemporary and future scenarios. Table 5-18 displays the percent difference between the future and contemporary scenarios at various percentiles 10th, 90th, 95th, 99th, and 99.9th for each of the model combinations: MM5I/CCSM, WRFG/CCSM,

CRCM/CCSM, and CRCM/CGCM3. To test whether the future and contemporary scenarios were statistically different, an independent, two-tailed T-Test at a 95th significance level was used. Results of this hypothesis test are displayed in Table 5-18, where the highlighted cells represent models that simulated statistically and significantly different values. Bright yellow cells denote significant with a 0.01 significance level, and light yellow represent a 0.05 significance level.

Table 5-18. Comparison of contemporary and future scenarios for the various climate models. Percent difference calculations are provided for each of the model combinations at each of the locations. Percent difference = [(Model/Obs) - 1] x 100%. Statistically different values are highlighted in light yellow (0.05 significance level) and bright yellow (0.01).

		Percent Difference Between Future and Contemporary Scenarios Percentiles					
Site ID	Model	10 th	90 th	95 th	99 th	99.9 th	Mean
KMCW	MM5I/CCSM	-60.09	-24.49	-24.88	-29.18	-32.71	-28.54
	WRFG/CCSM	-5.82	-7.21	-6.07	-4.90	-5.19	-5.34
	CRCM/CCSM	-5.82	-7.21	-6.07	-4.90	-5.19	-6.15
	CRCM/CGCM3	-6.66	-2.67	-2.85	-2.63	-1.76	-3.30
KLAF	MM5I/CCSM	-32.15	-27.68	-31.31	-37.46	-43.11	-26.15
	WRFG/CCSM	-4.42	-9.74	-9.30	-7.13	-9.37	-6.50
	CRCM/CCSM	-6.03	-0.89	-0.24	0.51	0.06	-2.19
	CRCM/CGCM3	-4.37	-2.30	-2.13	-1.76	-1.14	-2.55
KHSI	MM5I/CCSM	-64.38	-58.78	-57.21	-50.83	-48.20	-54.75
	WRFG/CCSM	-7.49	-6.06	-7.58	-7.88	-8.49	-5.66
	CRCM/CCSM	-6.79	1.57	1.77	1.75	2.26	0.77
	CRCM/CGCM3	-15.22	-2.27	-3.40	-4.68	-5.11	-3.14
KLBL	MM5I/CCSM	-64.50	-49.36	-51.13	-53.77	-55.31	-44.92
	WRFG/CCSM	-0.41	-4.19	-4.42	-2.33	2.08	-2.91
	CRCM/CCSM	-3.71	-2.14	-1.24	-0.59	1.44	-2.51
	CRCM/CGCM3	33.57	-12.97	-14.25	-16.31	-20.00	-12.26
KJMS	MM5I/CCSM	-44.29	-16.53	-15.71	-16.74	-19.69	-22.88
	WRFG/CCSM	-1.34	-5.78	-5.98	-6.78	-7.90	-4.31
	CRCM/CCSM	-1.55	0.67	0.76	1.81	2.09	-0.77
	CRCM/CGCM3	0.34	-2.78	-2.64	-6.44	-7.73	-2.54
	MM5I/CCSM	-12.54	-30.11	-30.16	-29.46	-31.05	-24.37

Table 5-18 continued

KHOU	WRFG/CCSM	-2.95	-1.85	-1.46	-2.34	-3.03	-2.33
	CRCM/CCSM	-0.84	-3.48	-2.90	-2.11	-1.50	-2.86
	CRCM/CGCM3	-0.50	-1.01	-1.50	-3.30	-2.86	-1.90
KFTY	MM5I/CCSM	-39.46	-43.88	-45.34	-45.27	-45.85	-38.26
	WRFG/CCSM	-1.59	-0.01	0.49	1.00	1.98	-1.25
	CRCM/CCSM	-0.95	-0.98	-0.55	-0.51	-0.31	-1.40
	CRCM/CGCM3	-3.47	-2.95	-2.45	-3.11	-3.69	-3.26

Focusing at the 10th percentile, the MM5I simulated a statistically significant difference among all of the locations in this study. This result demonstrates that the MM5I/CCSM unanimously simulates an overall decreasing trend in the low-end winds (10th percentile) ranging from as large as -64.5% at Liberal, KS to a small change of -12.5% at Houston, TX. The remaining climate models show occasional signals of statistically significant trends between the future and contemporary scenarios. Hastings, NE, is the only location to have a unanimous (statistically significant) diminishing trend in wind speeds across all model combinations. On the other hand, Jamestown, ND, and Houston, TX, show the least significant trend (increasing or decreasing) throughout all the models (with the exception of the MM5I/CCSM) at the 10th percentile. The only model to show a statistically significant (with a 0.05 significance level) percent increase between the future and contemporary scenarios is the CRCM/CGCM3 at Liberal, KS.

Looking at the high-end winds, there is a visibly vaguer trend amongst the models and cities as to what trends are being simulated. The MM5I/CCSM displays an undisputed decreasing trend that is statistically significant throughout the 90th, 95th, 99th, and 99.9th percentiles at each of the cities. The WRFG/CCSM shows a significant percent decrease at Mason City, IA, Lafayette, IN, Hastings, NE, and Jamestown, ND. Although statistically insignificant, the WRFG/CCSM simulates a positive trend at two of the three remaining locations (Liberal, KS, and Atlanta, GA).

The overall mean showed significant trends amongst nearly all the cities and climate models (Table 5-18). Mason City, IA, and Atlanta, GA, are the only two cities with a unanimous percent decrease that was statistically significant (with 0.01 or 0.01 significance levels) across all models. More specifically, the MM5I/CCSM simulated the largest magnitude difference (-28.5 and -38.3% respectively) at those two locations.

The percent difference simulated by the MM5I/CCSM is often times as much as one order of magnitude larger than the other climate models. The only other model to simulate a statistically different percent change in the order of 10 is the CRCM/CGCM3 at Hastings, NE, and Liberal, KS. This feature can be seen in Figure 5-10.

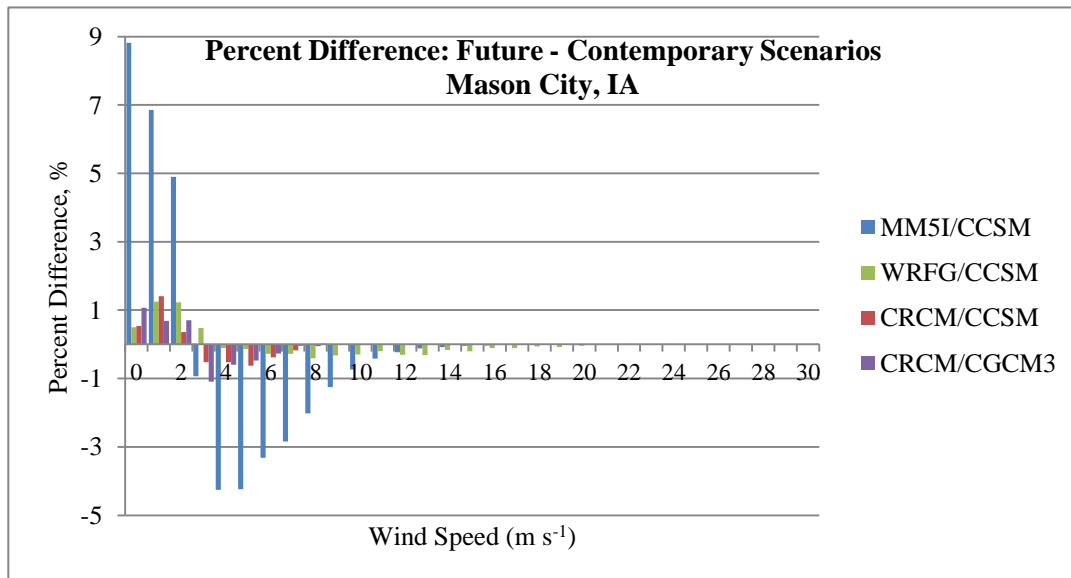


Figure 5-10. Percent difference between the future and contemporary model scenarios at Mason City, IA.

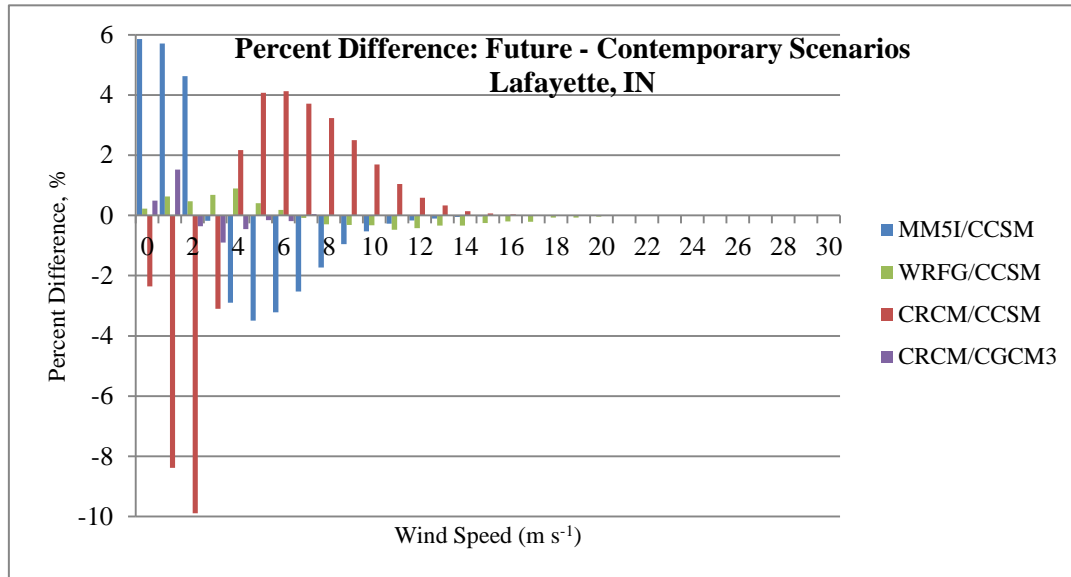


Figure 5-11. Percent difference between the future and contemporary model scenarios at Lafayette, IN.

Figure 5-10 shows the percent difference between the future and contemporary model scenarios at Mason City, IA. This plot includes the MM5I/CCSM, WRFG/CCSM, CRCM/CCSM, and CRCM/CGCM3 model scenarios. There is a general trend among the models that shows an increasing trend in wind speeds $\leq 2 \text{ m s}^{-1}$ and decreasing elsewhere. The MM5I/CCSM (blue) produces the largest magnitude of percent difference across all wind speeds compared to all other model combinations. Aside from the magnitude difference, the models show similar patterns overall regarding the shape of the distribution.

Figure 5-11 shows the percent difference between future and contemporary model scenarios at Lafayette, IN. Similar to results seen in Mason City, IA, the MM5I/CCSM (blue), there is a large (4-6%) increase in winds $\leq 2 \text{ m s}^{-1}$ and decreases elsewhere. A unique feature displayed only at this location is that the CRCM/CCSM (red) simulates a significant decreasing trend in low wind speeds (0.00 to 5.00 m s^{-1}) where the other model scenarios show an increasing trend. The magnitude of the decreasing trend displayed by the CRCM/CCSM is as large as 8 to nearly 10%. This feature is not shown in any other model

scenario or location. Lastly, the WRFG/CCSM (green) displays an increasing trend into larger wind speeds compared to at Mason City, IA, where there is an increase in winds $\leq 6 \text{ m s}^{-1}$ and then decreases elsewhere.

Features in the other five cities are relatively similar to those of Mason City, IA, thus, were not included in the body of the paper. Difference plots of each of the remaining cities are provided in Appendix D.

5.6.3 Seasonal distributions

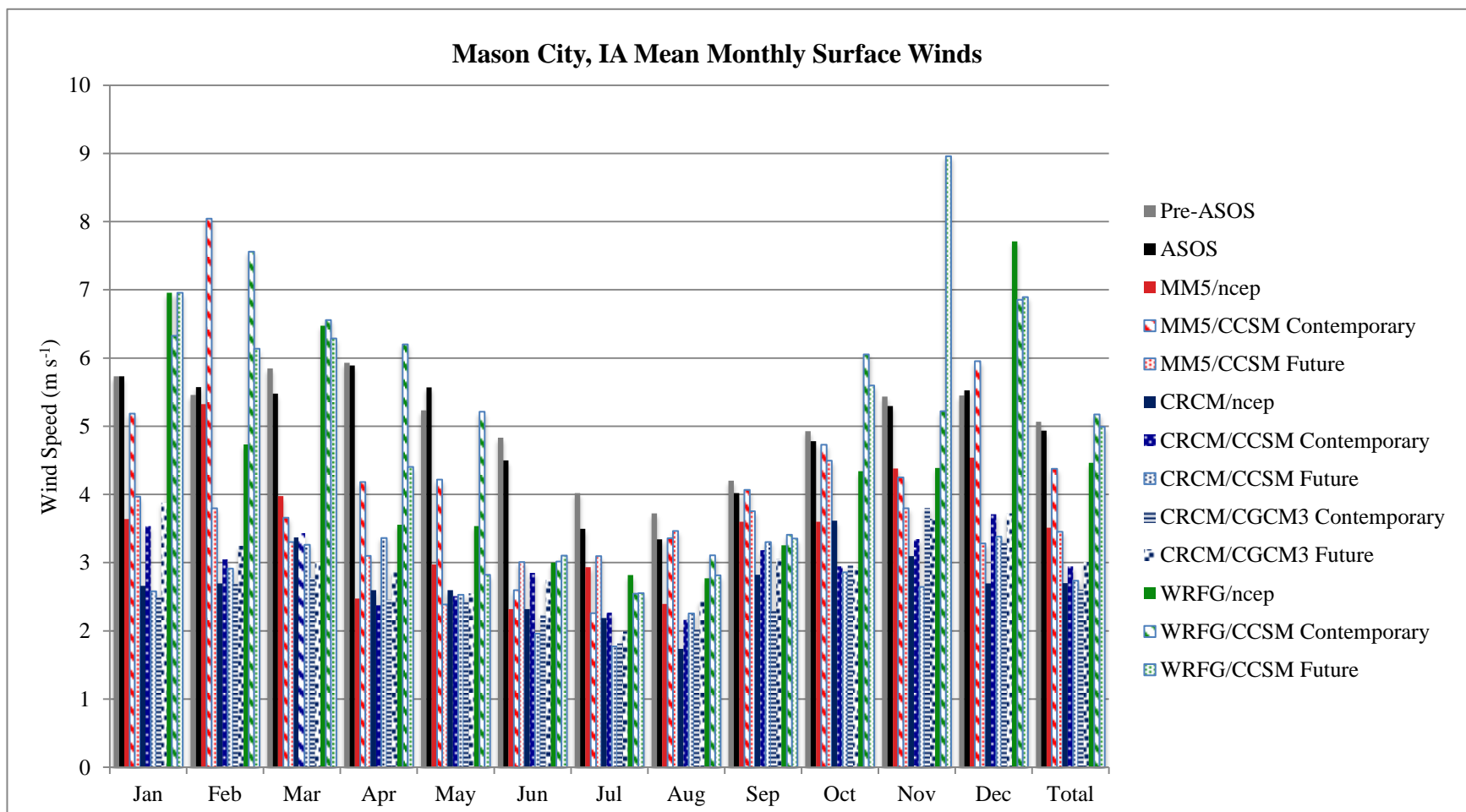


Figure 5-12. Mean monthly surface winds at Mason City, IA. Comparison among observational and various models (NCEP, contemporary, and future).

This section provides insight into the seasonal changes presented between the future and contemporary model scenarios. An overview of model-simulated seasonal trends at Mason City, IA is illustrated in Figure 5-12. This figure also displays observational data. General qualitative inferences that can be drawn from this plot are that wind speeds are generally at their seasonal peak during the months of November, December, February, and March; whereas, winds are seasonally at their lowest in June, July, and August. Seasonal plots with model and observational comparisons for each of the other sites are located in Appendix E. Recall, in Section 5.5.1 and 5.5.2 there was an overall negative bias at each of the locations except (Houston, TX, and Atlanta, GA) between the observational data and the models with NCEP reanalysis data as well as the models in the contemporary scenario. These bias features are visible in Appendix E, particularly so with Houston, TX, and Atlanta, GA, which have a large positive bias.

Furthermore, Table 5-15 gives a quantitative overview of seasonal distributions which are simulated by each of the model scenarios. Mean monthly wind characteristics in model simulations with contemporary and future scenarios were described in Sections 5.3.4 and 5.4.4 respectively.

Table 5-15. Percent difference between mean monthly wind speeds simulated for future and contemporary scenarios.

Difference (Future - Contemporary) % Diff = [(Future/Contemporary) -1] x 100%														
		Jan	Feb	Mar	Apr	May	Jun	Jul	Aug	Sep	Oct	Nov	Dec	Total
MM5I/ CCSM	KMCW	-23.52	-52.79	-9.66	-25.82	-43.46	15.80	37.03	3.20	-7.76	-4.98	-10.68	-44.85	-21.05
	KLAF	12.59	-20.38	-16.58	-9.92	-26.89	42.57	-8.48	-15.04	-10.15	3.03	-10.60	-29.71	-9.98
	KHSI	-30.98	-56.39	-30.99	-66.15	-63.55	-4.39	-10.50	5.43	-20.17	-7.61	42.79	-22.49	-28.69
	KLBL	-38.03	-45.96	-45.39	-37.61	-14.32	0.47	-0.95	21.10	-26.55	-13.27	-25.57	-28.41	-27.50
	KJMS	-31.68	-47.13	-9.68	-25.24	-30.87	19.10	29.75	43.39	-12.94	-12.65	26.59	-20.89	-12.49
	KHOU	27.66	-4.82	-31.71	-22.56	8.49	24.69	-25.81	26.96	-13.08	-0.14	7.61	-0.98	-1.52
	KFTY	34.71	-48.34	3.58	-62.80	-40.88	26.73	-10.63	-20.89	-21.66	-27.35	-17.01	-33.35	-24.38
WRFG/ CCSM	KMCW	9.96	-18.86	-4.08	-28.97	-45.82	2.91	0.22	-9.50	-1.69	-7.54	71.60	0.55	-3.52
	KLAF	18.83	-21.96	10.76	-32.79	-37.30	17.69	-4.85	-10.41	-5.99	-6.27	33.50	-7.37	-5.29
	KHSI	-28.11	-40.73	-20.26	0.62	-31.26	-5.72	-0.36	9.98	-12.50	2.58	-2.02	-13.35	-13.86
	KLBL	3.73	-19.89	-31.54	-20.39	-43.86	13.05	15.08	24.54	-17.31	-20.03	-19.52	36.99	-10.84
	KJMS	-3.53	-49.90	-11.93	-20.40	-13.28	-4.71	1.90	-5.65	-11.88	5.97	44.21	18.45	-7.04
	KHOU	35.95	9.15	-29.49	-11.59	7.85	8.33	-16.60	8.69	5.28	-12.86	-2.11	7.96	0.30
	KFTY	41.00	20.71	22.39	14.33	8.74	43.76	-1.62	-11.31	-9.76	7.42	17.74	2.88	13.04
CRCM/ CCSM	KMCW	-27.01	-4.38	-4.89	41.60	0.80	-31.35	-21.80	4.46	3.78	-2.98	-20.91	-8.82	-7.17
	KLAF	-21.35	23.70	-41.34	48.12	26.47	6.54	-26.92	-22.31	-4.35	16.62	38.09	31.79	3.07
	KHSI	-40.14	3.75	-5.72	12.07	6.00	-4.49	0.21	2.06	40.49	5.91	6.02	-11.03	-0.76
	KLBL	26.89	-10.78	15.67	8.04	-9.99	27.06	7.71	-6.94	10.64	7.43	-11.70	-29.55	0.76
	KJMS	-37.31	24.07	-10.77	25.69	1.19	6.82	-30.07	10.58	31.33	21.75	14.06	74.63	9.64
	KHOU	-0.51	19.59	-42.43	-0.51	-3.64	22.60	15.11	46.72	23.78	33.83	-7.83	-24.54	1.50
	KFTY	4.39	18.48	-28.56	8.69	-0.31	-36.53	-0.48	-17.06	1.20	9.49	14.58	17.79	-0.73
CRCM/ CGCM3	KMCW	56.00	20.51	8.28	16.77	5.35	22.86	9.48	21.30	32.92	-1.28	-4.16	13.11	15.42
	KLAF	15.62	21.78	-17.79	7.12	56.65	-4.67	30.64	17.87	4.95	-5.10	7.07	-38.75	3.11
	KHSI	5.98	14.40	5.37	-0.42	1.08	4.47	11.10	23.31	38.43	5.52	19.38	-5.89	9.15
	KLBL	-12.79	45.22	4.93	-8.95	-7.18	6.03	13.06	24.95	56.89	-14.03	-1.69	-7.07	5.05
	KJMS	46.69	22.28	-16.64	19.75	27.07	23.50	30.88	0.53	30.83	16.80	16.13	-24.28	12.76
	KHOU	-13.99	23.15	-12.60	-25.32	18.72	17.35	10.48	32.04	42.24	0.84	-3.84	-10.61	2.99
	KFTY	5.69	6.75	-8.33	-18.41	30.23	2.81	47.31	10.25	-9.68	-5.73	19.12	-13.97	2.11

There is large variation in percent difference calculations among the seven cities as well as the model scenarios. Our primary focus for this study is on model comparisons, thus, not as much emphasis will be placed on analyzing variation among cities.

There is an increasing trend in mean monthly wind speeds (3.20 to 37.0%) during the months of June, July, and August within the MM5I/CCSM scenarios (Table 5-15). Recall, June, July, and August are typical months where wind speeds are at their seasonal minimum compared to other months. This observation of positive differences during these months could infer that seasonal minimum winds are simulated to increase between the periods of the contemporary and future scenarios (1968-2000 and 2038-2070, respectively). There are exceptions to this trend, such as a percent increase during the month of January at Lafayette, IN, Houston, TX, and Atlanta, GA; an increase during March in Atlanta, GA; last, there was an increase during October at Lafayette, IN and November at Hastings, NE, Jamestown, ND, and Houston, TX. Overall, there is a general negative trend throughout the majority of the months across all cities. Magnitudes of percent differences range from an increase of 37.3% to a decrease of 66.2%.

Overall, the contemporary (Table 5-11 through Table 5-14) and future scenarios (Table 5-11 through Table 5-14) appear to simulate the general timing of seasonal minimum winds (June, July, and August), whereas, they do not simulate the maximum winds with as much accuracy (March, April, and May) (Table 5-6 through Table 5-8).

CHAPTER 6

SUMMARY AND CONCLUSIONS

In this study, we analyzed surface wind speed trends in observational and model data. We focused on “extreme” wind speeds, both at the high and low end as well as seasonal trends. We found that there is a difference in the observational dataset over the period of study as a result of the introduction of automated wind speed measurements in the late 1990s. The primary difference was observed at wind speeds $\leq 1.54 \text{ m s}^{-1}$ (3 kts) where there was an increase (~2.5 – 11 %) in these low winds at all of the cities except at Liberal, KS. However, it is not clear whether the difference in low wind speeds can be completely attributed to the introduction of ASOS instrumentation or if in fact, wind speeds have actually decreased to some degree. Based on the fact that there is a large shift in instrumentation mid-way through the observational dataset, one may make inferences, not conclusions, on the long-term trends of surface wind speeds. Also, we will exercise caution when making conclusions regarding comparisons between observational and model-simulated data.

The main focus of this project was to analyze the simulation of surface wind speeds produced by climate models within the NARCCAP data archive. Initially, we evaluated the output from the MM5I, WRFG, and CRCM with NCEP reanalysis boundary conditions, and then we analyzed the same RCMs, but with contemporary and future scenario boundary conditions. Boundary conditions for the future scenario were comprised of the SRES A2 emissions scenario for the 21st century. This emissions scenario was selected for the NARCCAP data archive based on its high-emission, high-impact projections.

As concluded in Section 5.5.1 and 5.5.2, the NCEP-driven simulations and contemporary climate simulations do contain biases compared to observed data for the same time periods. There is a general negative bias in both the climate models with NCEP reanalysis data as well as the contemporary climate models at all of the locations except Houston, TX, and Atlanta, GA, which shows a positive bias. Appendix E shows an overall depiction of how the observational data compares with each of the model scenarios. Additionally, it is clear that the CGCM3 is responsible for introducing significant error into the contemporary scenario at Mason City, IA, Lafayette, IN, Hastings, NE, and Liberal, KS. This is something to take into account when drawing conclusions on the accuracy of the future scenario trends as well as the overall comparison between the future and contemporary climates.

The most noteworthy finding in this study is in regards to model-simulated low-end winds. It is evident that wind speeds at the 10th percentile exhibit significant diminishing trends, that is, the frequency in which extremely low winds are occurring has increased throughout the last 3 decades. This conclusion is supported throughout the observational portion of this study (*note: trends may be partially/fully attributed to introduction of ASOS*) as well as within the contemporary model-simulated analysis. A predominant feature in model-simulated near-calm winds is simulated by the MM5I (NCEP, contemporary, and future scenarios); this RCM displays an overwhelmingly large occurrence of extremely low winds. This unusual feature was not thoroughly investigated, but rather, only addressed as a potential issue.

Comparing the future and contemporary model scenarios at the 10th percentile, it is apparent that there is an overall decreasing trend in wind speeds between the two periods: 1968-2000 and 2038-2070. The MM5I simulated a statistically significant diminishing trend amongst all of the locations in this study at the 10th percentile. This result supports the overall tendency

that the MM5I/CCSM simulates an overall decreasing trend in the low-end winds (10^{th} percentile).

Looking at the high-end winds, there is significantly less clarity amongst the models and cities as to what trends are being simulated; more specifically, with the exception of the MM5I/CCSM, the trends are generally statistically insignificant. The MM5I/CCSM displays an undisputed decreasing trend that is statistically significant throughout the 90^{th} , 95^{th} , 99^{th} , and 99.9^{th} percentiles at each of the cities. With these mixed results, it is not appropriate to declare concrete results regarding model representation of trends in high-end surface winds.

The only model to simulate a unanimously diminishing feature in both the high and low-end winds is the MM5I/CCSM. Furthermore, it is also interesting to note that the percent difference simulated by this climate model was often as much as one or even two orders of magnitude larger than the other climate models. The only other model to simulate a statistically different percent change in the order of 10 is the CRCM/CGCM3 at Hastings, NE, and Liberal, KS. Difference plots in Appendix D illustrated these percent changes between the future and contemporary scenarios.

Large variation was seen amongst the climate models in regards to seasonal trends simulated in the climate models with contemporary scenario boundary conditions; it appears that trends produced by the CRCM/CGCM3 do not resemble the other model scenarios (MM5I/CCSM, WRFG/CCSM, and CRCM/CCSM), which could infer that the GCM plays a large role in these monthly mean values. Another noteworthy feature is the small variation in monthly mean wind speeds at Mason City, IA, and Lafayette, IN, by the CRCM/CCSM. Overall, the contemporary and future scenarios appear to simulate the general timing of minimum winds

(June, July, and August), whereas, they do not simulate the maximum winds with accuracy (March, April, and May).

The goal of this research project was not to compare model vs model, but rather, to determine if the models can generally simulate observed surface wind speed characteristics with some level of confidence. Comparing results found in this study to those done by Pryor (2010), it was concluded that there is a clear trend of diminishing wind speeds at the 90th percentile and the annual mean winds within the observational datasets as well as with the MM5 RCM, which match results found herein. Pryor et al. (2010) also showed that there was rather inconclusive evidence of significant trends among the other models analyzed because of observational-to-model and model-to-model discrepancies. Pryor et al. (2010) attributed these differences to be a result of variations in orographic properties in the model fields, spatial resolution, and vertical interpolation of the wind speeds to 10 m.

Although it is not clear quantitatively how much wind speed trends are influencing evaporative processes, it is, however, definitive that surface winds do indeed play a role in evaporation in the hydrologic cycle. Based on the results of this study, the “stilling” of surface wind speeds will act to lower evaporation. A decreasing trend in evaporation and evapotranspiration could mean the following agricultural outcomes: crops will need less water to function properly, thus, leading to higher water use efficiency; less evapotranspiration means less energy being removed from the plant surface, resulting in an increase in internal crop temperature, which might be an adverse outcome of “stilling” wind speeds. Also, the increase in the occurrence of low or near-calm winds might also indicate lesser effective pollination for crop reproduction since plants rely on wind as a mechanical force to spread pollen downwind.

Overall, the focus of this study was not to deduce trends in agricultural or hydrological processes, but rather, to identify wide-ranging outcomes of a changing wind climate.

A changing surface wind climate can be the result of innumerable varying meteorological and environmental factors; consequently, to be able to firmly quantify which element or combination of elements contribute to trends in wind speeds would be difficult (Pryor et al., 2010).

Based on recent reports by the IPCC (2013b), a few overarching pieces of evidence are presented which may partially explain the evolving surface wind field which has been shown herein with the analysis of observational data and model scenarios: mean sea level pressure (MSLP) changes, decreased storm passage in the mid latitudes in the northern hemisphere, as well as an observed shift in the tracks of storm passage (IPCC, 2013b) are suggested as factors related to climate change.

According to the IPCC (2013b), MSLP under representative concentration pathway (RCP) 8.5 displays a significant increasing trend during the months of June, July, and August throughout the South Eastern United States by the year 2100. This model-simulated change implies that the Bermuda High will likely strengthen and could act to enhance the low level jet in the Central United States during these summer months. As this semi-permanent region of high pressure intensifies, its ridges extend further westward, thus, leading to a tighter pressure gradient between the high pressure region and the nearby synoptic pattern, thus, resulting in an enhanced nocturnal LLJ throughout the Great Plains. On the other hand, MSLP changes with time are shown to be generally small, such that they are statistically insignificant during the winter months (December, January, and February) over the United States (IPCC, 2013b).

Furthermore, evidence has also shown that the frequency of cyclone passage in the mid latitudes in the northern hemisphere will decrease by the year 2100 (based on RCP 8.5 scenario) (IPCC, 2013b). Wind speeds are directly impacted by cyclone passage, and are directly proportional to the pressure gradient. If the frequency of cyclone passage decreases with time, surface wind speeds will also decrease. Another factor which influences wind speeds at the surface is the track of cyclone passage. The IPCC AR5 states that there is substantial uncertainty revolving around the projections of changes in storm tracks throughout the NH.

According to the IPCC (2013a), many extreme events are the result of natural climate variability. Natural variability and anthropogenic forces will collectively be significant factors in shaping future extreme events in a changing climate. Many of the above mentioned factors which influence surface winds are based on variations in temperature. Ultimately, thermal forces drive much of the feedback mechanisms in our planet's climate, and can be viewed as pivotal in understanding our evolving climate.

REFERENCES

- Abhishek, A., J. Y. Lee, T. C., Keener, and J. Y. Yang, 2010: Long-term wind speed variations for three midwestern U.S. cities, *J. of the Air & Waste Management Association*, **60(9)**, 1057-1065.
- American Lung Association, 2013: State of the Air. (<http://www.stateoftheair.org/>)
- Arrakis, 2004: Wind resources, 34 (<http://www.arrakis.nl/files/WindResources.pdf>)
- Automated Surface Observing System (ASOS), 1998: User's Guide, National Oceanic and Atmospheric Administration, Department of Defense, Federal Aviation Administration, United States Navy.
- ADEM, ASOS and Met Data Processing Subgroup. May 15-17, 2007. EPA R/S/L Modelers Workshop.
- Deaves, D. M. and I. G. Lines, 1998: The nature and frequency of low wind speed conditions. *J. Wind Eng. Ind. Aerodynamics*, **73(1)**, 1-29.
- DeGaetano, A. T., 1997: A quality-control routine for hourly wind observations. *J. Atmos. Oceanic Technol.*, **14**, 308–317.
- DeGaetano, A. T., 1998: Identification and implications of biases in US surface wind observation, archival, and summarization methods. *Theor. Appl. Climatol.*, **60**, 151–162
- Della-Marta et al., 2009: The return period of wind storms over Europe. *Int. J. Climatol.*, **29**, 437–459.
- EPA, 1997: Analysis of the affect of ASOS-derived meteorological data on refined modeling.
- Federal Meteorological Handbook No. 1 Surface Weather Observations and Reports FCM-H1-2005 Washington, D.C. September 2005.
- Hatfield, J. L., T. J. Sauer, and J. H. Prueger, 2001: Managing soils to achieve greater water use efficiency: A review. *Agron. J.*, **93**, 271-280.
- Hong, S. U., Y. Noh, and J. Dudhia, 2006: A new vertical diffusion package with an explicit treatment of entrainment processes. *Mon. Wea. Rev.*, **134**, 2318–2341.
- IPCC, 2013a: Managing the risks of extreme events and disasters to advance climate change adaptation. Special report of the Intergovernmental Panel of Climate Change. Cambridge University Press, The Edinburgh Building, Shaftesbury Road, Cambridge CB2 8RU ENGLAND, 582.
- , 2013b: Long-term Climate Change: Projections, Commitments and Irreversibility. In: Climate Change 2013: The Physical Science Basis. Contribution of Working Group I to the

Fifth Assessment Report of the Intergovernmental Panel on Climate Change [Stocker, T.F., D. Qin, G.-K. Plattner, M. Tignor, S.K. Allen, J. Boschung, A. Nauels, Y. Xia, V. Bex and P.M. Midgley (eds.)]. Cambridge University Press, Cambridge, United Kingdom and New York, NY, USA.

Kalnay et al., 1996: The NCEP/NCAR 40-year reanalysis project, *Bull. Amer. Meteor. Soc.*, **77**, 437-470.

Kaganov, E. I., A. M. Yaglom, 1976: Errors in wind-speed measurements by rotation anemometers, *Bound. Layer Meteorol.*, **10**, **1**, 15-34.

Klink, K., 1999a: Climatological mean and interannual variance of United States surface wind speed, direction, and velocity. *Int. J. Climatol.*, **19**, 471–488

Klink, K., 1999b: Trends in mean monthly maximum and minimum surface wind speeds in the coterminous United States, 1961–1990. *Climate Res.*, **13**, 193–205.

Klink, K., 2002: Trends and interannual variability of wind speed distributions in Minnesota, *J. Clim.*, **15**, 3311–3317.

Mage, D. T., 1967: Frequency distributions of hourly wind speed measurements, *Atm. Env.*, **14**, **3**, 367-374.

McInnes, K.L., T.A. Erwin, and J.M. Bathols, 2011: Global Climate Model projected changes in 10 m wind speed and direction due to anthropogenic climate change. *Atmos. Science Letters*, 1341.

McKee, T.B., N.J. Doesken, C.A. Davey, and R.A. Pielke, Sr., 2000: Climate data continuity with ASOS. Report for period April 1996 through June 2000. Climo Report 00-3, November, 77 pp.

Mearns, L. O., Ray Arritt, Sébastien Biner, Melissa S. Bukovsky, Seth McGinnis, Stephan Sain, Daniel Caya, James Correia Jr., Dave Flory, William Gutowski, Eugene S. Takle, Richard Jones, Ruby Leung, Wilfran Moufouma-Okia, Larry McDaniel, Ana M. B. Nunes, Yun Qian, John Roads, Lisa Sloan, and Mark Snyder, 2010: The North American Regional Climate Change Assessment Program: Overview of Phase I results. *Bull. Amer. Meteor. Soc.* (submitted November 2010).

Mearns, L.O., et al., 2007, updated 2012. The North American Regional Climate Change Assessment Program dataset, National Center for Atmospheric Research Earth System Grid data portal, Boulder, CO.

Meehl, G. A., et al., 2000: An introduction to trends in extreme weather and climate events: Observations, socioeconomic impacts, terrestrial ecological impacts, and model projections. *Bull. Amer. Meteor. Soc.*, **81**, 413–416.

Munn, R. E., 1976: Air Pollution Meteorology. *Manual of urban air quality management.* European Series, 101-126.

NOAA Satellite and Information Service, cited 2013: Climate maps of the United States. [Available online at <http://cds.ncdc.noaa.gov/cgi-bin/climaps/climaps.pl>]

Kanamitsu, M., W. Ebisuzaki, J. Woollen, S-K Yang, J.J. Hnilo, M. Fiorino, and G. L. Potter, 2002: NCEP-DOE AMIP-II Reanalysis (R-2). *Bull. Amer. Meteor. Soc.*, **83**, 1631-1643.

Okin, G.S., D.A. Gillette, and J.E. Herrick, 2006: Multi-scale controls on and consequences of aeolian processes in landscape change in arid and semi-arid environments. *J. of Arid Environ.*, **65**(2), 253-275.

Pryor, S. C., R. J. Barthelmie, D. T. Young, E. S. Takle, R. W. Arritt, D. Flory, W. J. Gutowski Jr., A. Nunes, and J. Roads, 2010: Wind speed trends over the contiguous United States, *J. Geophys. Res.*, **114**, 14105.

Pryor, S. C., and J. T., Schoof, 2010: Importance of the SRES in projections of climate change impacts on near-surface wind regimes. *Meteor Zeitschrift*, **19**(3), 267-274.

Roderick, M. L., M. T. Hobbins, and G. D. Farquhar, 2007a: Pan evaporation trends and the terrestrial water balance. I. Principles and observations, *Geography Compass*, **3**(2), 746-760.

-----, -----, -----, 2007b: Pan evaporation trends and the terrestrial water balance. II. Energy balance and interpretation, *Geography Compass*, **3**(2), 761-780.

Rong, Y. S., X. N. Zhang, and L. Y. Bai, 2012: Pan evaporation change and its impact on water cycle over the upper reach of Yangtze River. *Chinese J. Geophys.*, **55**(5), 488–497.

Seginer, Ido, 1971: Wind effect on the evaporation rate. *J. Appl. Meteor.*, **10**, 215–220.

Smith, F. B., 1993: Low wind speed meteorology, for Cambridge Atmospheric Dispersion Modeling Course.

Stewart, D. A., and O. M. Essenwanger, 1978: Frequency distribution of wind speed near the surface. *J. Appl. Meteor.*, **17**, 1633–1642.

Takle, E. S., and J. M. Brown, 1976: Wind and wind energy in Iowa. Final report to the Iowa Energy Policy Council, Des Moines, 132 pp.

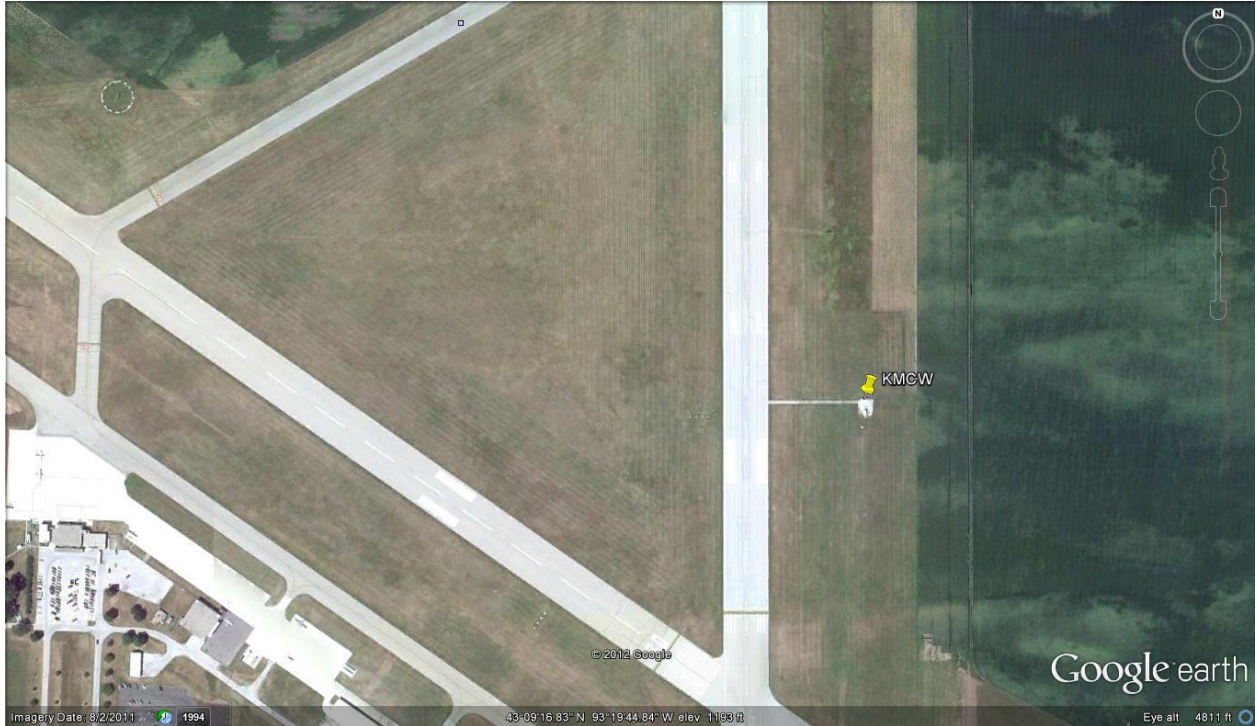
-----, -----, and W. M. Davis, 1978: Characteristics of wind and wind energy in Iowa. *Iowa State J. Res.*, **52**, 313-339.

- , -----, 1978: Note on the use of Weibull statistics to characterize wind speed data. *J. Appl. Meteor.*, **17**, 556-559.
- Tuller, S. E., and A. C. Brett, 1984: The characteristics of wind velocity that favor the fitting of a Weibull distribution in wind speed analysis. *J. Climate Appl. Meteor.*, **23**, 124–134.
- United Nations Environmental Program, 1990: Desertification Revisited. *Meeting on the Assessment of Desertification*, UNEP-DP/PAC, Nairobi, Kenya, 344.
- Vautard, R., J. Cattiaux, P. Yiou, J.-N. Thepaut, and P. Ciais, 2010: Northern Hemisphere atmospheric stilling partly attributed to an increase in surface roughness. *Nat. Geosci.*, **3(11)**, 756-761.
- Zuo H C, Bao Y, Zhang C J, et al., 2006: An analytic and numerical study on the physical meaning of pan evaporation and its trend in recent 40 years. *Chinese J. Geophys.*, **49(3)**, 680-688

APPENDIX A

ASOS SITE INFORMATION

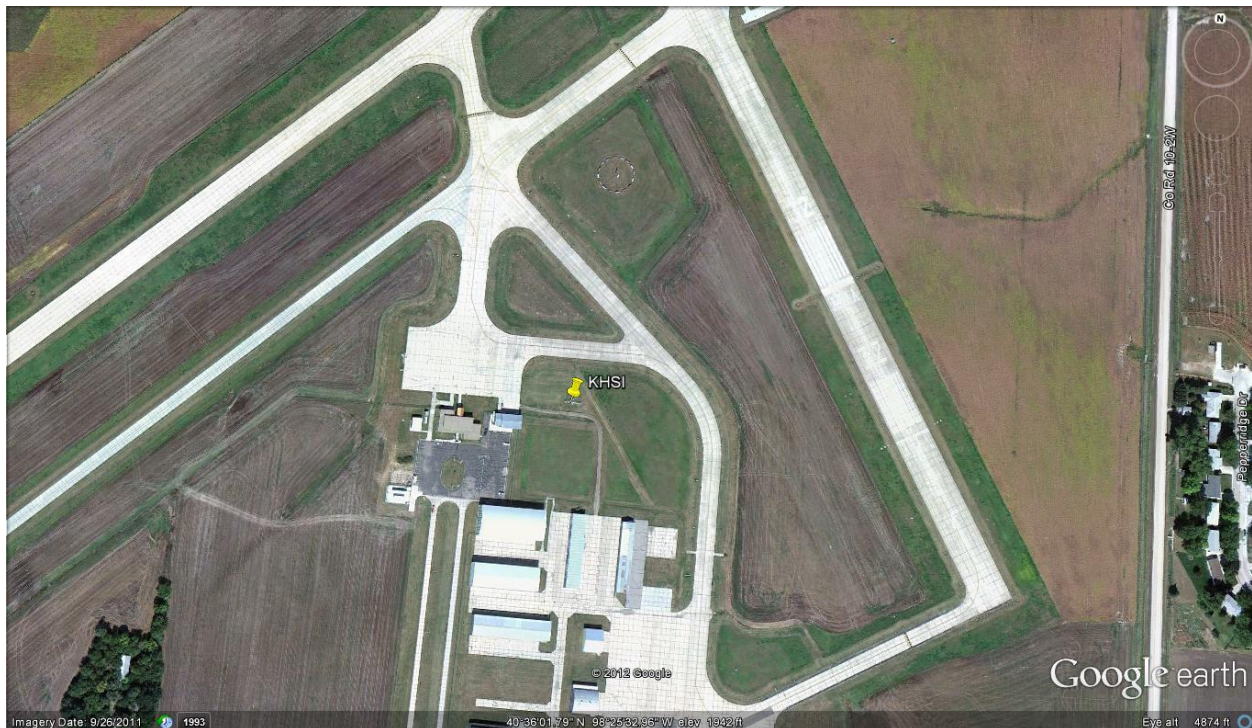
Satellite images of each of the seven cities are given in the following order: Mason City, IA, Lafayette, IN, Hastings, NE, Liberal, KS, Jamestown, ND, Houston, TX, and Atlanta. The location of the ASOS instrumentation is denoted by a yellow pin.



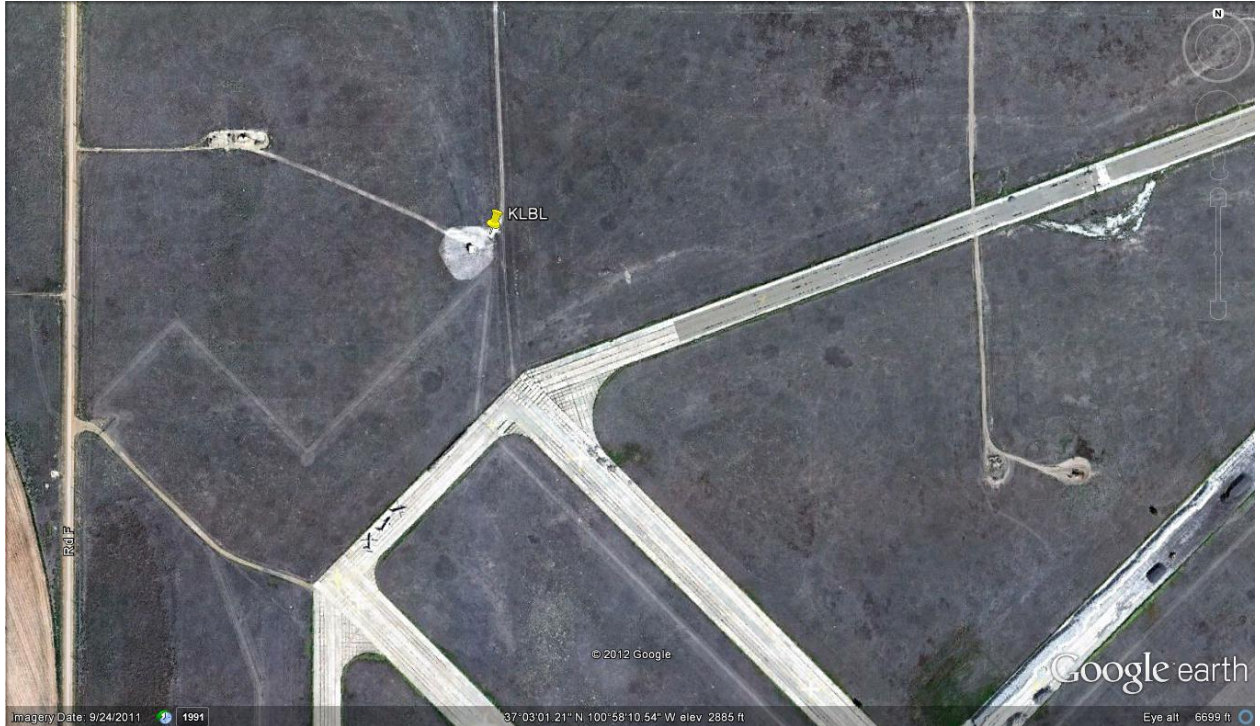
Mason City, IA



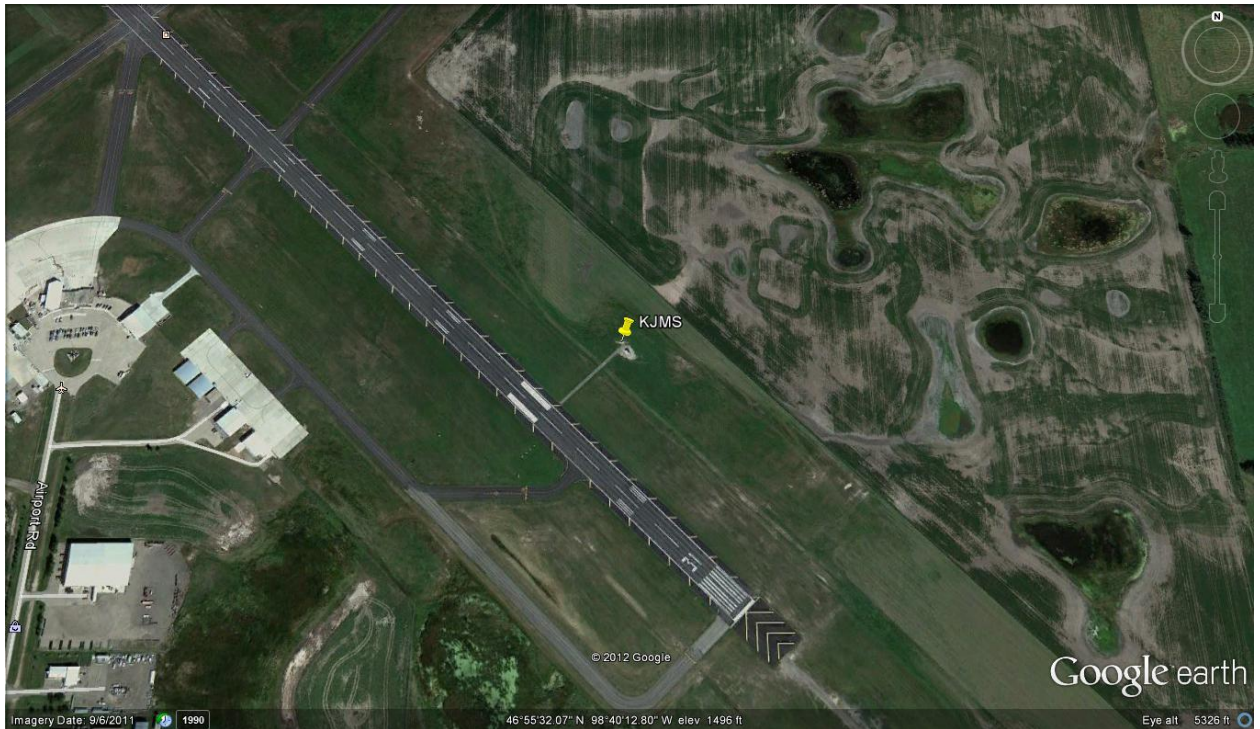
Lafayette, IN



Hastings, NE



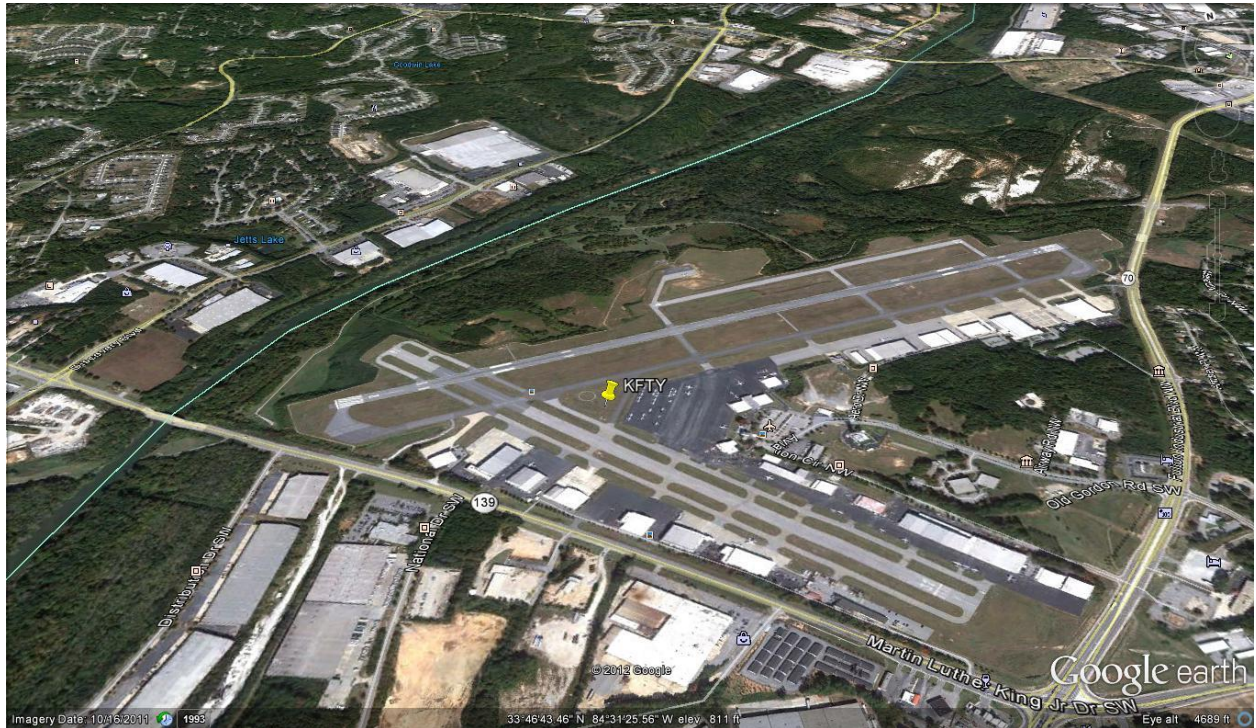
Liberal, KS



Jamestown, ND



Houston, TX

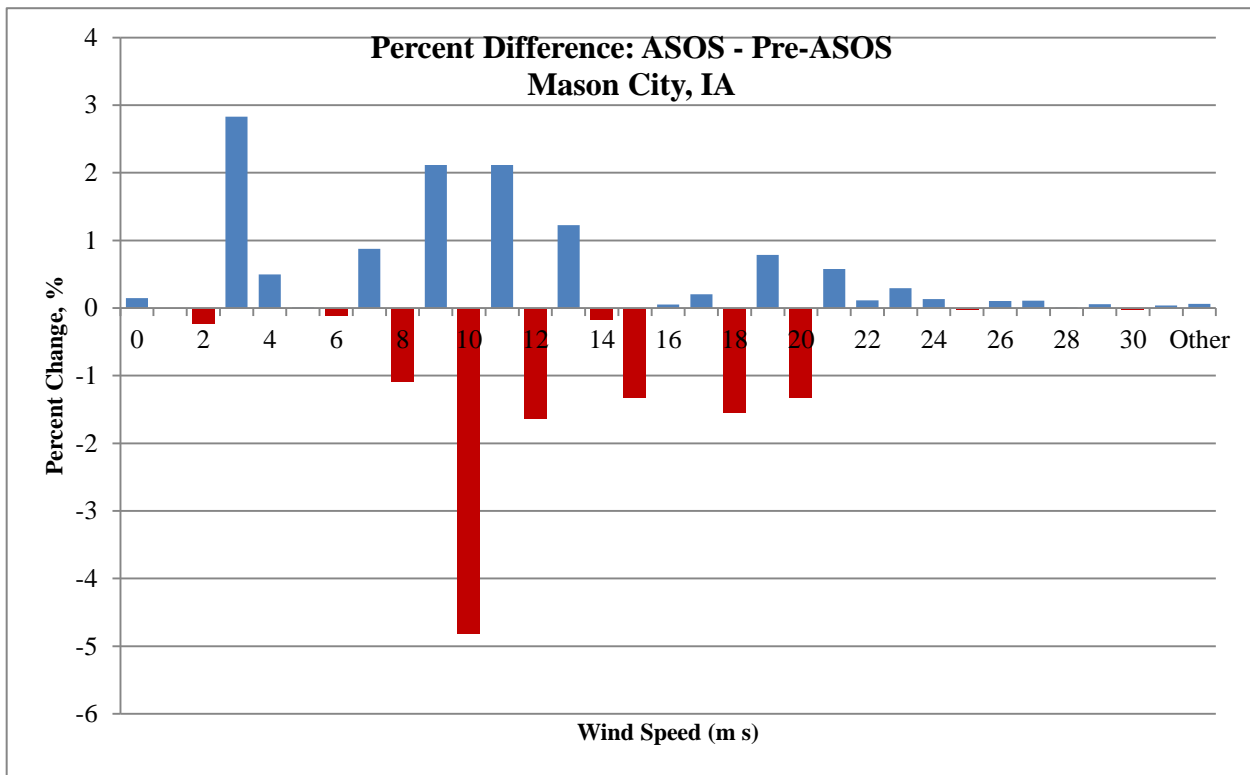


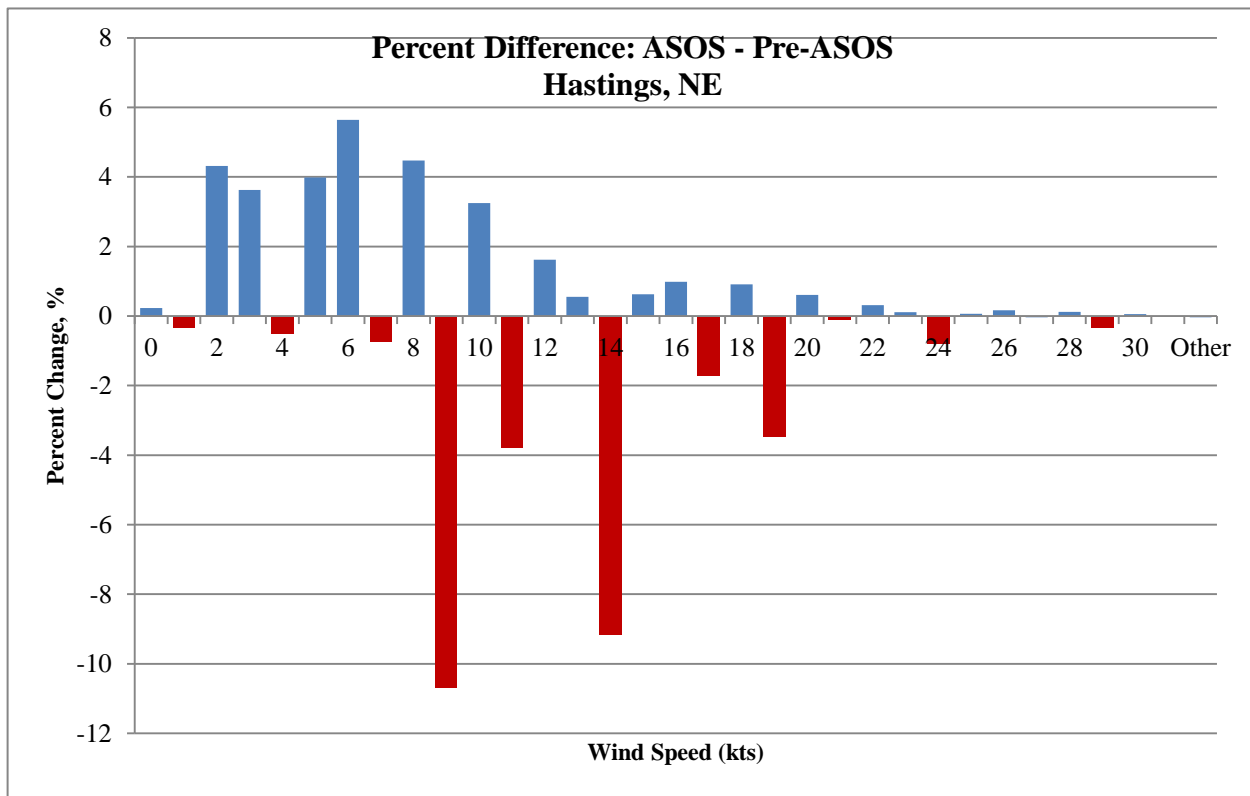
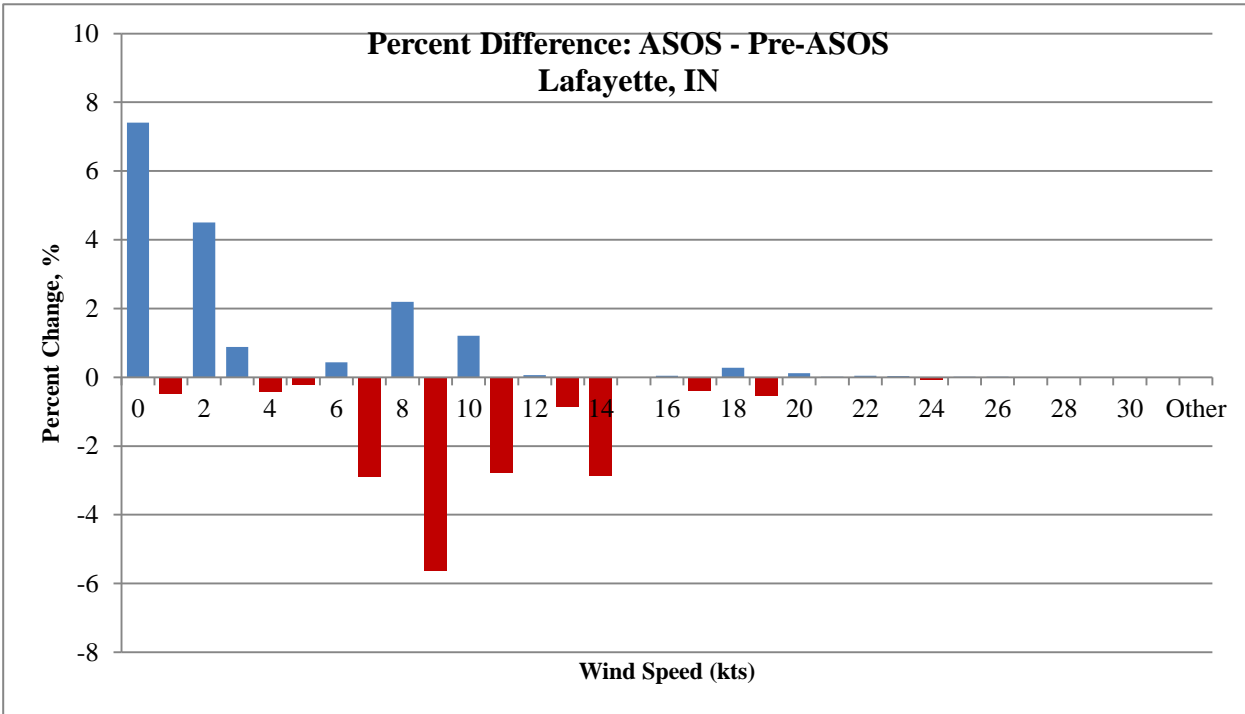
Atlanta, GA

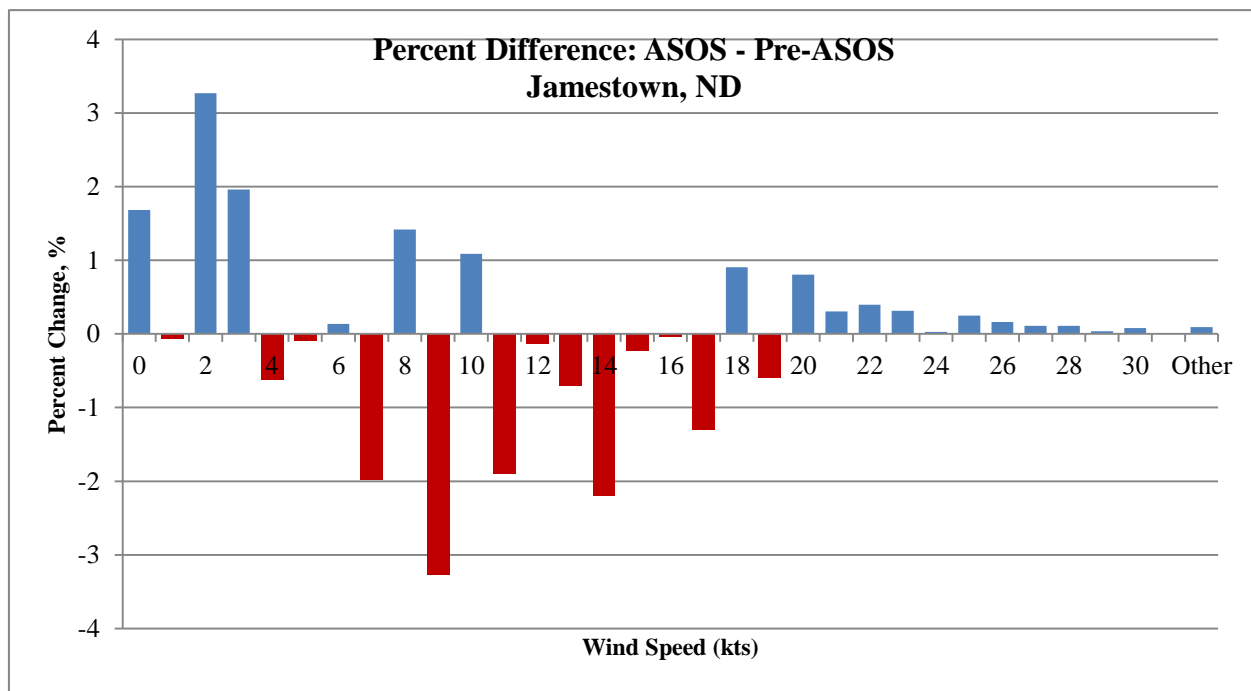
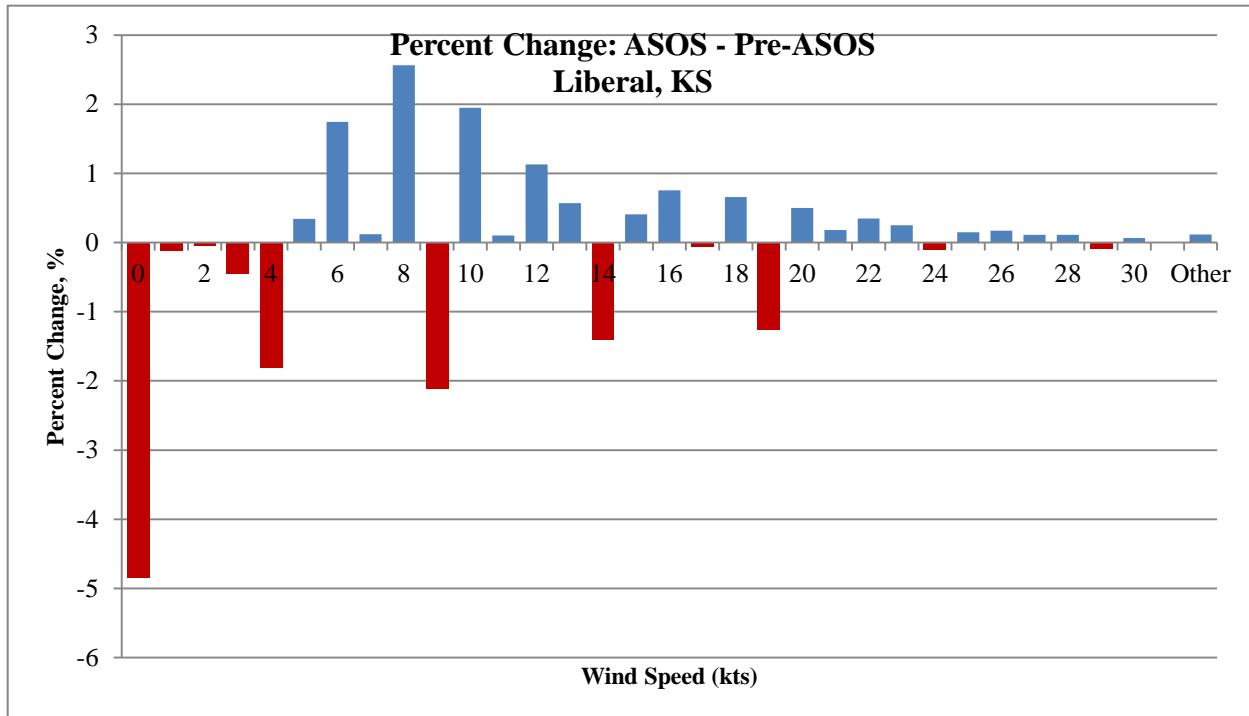
APPENDIX B
PERCENT DIFFERENCE: ASOS – PRE-ASOS

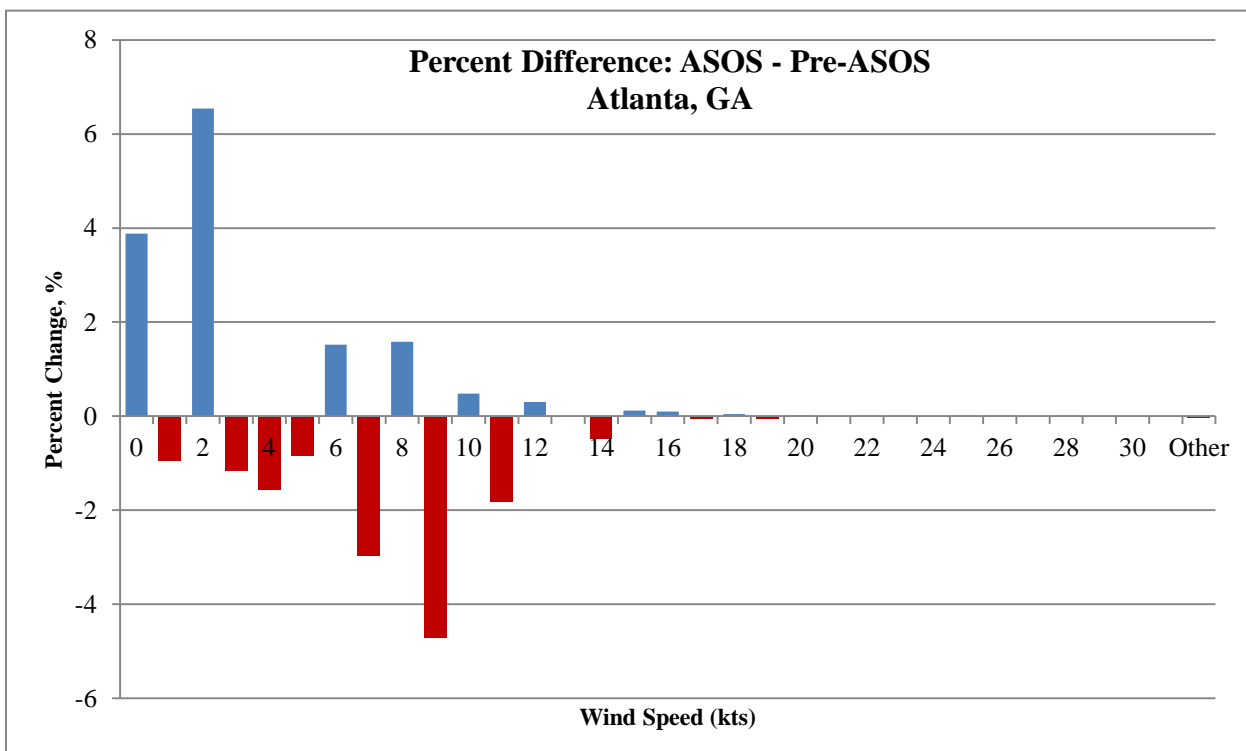
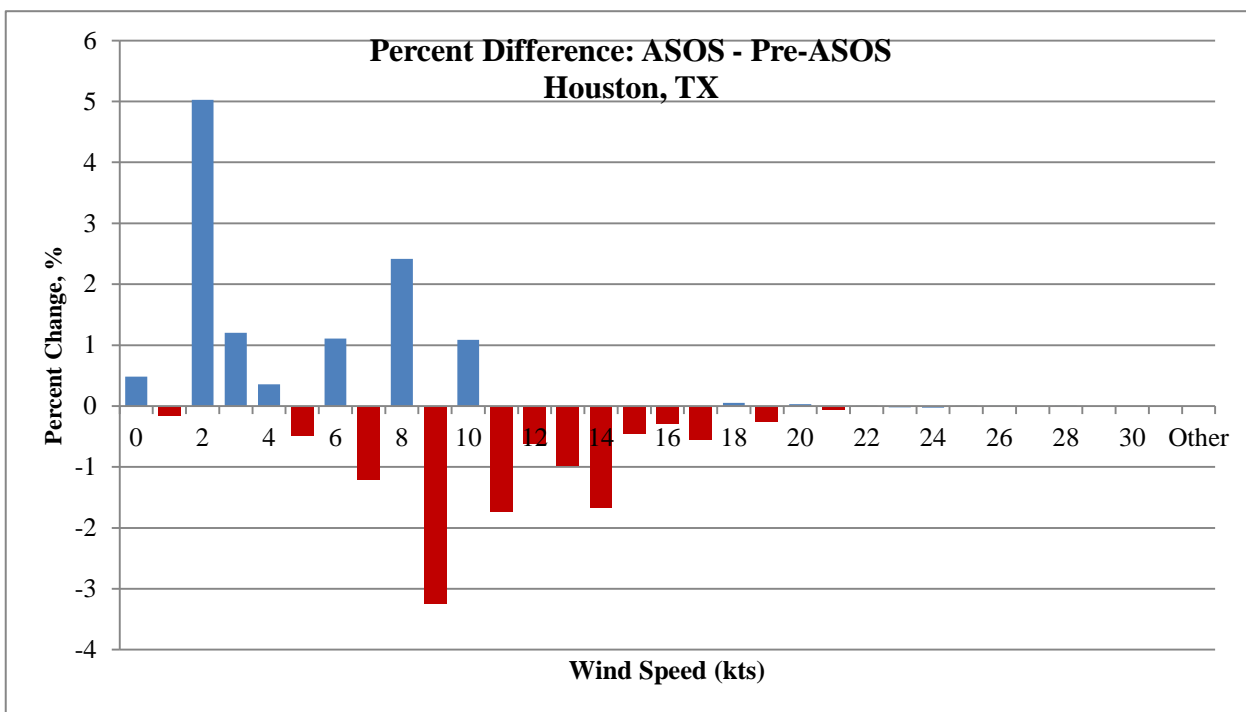
Within this appendix are plots which illustrate the percent difference in observed wind speeds between ASOS and Pre-ASOS datasets. Each of the seven cities is displayed below.

$$\% \text{Diff} = [(ASOS/\text{Pre-ASOS}) - 1] \times 100$$





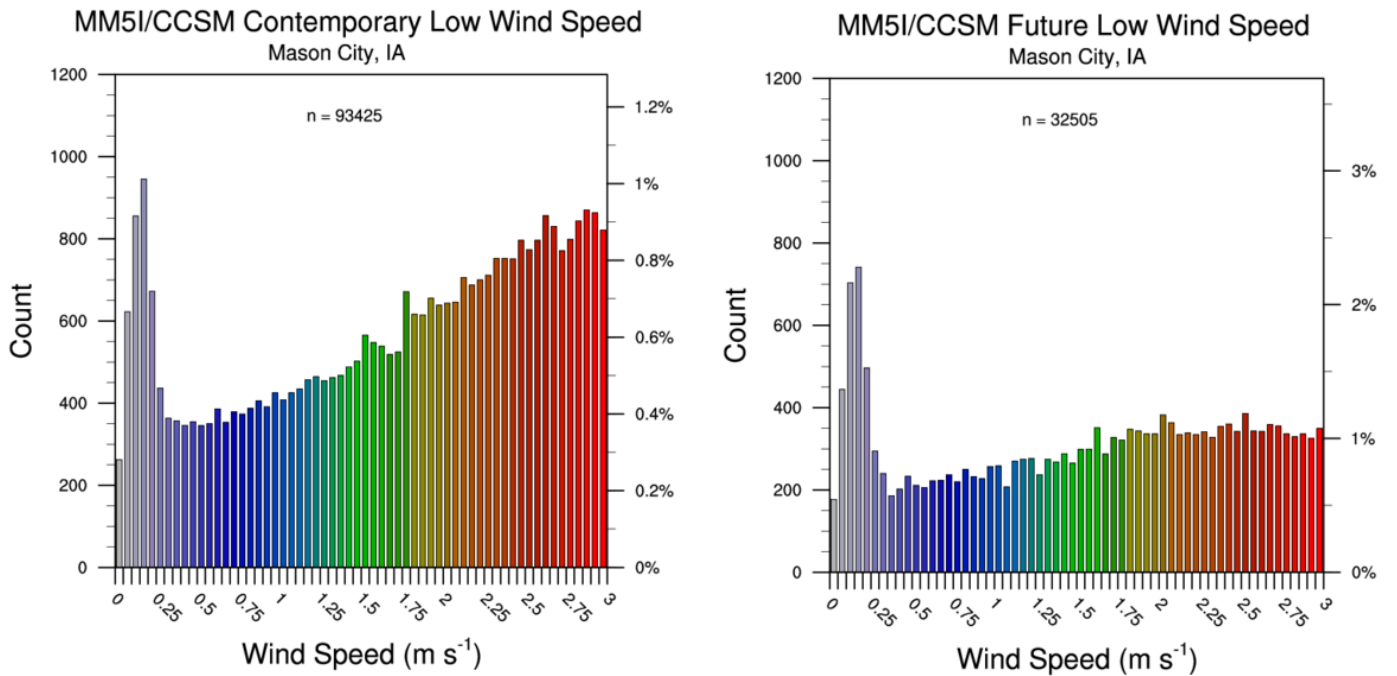
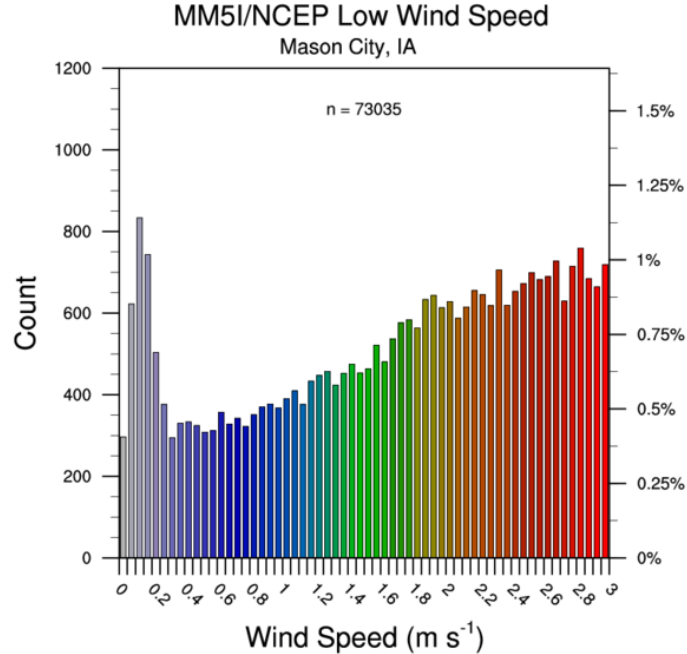




APPENDIX C1

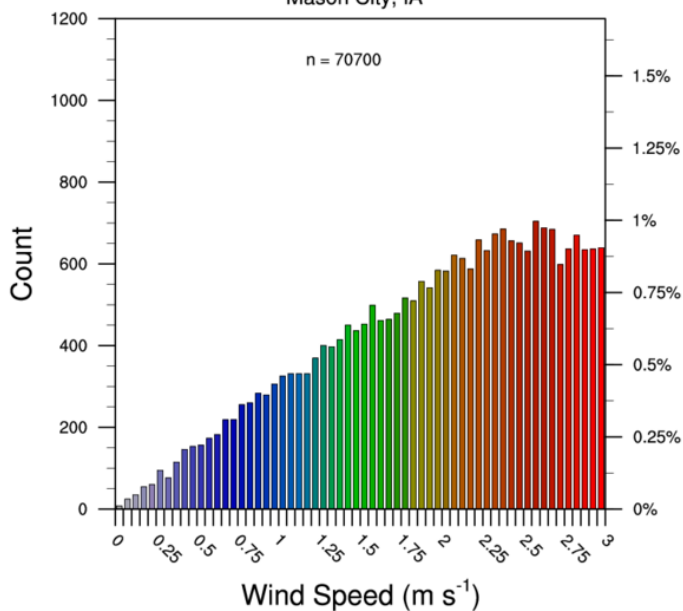
LOW WIND SPEED ANALYSIS: MASON CITY, IA

This appendix provides annual distributions of low wind speeds for MM5I, WRFG, and CRCM regional models with different forcing for Mason City, IA.



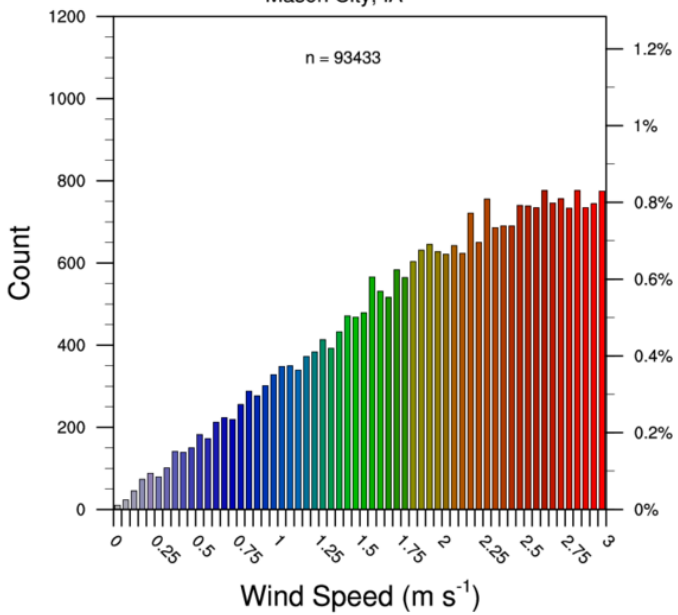
WRFG/NCEP Low Wind Speed

Mason City, IA



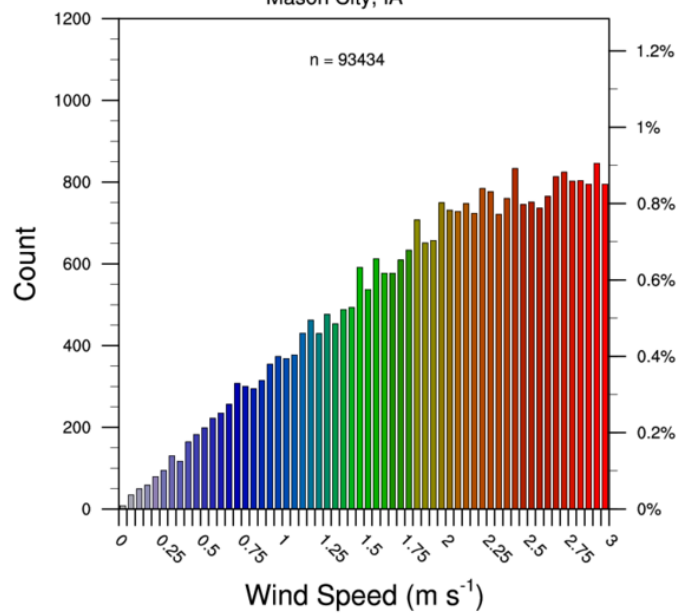
WRFG/CCSM Contemporary Low Wind Speed

Mason City, IA

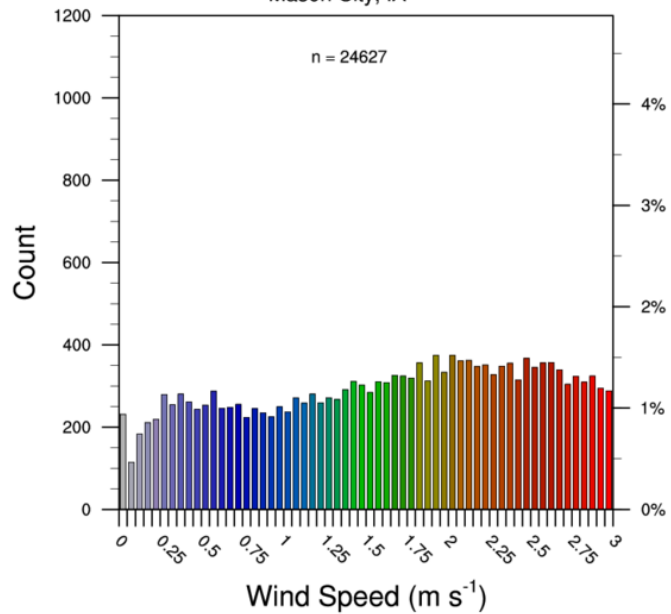


WRFG/CCSM Future Low Wind Speed

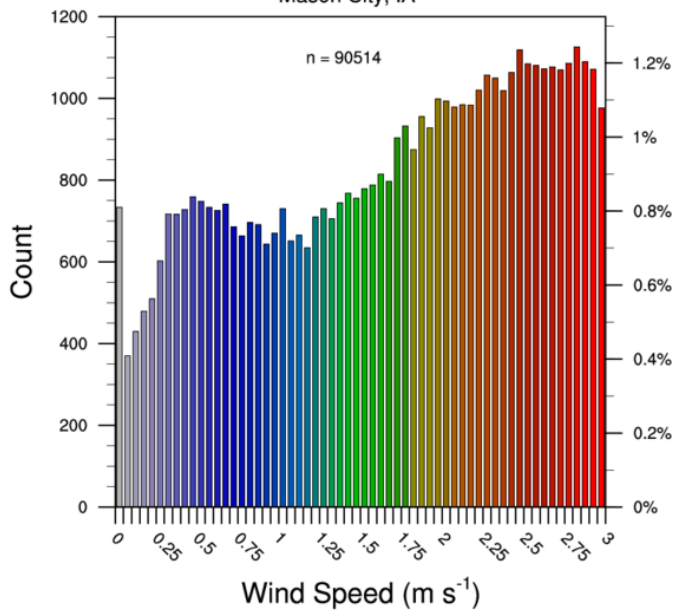
Mason City, IA



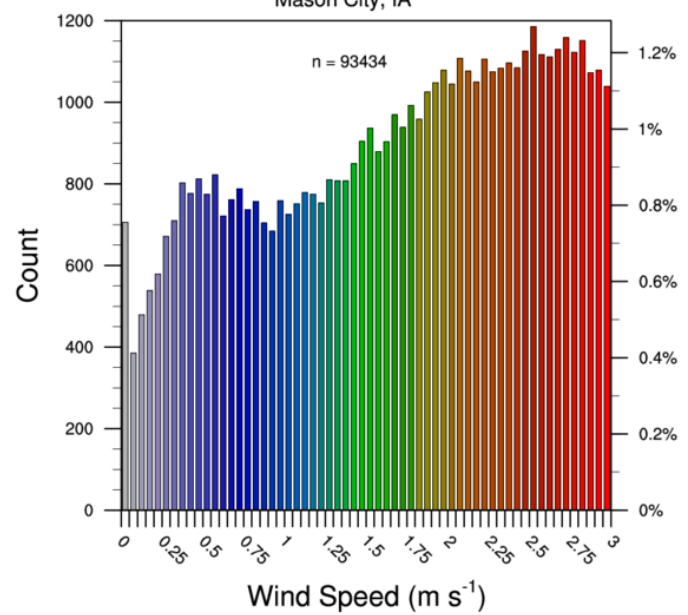
CRCM/NCEP Low Wind Speed
Mason City, IA

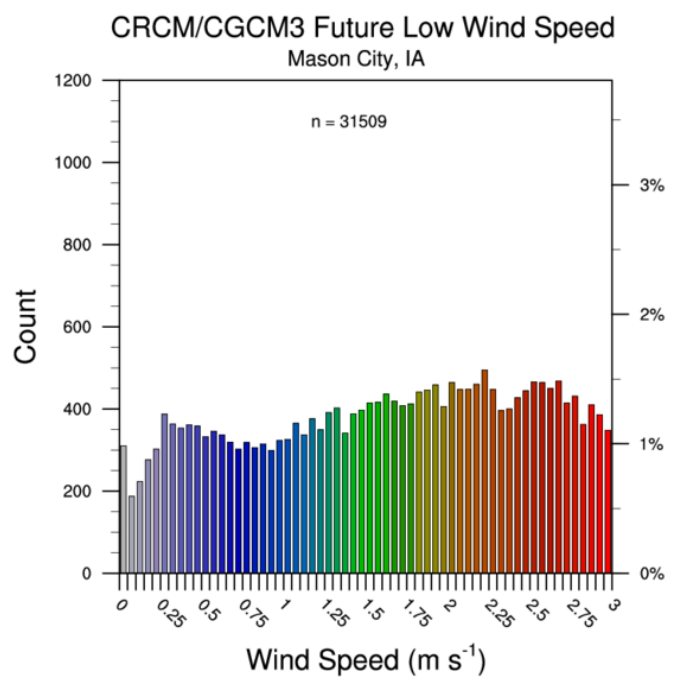
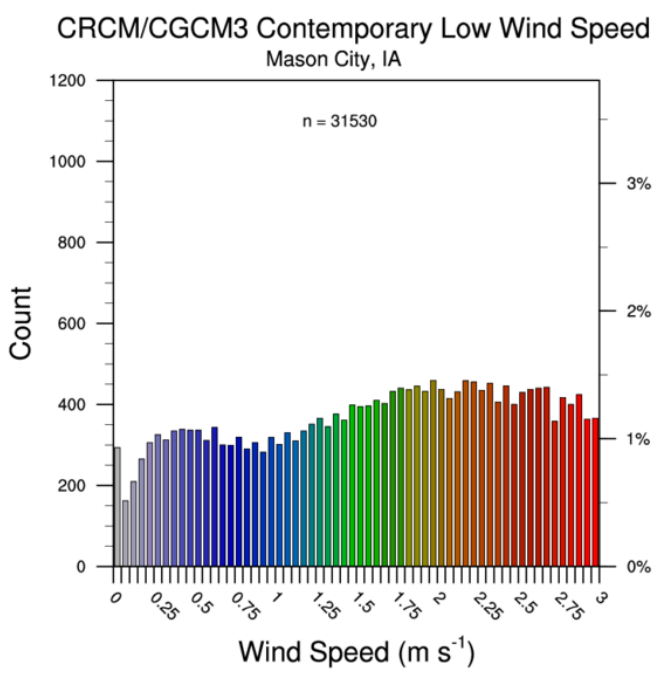
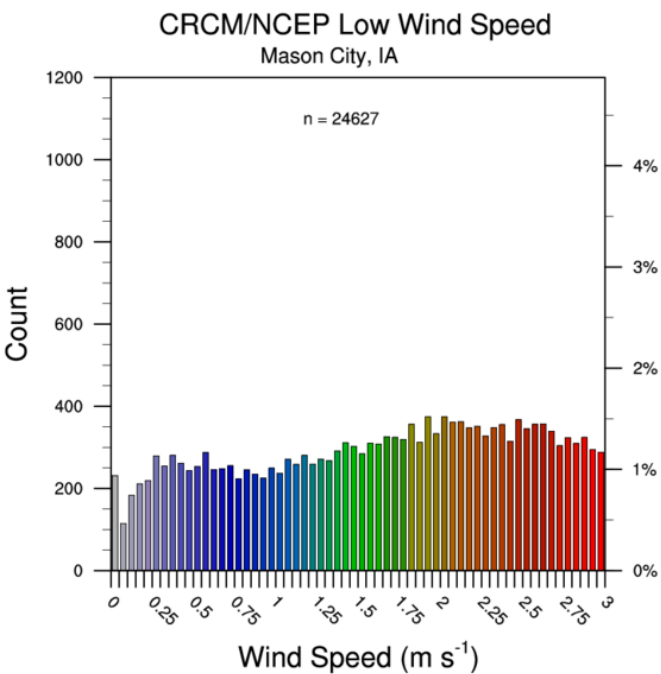


CRCM/CCSM Contemporary Low Wind Speed
Mason City, IA



CRCM/CCSM Future Low Wind Speed
Mason City, IA

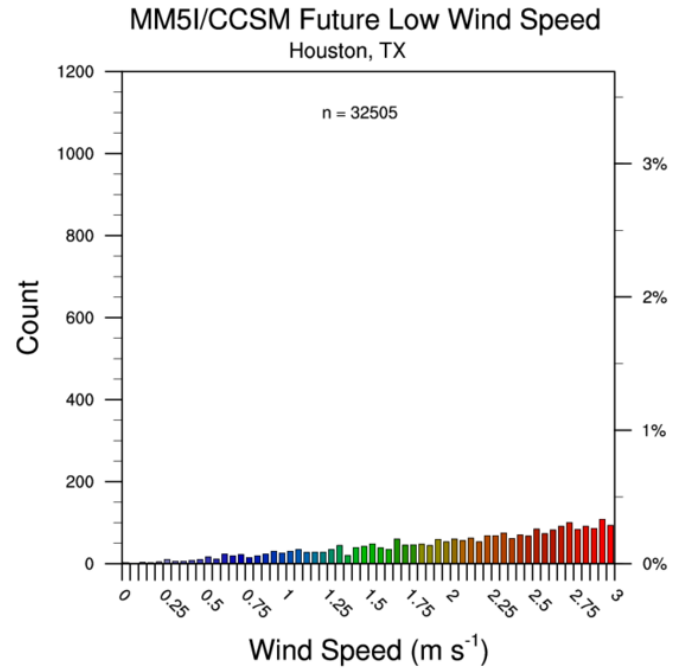
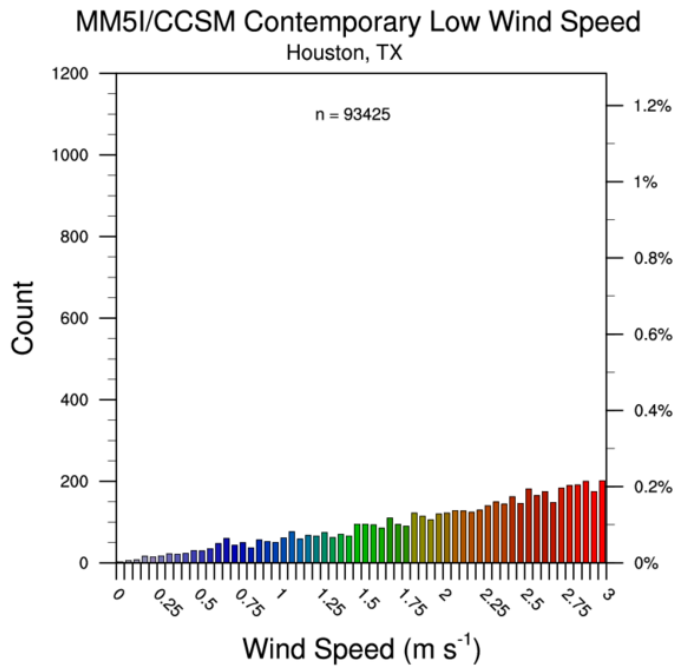
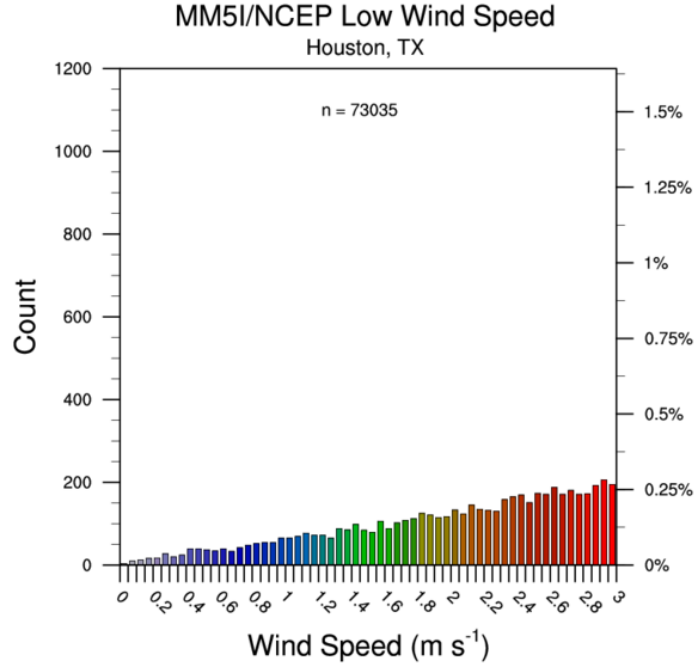


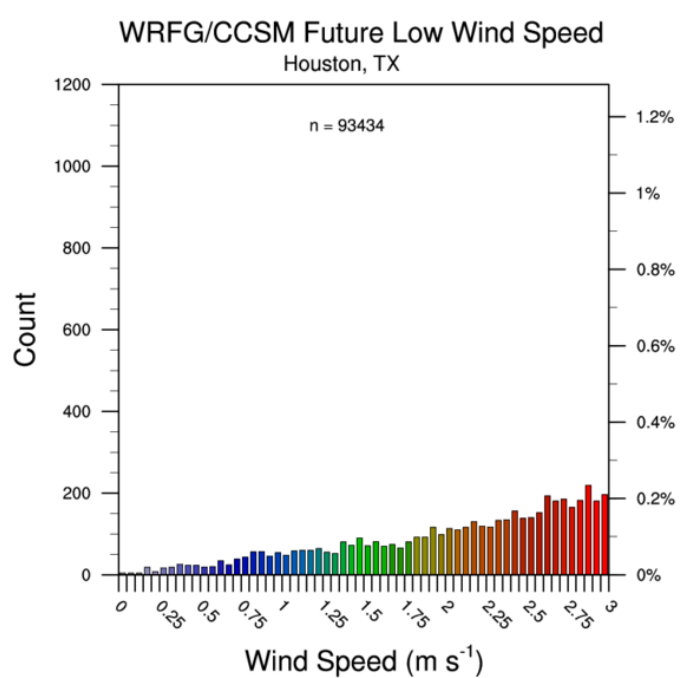
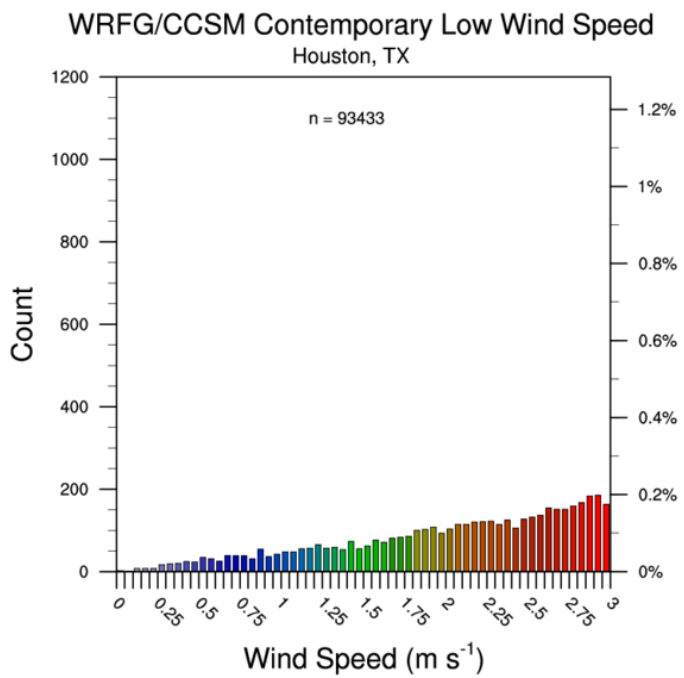
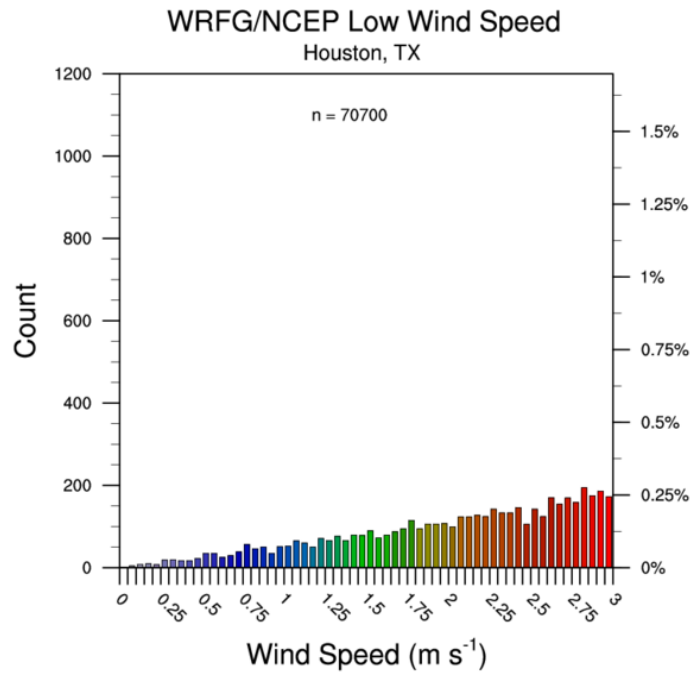


APPENDIX C2

LOW WIND SPEED ANALYSIS: Houston, TX

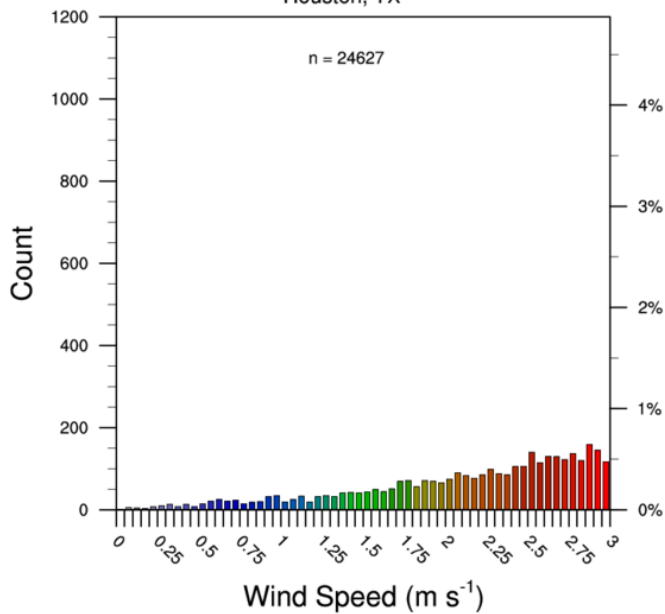
This appendix provides annual distributions of low wind speeds for MM5I, WRFG, and CRCM regional models with different forcing for Houston, TX.





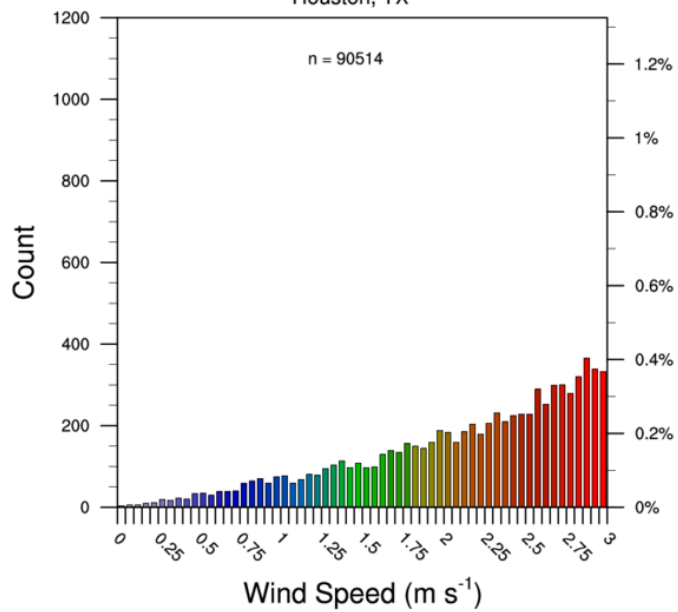
CRCM/NCEP Low Wind Speed

Houston, TX



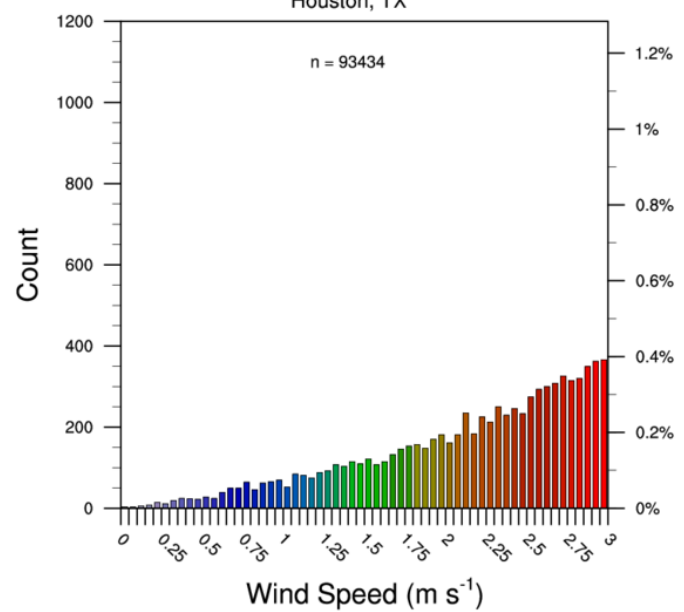
CRCM/CCSM Contemporary Low Wind Speed

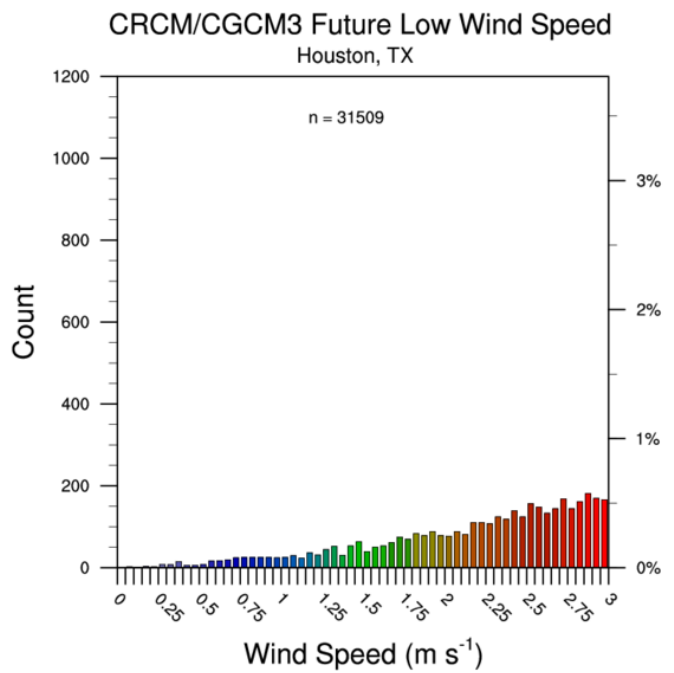
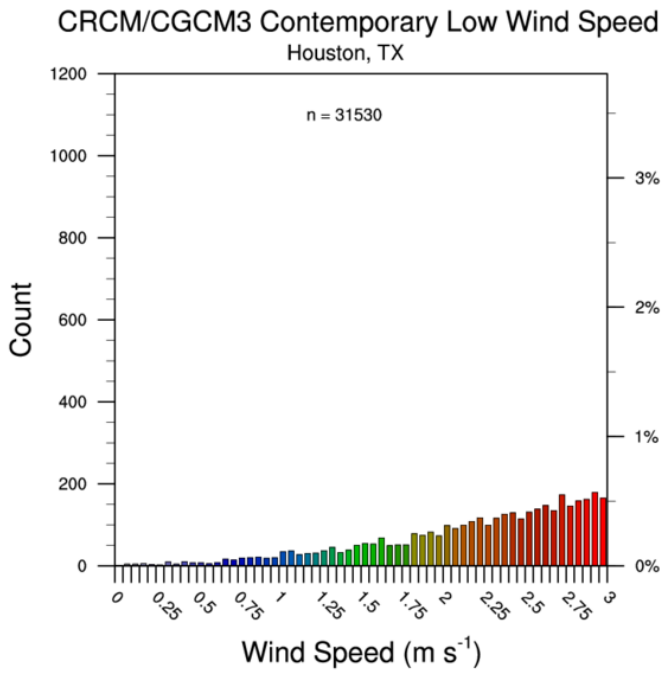
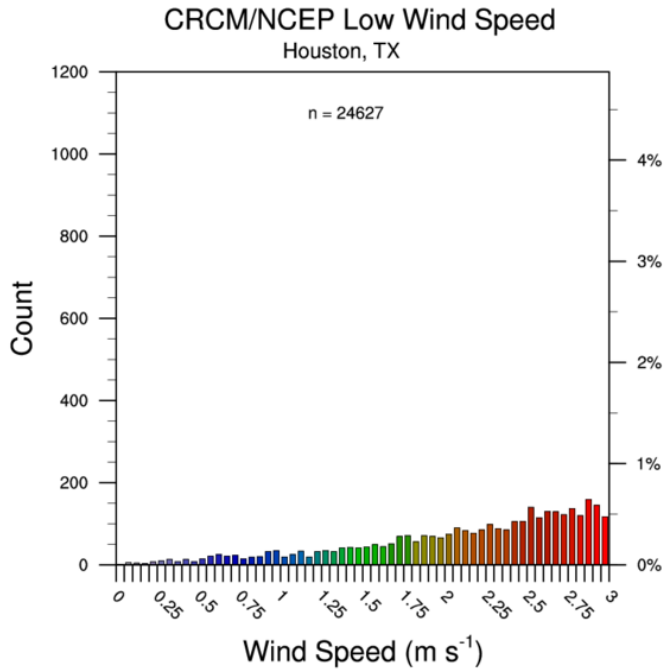
Houston, TX



CRCM/CCSM Future Low Wind Speed

Houston, TX

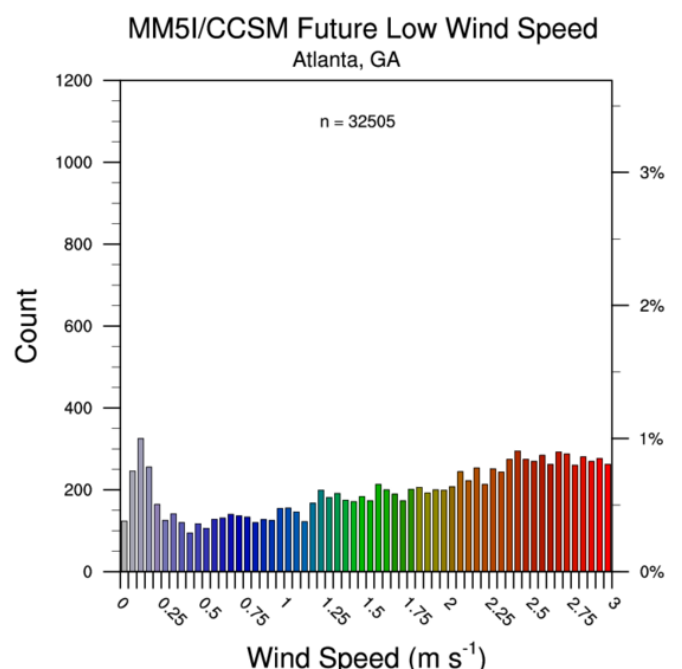
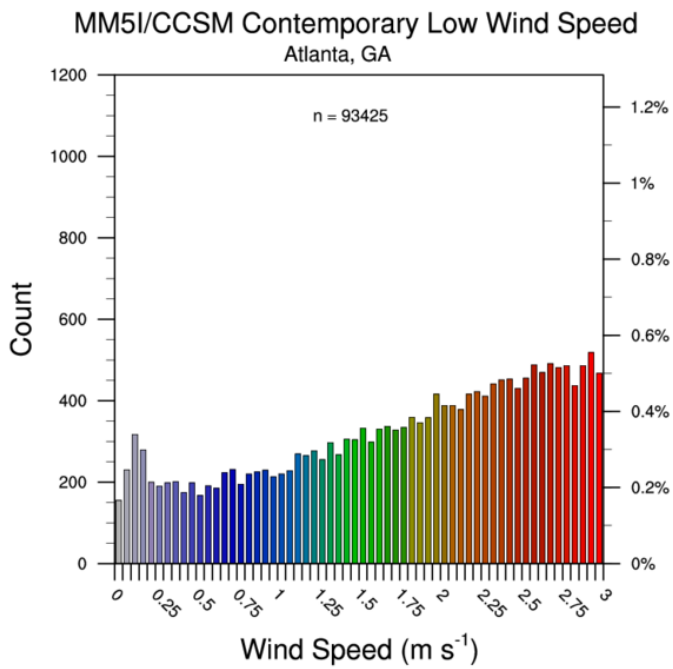
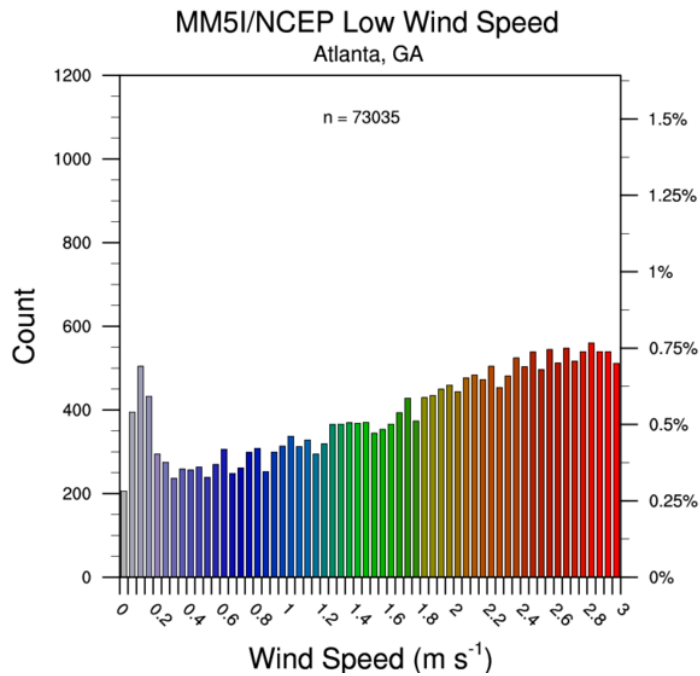


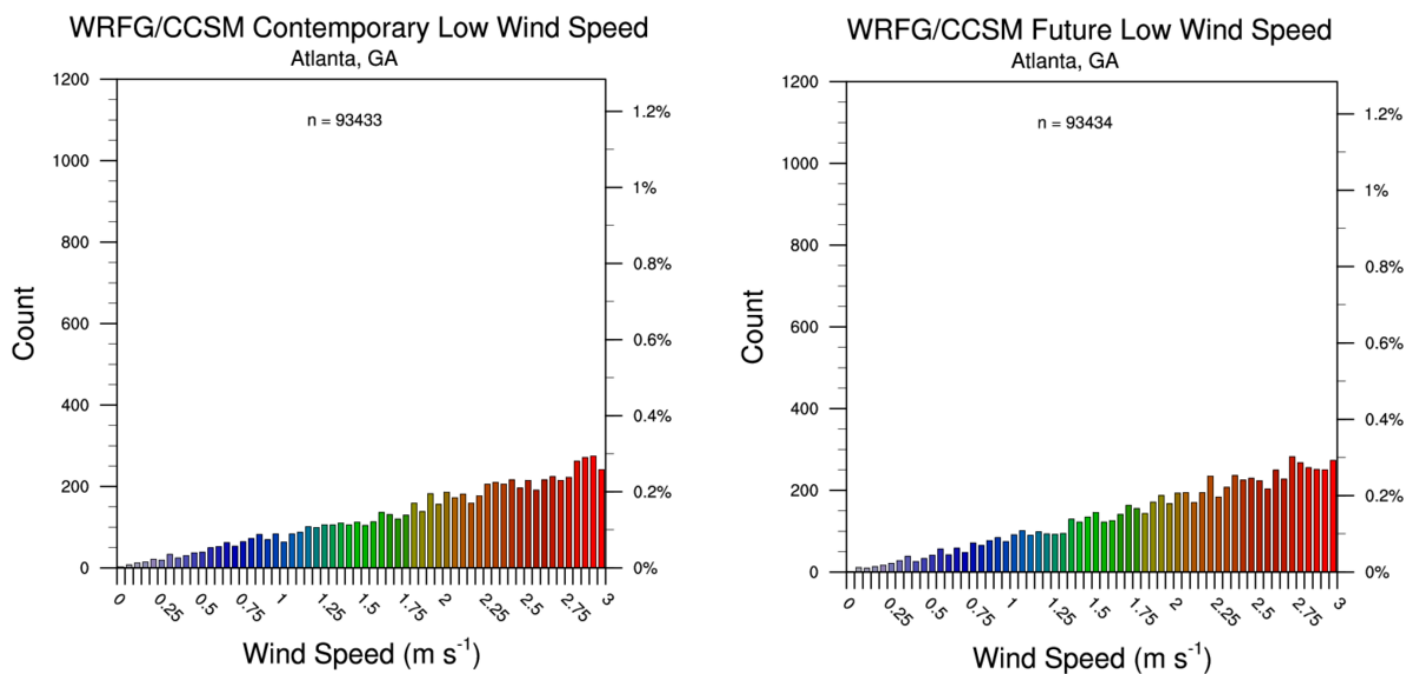
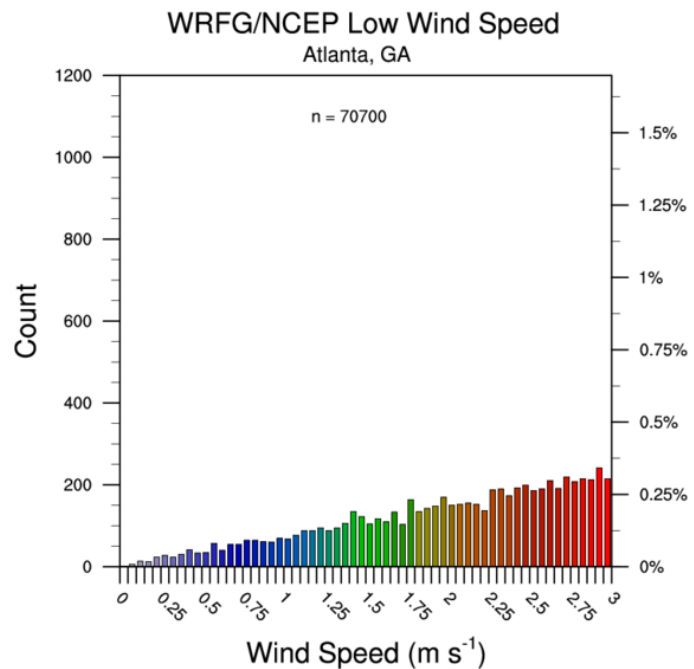


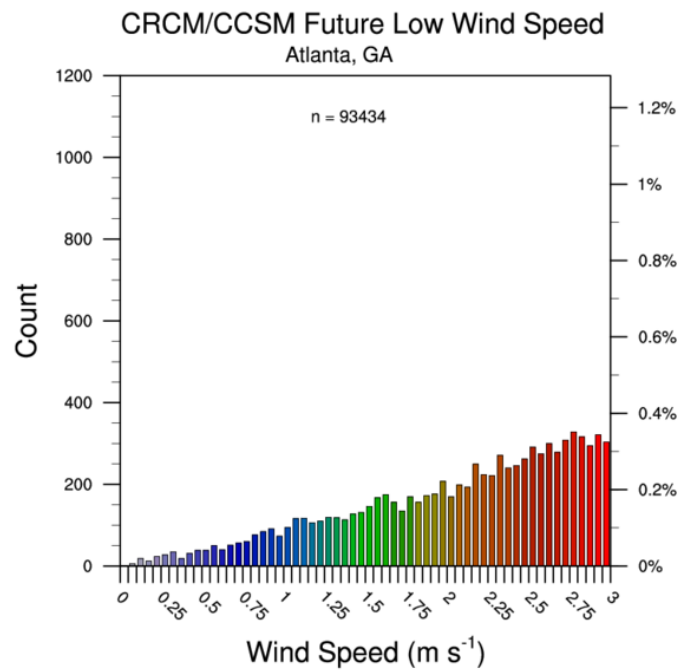
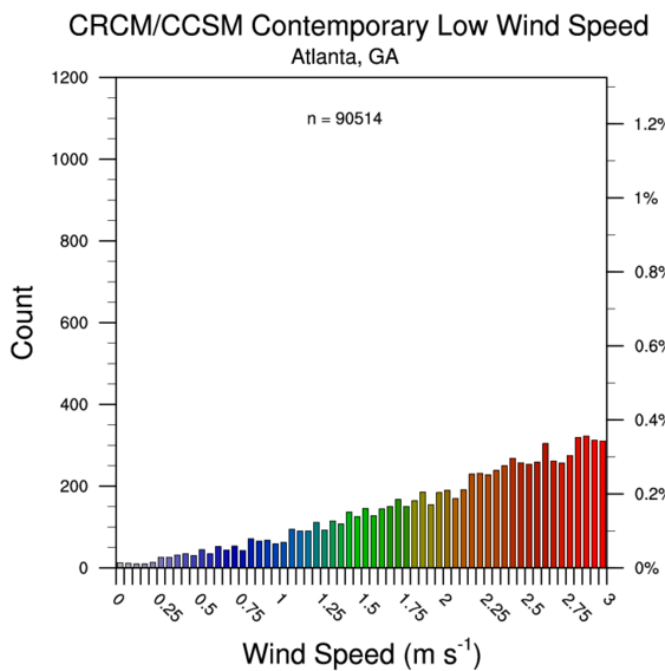
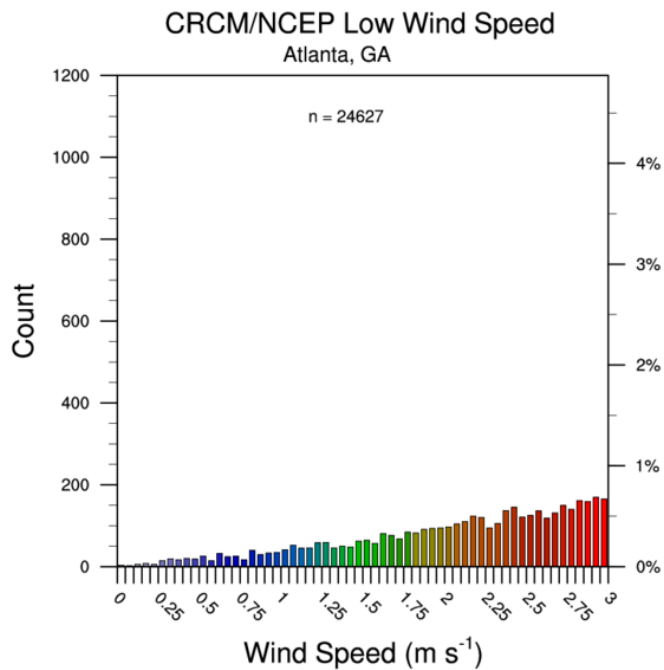
APPENDIX C3

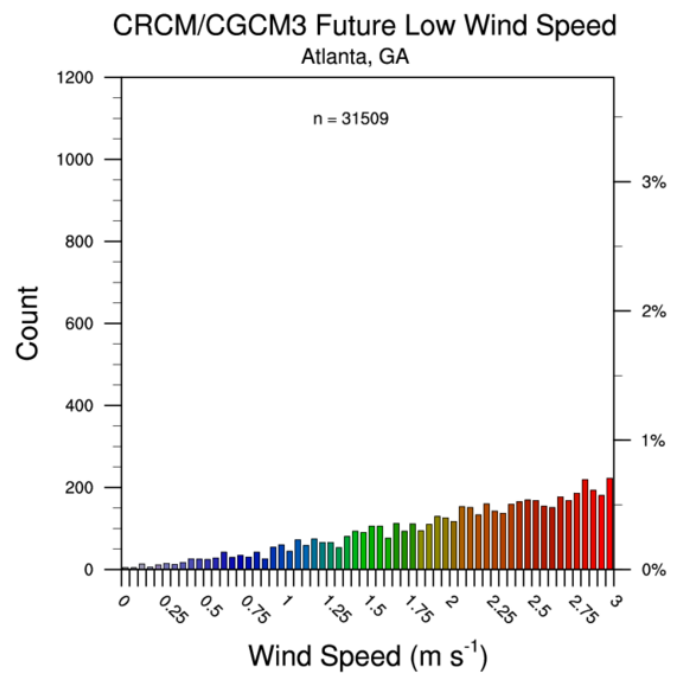
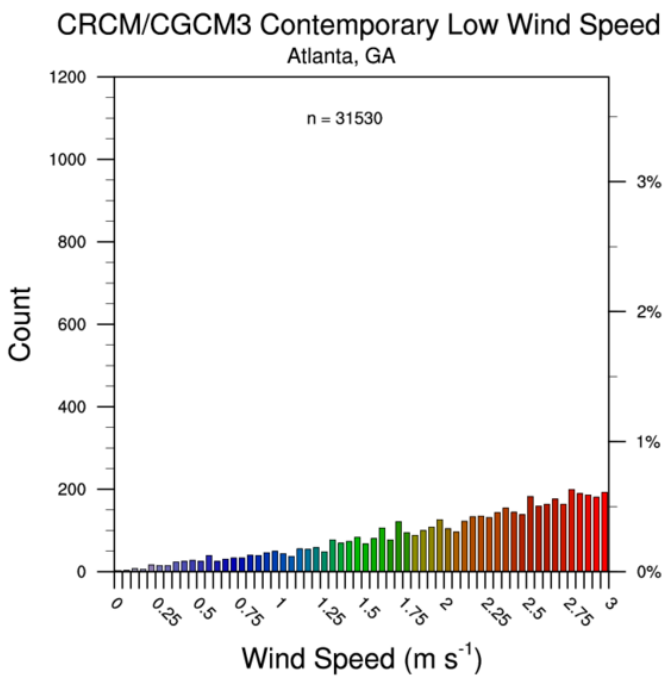
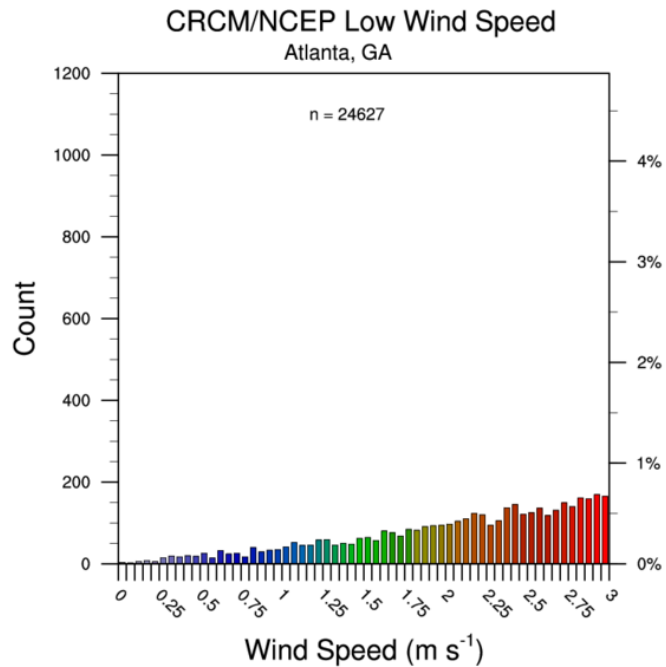
LOW WIND SPEED ANALYSIS: ATLANTA, GA

This appendix provides annual distributions of low wind speeds for MM5I, WRFG, CRCM regional models with different forcing for Atlanta, GA.





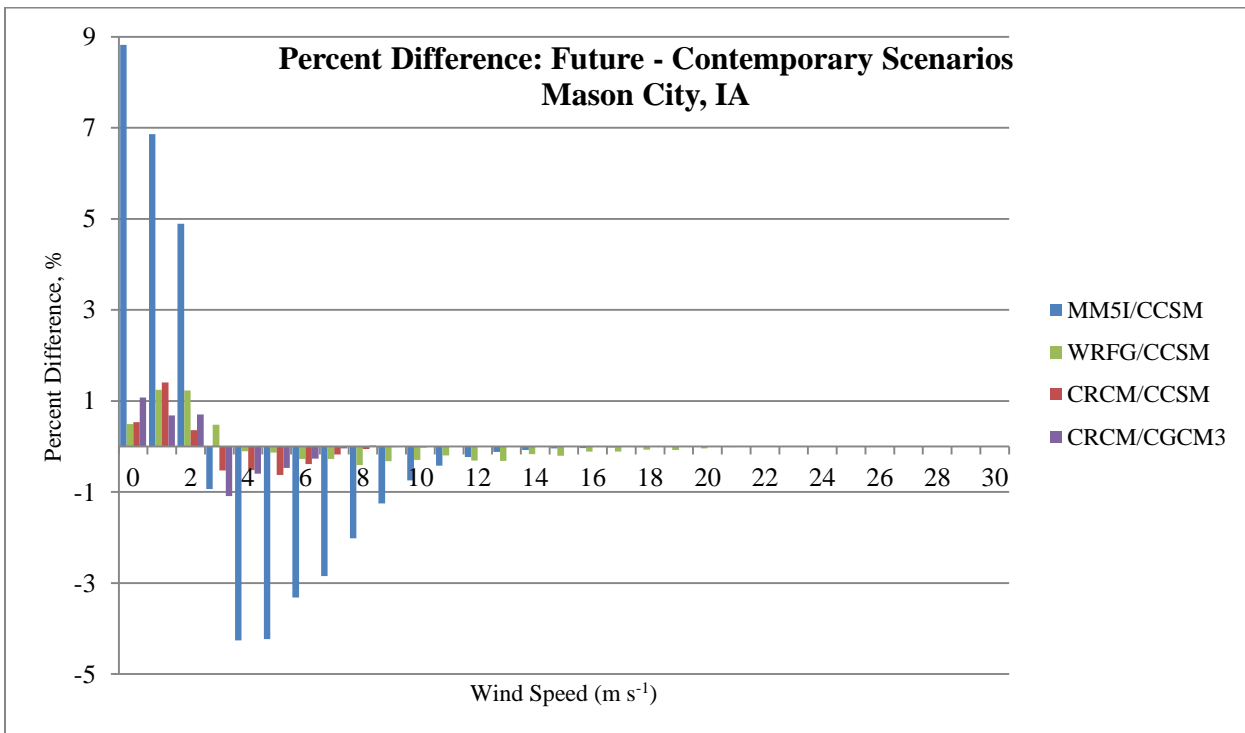


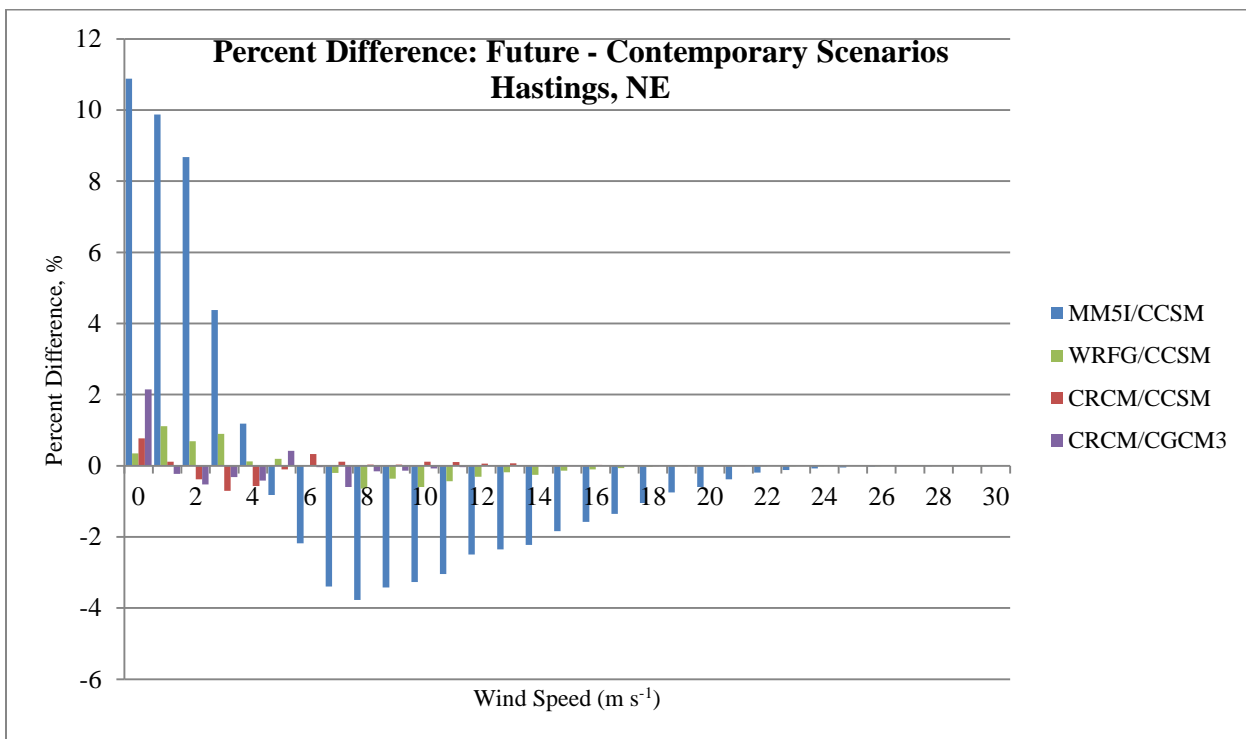
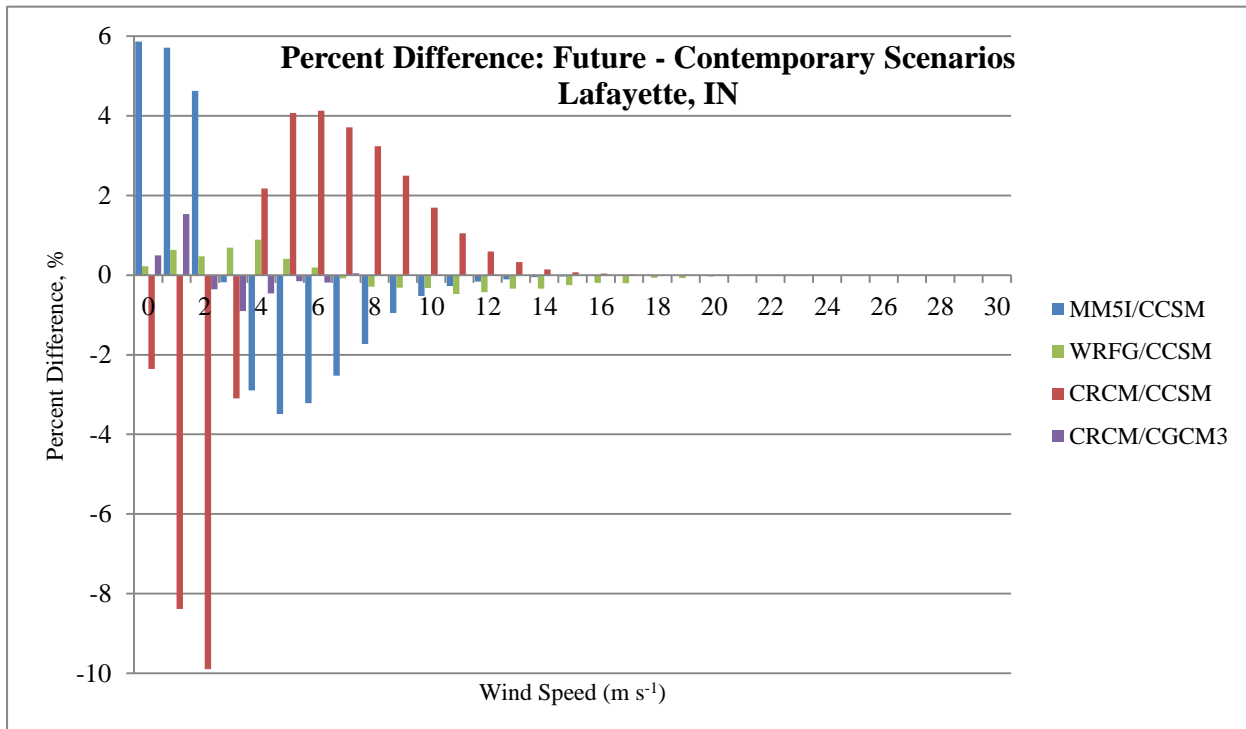


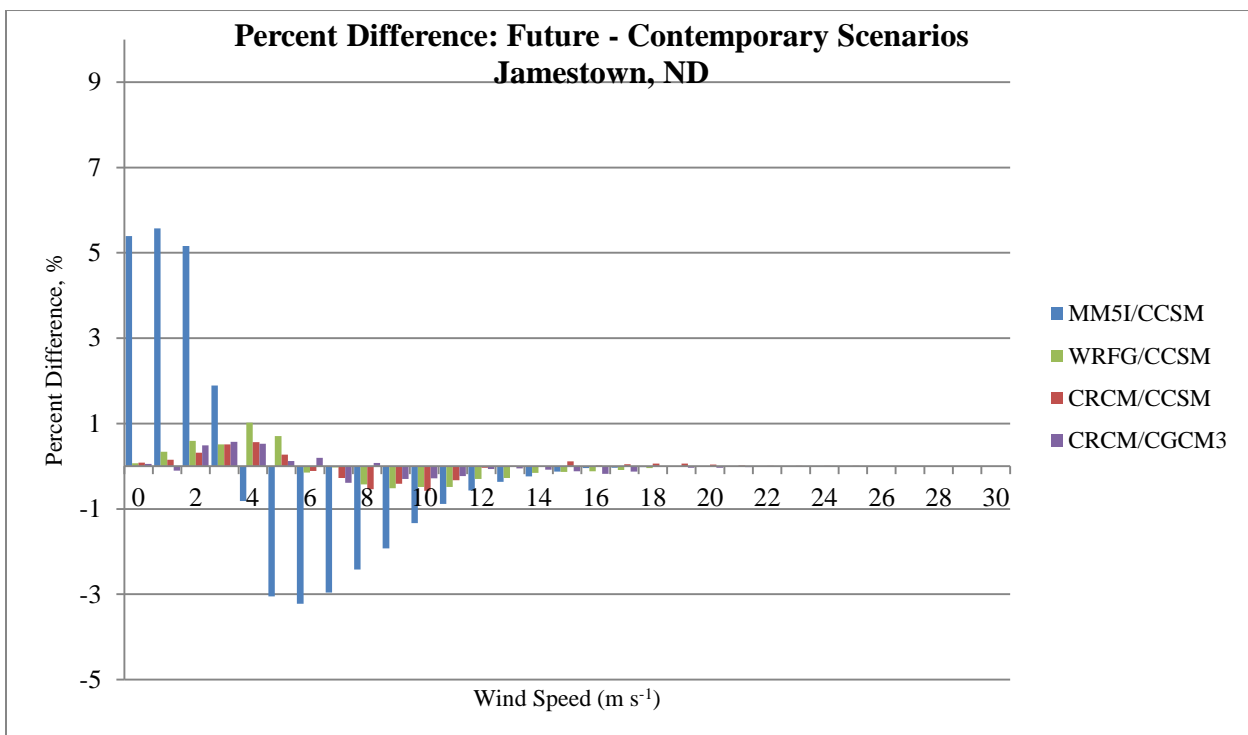
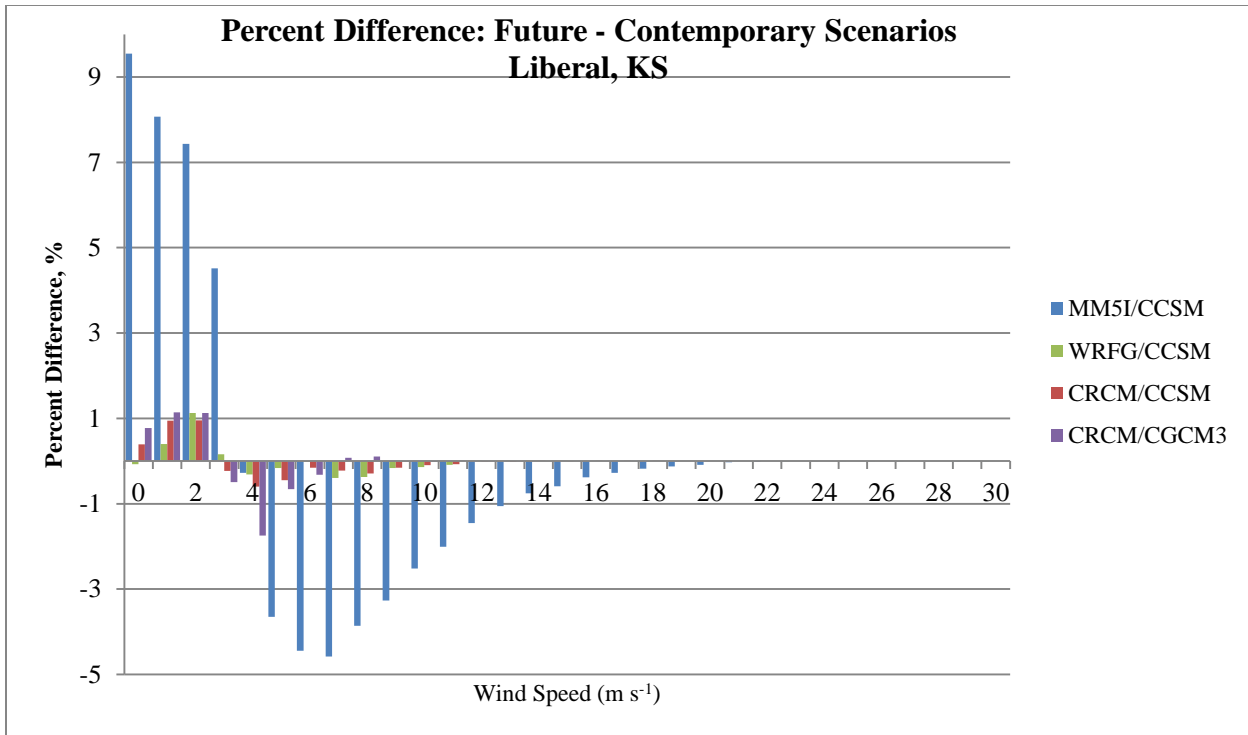
APPENDIX D

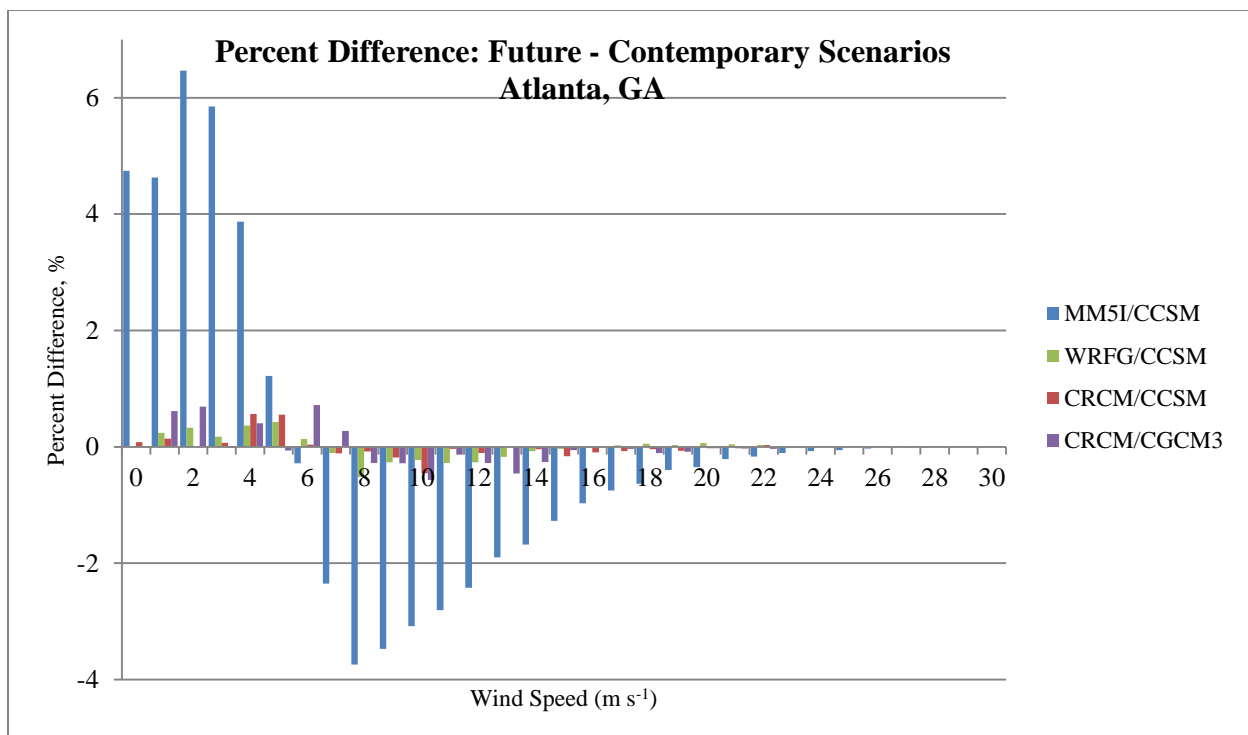
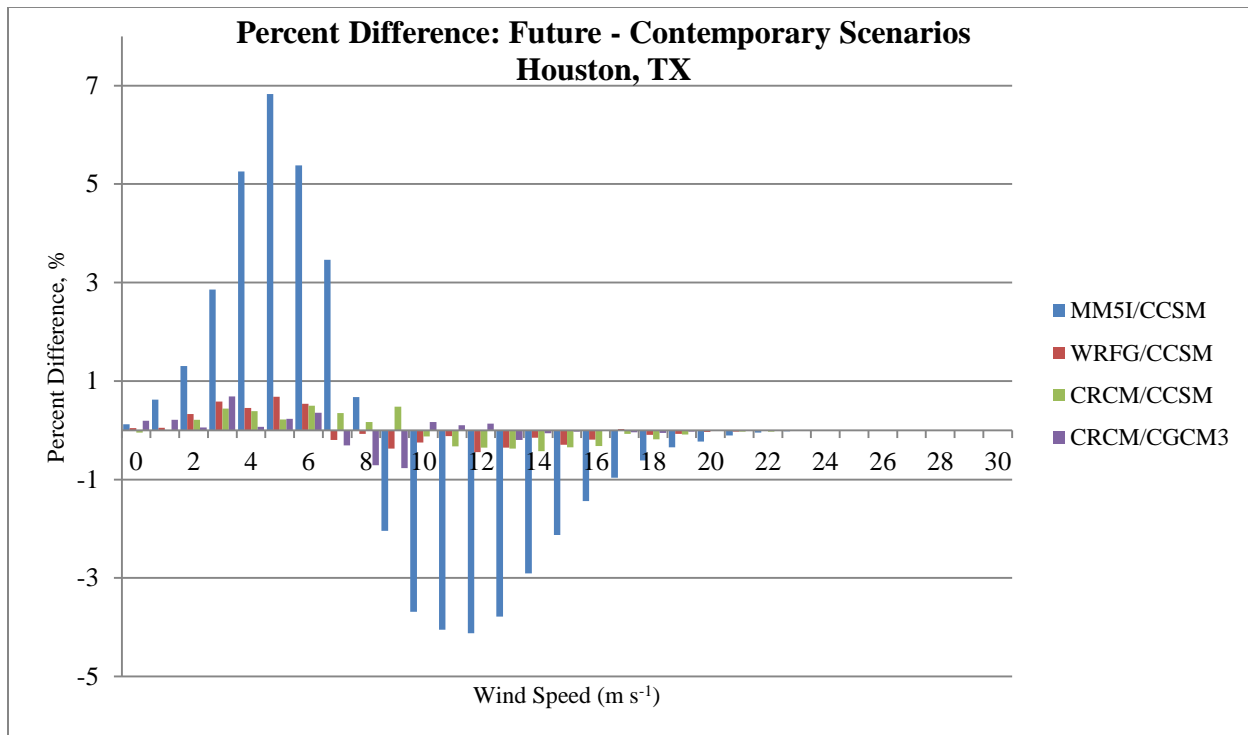
DIFFERENCE PLOTS: CONTEMPORARY AND FUTURE SCENARIOS

This appendix includes plots illustrating calculated percent difference in annual wind speeds between Future and Contemporary Scenarios at each of the seven cities. The following model combinations are plotted: MM5I/CCSM, WRFG/CCSM, CRCM/CCSM, and CRCM/CGCM3.









APPENDIX E

SEASONAL DISTRIBUTIONS

This appendix displays seasonal distributions (mean monthly winds) among observational data, NCEP, Contemporary, and Future model data at each of the seven locations. These plots allow for inter-model comparisons as well as model-to-observational comparisons to be drawn.

